Delay-robust distributed secondary frequency control for next-generation power systems: Stability analysis and controller synthesis

Sultan Alghamdi

Submitted in accordance with the requirements for the degree of
Doctor of Philosophy

School of Electronic and Electrical Engineering
University of Leeds

2^{nd} June, 2020

The candidate confirms that the work submitted is their own, except where work which has formed part of jointly authored publications has been included. The contribution of the candidate and the other authors to this work has been explicitly indicated below. The candidate confirms that appropriate credit has been given within the thesis where reference has been made to the work of others.

The work in Chapter 3 of the thesis has appeared in the following publications:

1. S. Alghamdi, J. Schiffer and E. Fridman, "Distributed Secondary Frequency Control Design for Microgrids: Trading Off L_2-Gain Performance and Communication Efforts under Time-Varying Delays," 2018 European Control Conference (ECC), Limassol, 2018, pp. 758-763.

   As the lead author, the candidate performed all the computational as well as simulation work and wrote the paper.

   Dr Johannes Schiffer, my supervisor, supervised the work, modified the text, proof-read the drafts, and made suggestions and corrections to the submitted paper.

   Prof. Emilia Fridman reviewed the final draft of the paper and provided some suggestions.

2. S. Alghamdi, J. Schiffer and E. Fridman, "Synthesizing Sparse and Delay-Robust Distributed Secondary Frequency Controllers for Microgrids," in IEEE Transactions on Control Systems Technology.

   As the lead author, the candidate performed all the computational as well as simulation work and wrote the paper.

   Dr Johannes Schiffer, my supervisor, supervised the work, modified the text, proof-read the drafts, and made suggestions and corrections to the submitted paper.

   Prof. Emilia Fridman reviewed the final draft of the paper provided some suggestions.

The work in Chapter 4 of the thesis has appeared in the following publication:

3. S. Alghamdi, J. Schiffer and E. Fridman, ”Conditions for Delay-Robust Consensus-Based Frequency Control in Power Systems with Second-Order Turbine-Governor Dynamics,” 2018 IEEE Conference on Decision and Control (CDC), Miami Beach, FL, 2018, pp. 786-793.

   As the lead author, the candidate performed all the computational as well as simulation work and wrote the paper.

   Dr Johannes Schiffer, my supervisor, supervised the work, modified the text, proof-read the drafts, and made suggestions and corrections to the submitted paper.

   Prof. Emilia Fridman reviewed the final draft of the paper provided some suggestions.

The work in Chapter 5 of the thesis has appeared in the following publication:

4. S. Alghamdi, N. Smith, J. Schiffer and P. Aristidou, ”Delay-Robust Distributed Secondary Frequency Control: A Case Study,” 2019 IEEE Milan PowerTech, Milan, Italy, 2019, pp. 1-6.

   As the lead author, the candidate performed all the computational as well as simulation work and wrote the paper.

   Nathan Smith was responsible for helping to set up the simulation and discuss the results.

   Dr Johannes Schiffer, my supervisor, supervised the work, modified the text, proof-read the drafts, and made suggestions and corrections to the submitted paper.

Dr Petros Aristidou, my supervisor, supervised the work, helped with setting up the simulation, modified the text, proof-read the drafts, and made suggestions and corrections to the submitted paper.

Abstract

Power systems worldwide are undergoing major transformation to enable a low-carbon future. These developments require new procedures for advanced control to ensure a stable and efficient system operation. Consensus-based distributed secondary frequency control schemes have the potential to ensure real-time frequency restoration and economic dispatch simultaneously in future power systems with significant contribution of renewable energy sources. However, owing to their distributed nature, these control schemes critically depend on communication between different controlled units. Thus, robustness against communication uncertainty is crucial for their reliable operation.

In this work, control design and stability analysis of delay-robust secondary frequency control in next-generation power systems are studied. The main contributions of the present thesis can be summarised as follows: (*i*) A design procedure for a consensus-based secondary frequency controller in microgrids is proposed that ensures robustness with respect to heterogeneous fast-varying communication delays and simultaneously provides the option to trade off the L_2-gain performance against the number of required communication links; (*ii*) The conditions for robust stability of a consensus-based frequency control scheme applied to a power system model with second-order turbine-governor dynamics in the presence of heterogeneous time-varying communication delays and dynamic communication topology are derived; (*iii*) The performance of the proposed consensus-based secondary frequency controller is analysed in a detailed model capturing the dynamic behaviour of a real system. The results provide insights to the robustness of the closed-loop system with respect to unmodelled (voltage and higher-order generator) dynamics as well as communication delays.

Acknowledgements

First of all, and most importantly, I would like to express my gratitude to my supervisors, **Dr Petros Aristidou** and **Dr Johannes Schiffer**, for their unlimited support, patient guidance and encouragement, and for the extremely useful advice and research insights and ideas. They have helped me out throughout my time as their PhD student. I was extremely blessed to have supervisors who cared so much about my research and academic development and who allocated much of their time to guide me - I am really grateful.

Special thanks go to my third supervisor, **Dr Benjamin Chong**, for all his support in my research work, for his extremely useful and helpful comments and suggestion on my thesis. Likewise, I would like to thank all co-authors on different research topics **Prof Emilia Fridman** and **Nathan Smith**, for their contributions, lessons, advice, and comments at various stages of my work.

I would like to thank all my group members and colleagues with whom I have shared the same workstation. My PhD years would have been far less enjoyable and instructive without them.

Last but not the least, I thank my father **Prof Mohammad Alghamdi** - I am beyond grateful to him for everything he has done and continues to do for me in his special ways. I honestly cannot thank him enough for always providing me with a never-ending supply of support, reassurance, and love. My gratitude to him is beyond words. I thank him for all the support and energy, and for everything he has done along the way. Without his support and guidance, I may never have reached where I am today.

Sultan

Abbreviations

AC alternating current
AGC automatic generation control
AVR automatic voltage regulator

DAE Differential-Algebraic Equation
DC direct current
DGU distributed generation unit

HV high voltage

LKF Lyapunov-Krasovskii functional
LK Lyapunov-Krasovskii
LMI linear matrix inequality
LV low voltage

MG microgrid
MV medium voltage

OLTC on load tap changers

PCC point of common coupling
PE power electronics

RAMSES RApid Multithreaded Simulation of Electric power Systems
RES renewable energy resource

SG synchronous machine

Contents

Declaration **ii**

Abstract **v**

Acknowledgements **vi**

Abbreviations **vii**

List of Figures **xi**

List of Tables **xiii**

1 Introduction **1**

1.1 Motivation . . . 1

1.1.1 The conventional power system . . . 1

1.1.2 Getting smart . . . 3

1.1.3 Overview of frequency control . . . 4

1.2 Contributions . . . 6

1.3 Related work . . . 8

1.4 Publications . . . 11

1.5 Thesis Outline . . . 12

2 Preliminaries in power systems and control theory **14**

2.1 Notation . . . 14

2.2 Preliminaries in power systems . . . 15

2.2.1 Reduced power systems model . . . 15

2.2.1.1 Modeling of synchronous generators 15
2.2.1.1.1 Swing equation 15
2.2.1.1.2 Turbine-governor dynamics 17
2.2.1.2 Simplified power network model 17
2.2.2 Microgrid model 19
2.2.2.1 Grid-forming inverter model 19
2.2.2.2 Microgrid network model 21
2.3 Preliminaries in control theory 22
2.3.1 Stability of time-delay systems 22
2.3.1.1 General Lyapunov-Krasovskii theorem 24
2.3.1.2 Choosing an appropriate Lyapunov-Krasovskii functional 26
2.3.1.2.1 Interval time-varying delay 26
2.3.1.3 Bounded techniques 27
2.3.1.3.1 Jensen's Inequality 27
2.3.1.3.2 A reciprocally convex approach 28
2.3.1.4 The descriptor method 29
2.3.2 Algebraic graph theory 30
2.3.3 Consensus protocol 31
2.3.4 L_2-Gain of dissipative systems 33

3 Delay-robust distributed secondary frequency control design for microgrids 35

3.1 Introduction 35
3.2 Distributed secondary frequency control in microgrid 36
3.2.1 Objectives and distributed control scheme 36
3.2.2 Closed-loop system 39
3.3 Controller synthesis 40
3.3.1 Coordinate transformation and error system 40
3.3.2 Problem statement 44
3.3.3 Main result 45

3.4 Numerical example 56

3.4.1 System description 56

3.4.2 Scenario 1: Heterogeneous communication delays 57

3.4.3 Scenario 2: Uniform communication delay ($\tau_r = \tau$ and $h_0 = 0$) 65

3.5 Summary 67

4 Conditions for delay-robust consensus-based frequency control in power systems 68

4.1 Introduction 68

4.2 Optimal consensus-based frequency control in power systems . . 69

4.2.1 Communication uncertainties: Time-varying delays and dynamic communication network 70

4.3 Robust stability in the presence of communication uncertainties 72

4.3.1 Coordinate transformation and reduction 72

4.3.2 Error system 76

4.3.3 Main result 77

4.4 Numerical example 82

4.5 Summary 85

5 Delay-Robust Distributed Secondary Frequency Control: A Case Study 86

5.1 Introduction 86

5.2 Test system descriptions 87

5.3 Delay-robust stability condition 89

5.4 Implementation of secondary frequency controller 90

5.4.1 Case 1: Tripping of 300MW generator g_2 in the North area 92

5.4.2 Case 2: Tripping of 750MW generator g_8 in the North area 93

5.4.3 Case 3: Loss of major corridor line 94

5.4.4 Discussion and summary 96

6 General Conclusions 98

6.1 Summary of work and main contributions 98

6.2 Directions for future work 100

Bibliography 103

List of Figures

1.1 Power system evolution 2

2.1 Synchronous machine model 16

3.1 Example of undirected connected graph 38

3.2 Schematic representation of islanded Subnetwork 1 of the CIGRE benchmark MV network 56

3.3 Frequency convergence at bus 9b for different values of κ. 59

3.4 Simulation results of the system (3.3.9) with $\kappa = 0.4656$ and $\gamma = 3.7092$, after being subjected to sinusoidal disturbances . . . 61

3.5 Simulation results of the system (3.3.9) with $\kappa = 0.4656$ and $\gamma = 3.7092$, after being subjected to disturbances: a step disturbance is applied to the electrical layer, while white noise is applied in the communication layer 61

3.6 Number of non-zero elements of $\mathcal{Z}$ for different values of γ . . . 63

3.7 Sparsity pattern of $\mathcal{L}$ for different values of γ 63

3.8 The convergence of the state p for generation unit $9b$ ($i = 6$) with different numbers of communication links 64

3.9 Simulation results with $\kappa = 2.6792$, $\gamma = 0.9637$, and $h = 100$ms . 66

3.10 Number of non-zero elements of $\mathcal{Z}$ for different values of γ . . . 66

4.1 Kundur's two-area-four-machine test system 82

4.2 Simulation results with $\kappa = 17.4898$, $h_1 = 0.1s$, $h_2 = 0.5s$. 84

5.1 Schematic representation of the Nordic test system 88

5.2 Flowchart of selection of the controller's parameters. 91
5.3 The feasibility map of condition (4.3.9) with different maximum communication delays. 92
5.4 Case 1: Frequency deviation 92
5.5 Case 2: Frequency deviation 93
5.6 Case 2: Bus voltage deviation at bus 1044 in Central area . . . 94
5.7 Case 2: Total active power output from the participating generators 94
5.8 Case 2: Convergence of controller outputs 95
5.9 Case 3: Frequency deviation 95
5.10 Case 3: Bus voltage of bus 1044 in Central area 96
5.11 Case 3: Total active power output from the participating generators 96

List of Tables

3.1 Results for κ and γ obtained from solving the optimization problem (3.3.12) in 'Design step 1' for different values of α and β . . 60

5.1 Comparison between the employed models in the control design and stability analysis and case study of this Chapter 87

5.2 The Participating generators 90

Chapter 1

Introduction

1.1 Motivation

1.1.1 The conventional power system

The history of power systems goes back to 1882 when Tomas Edison built the first direct current (DC) power system consisting of a generator, cable, loads [1]. From that time, the evolution of the power grid influenced by the economic and political factors has continued through small alternating current (AC) power systems to the current large-interconnected power systems [1, 2], see Fig 1.1.

Conventional power systems worldwide share the same basic hierarchical structure. This structure is mainly comprised of [1, 3]: (*i*) power plants that include different types of generation sources gas, coal, and nuclear; (*ii*) transmission system that transfers the power from the generation side to the load side; (*iii*) Costumers Load. The generation sources are connected to the high voltage (HV) level and mostly are thermal power plants [4]. Furthermore, transmission and distribution systems and the customers' loads are mainly located at the medium voltage (MV) and low voltage (LV) levels, as shown in Fig. 1.1. Power systems are seeing a growing demand to integrate more renewable energy resources (RESs) for a more sustainable, low-carbon future. The increasing penetration of economical and environmentally friendly RESs introduces enormous challenges for conventional power systems operation and

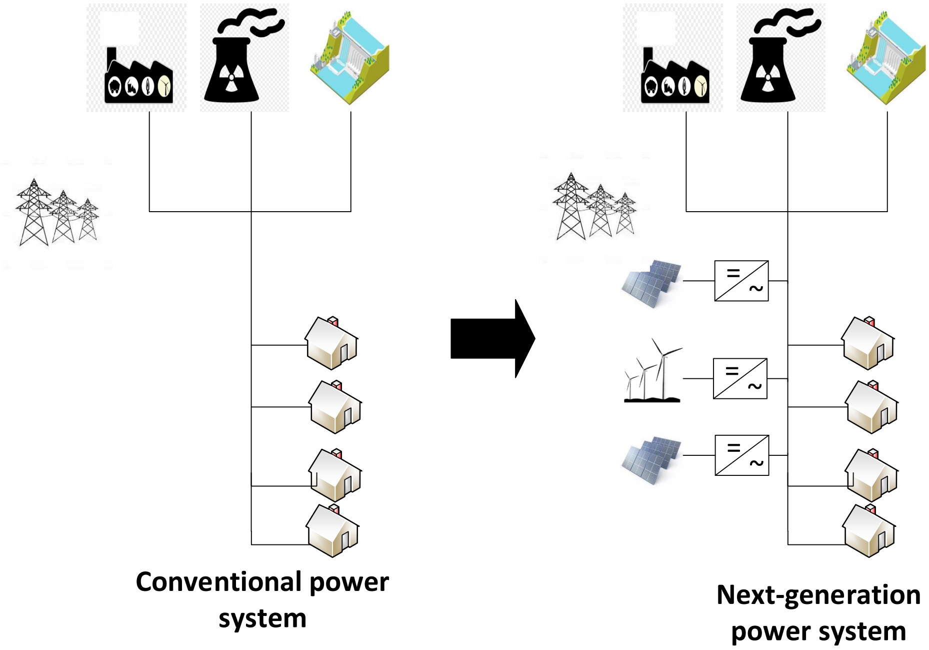

Figure 1.1: Power system evolution

control due to the following facts [5–8]:

i) Most RESs are small-scale distributed generation units (DGUs) , which are connected to the MV and LV levels via power electronics (PE) converters, as shown in Fig 1.1. Consequently, the replacement of a few bulk conventional fossil fuels based power plants with a large number of small-scale DGUs significantly increases the complexity of balancing demand and generation in real-time [9].

ii) Most of the RESs are DC sources, and therefore DC/AC converters (inverters) are usually required to interface the generation units to an AC network. In such scenarios, it is essential to recognize that the inverters' physical dynamics significantly differ from conventional synchronous generator dynamics [10] and the increasing integration of inverter-interfaced units results in reduced system inertia leading to low-inertia power systems.

Conventional power systems are being stressed by the above facts, which was not considered when most of them were built. The next generation-power systems, also known as smart grids [3, 5, 6], are expected to address these challenges and assure a more reliable, environmentally friendly, and robust grid.

1.1.2 Getting smart

There is a trend in the power industry and many governments to believe that smart grid technology is the key solution to the challenges mentioned above in the power system [6, 11]. In order for the grid to become smart, it is required to have the ability to merge communication technology and data information with power systems. Moreover, the smart grid is expected to address the following features [6].

- The ability to smoothly host any kind of generation units (rotational synchronous generators and inverter-interfaced units) while being robust against both physical and cyber disturbance events.

- The ability to operate economically and improve the security and quality of supply.

The notion of next-generation power system, i.e., smart grid, does not request a replacement of the current power system rather than a modification of its capabilities. The latter motivates the concept of microgrids (MGs). A MG is a small-scale power system, which is composed of a combination of DGUs, energy storage devices and loads at the distribution level [5]. MGs can be either connected to the main grid through a point of common coupling (PCC) or operated autonomously, i.e., in islanded mode [5, 12]. Thus, future power systems could be operated as a cell-structure of interconnected MGs [13].

Based on the above facts about smart grids, communication technology is considered as one of the most important components in power systems. Employing communication networks in power system applications introduces issues linked to communication uncertainties such as time delays, which lead to complicating the control design and may even deteriorate the system performance [14]. Among these challenges, robust frequency regulation is a very fundamental operational objective of next-generation power systems to which the present thesis is dedicated.

1.1.3 Overview of frequency control

The paramount principle in power systems is to maintain the balance between generation and load. If any imbalance occurs resulting, for instance, from sudden loads connected (or disconnected) or generating units tripped, the frequency deviates from its nominal value. If the frequency deviates by an unacceptable amount, then the protection system will be triggered, causing cascaded tripping of the generation units that might lead to a blackout [9]. The task of preserving the frequency close to the nominal value (and thus achieving the system power balance) is called frequency control. This task is traditionally achieved by hierarchical control layers: primary, secondary, and tertiary control [1].

- **Primary control.** The primary layer is performed through the governors of the turbine in the synchronous machine (SG) to increase (or decrease) the injection power to achieve the power balance between generations and demands. This controller is a fully decentralized controller with the time response between milliseconds to seconds. However, a well-known drawback of primary control is a steady-state frequency deviation from its nominal [15].

- **Secondary control.** The objective of this control layer is to adjust the active power setpoints to compensate for the steady-state frequency deviation. This controller is usually deployed via a centralized automatic generation control (AGC). To perform this task, the employment of a communication network is required, and its time response ranges between 30 seconds and 15 minutes [16].

- **Tertiary control.** The tertiary control layer is a centralized control layer that is mainly concerned with the energy management.

The resilience of future power systems is limited by the reliance of centralized approaches on a single control centre; thus, making them vulnerable to single-point failures. In addition, the need to minimize the complexity of communication infrastructures to achieve better scalability makes centralized schemes inefficient [17]. These challenges can be addressed with the use of new, distributed, schemes, which have advantages over centralized ones [18, 19]. The function of the distribution scheme requires exchanging information between neighbours. Thus, ensuring robustness with respect to communication uncertainties is mandatory [20, 21]. The main objectives of this thesis are as follows:

i) To investigate the problem of delay-robust distributed secondary frequency control in MGs and its corresponding challenges: the shape of communication topology and disturbance attenuation.

ii) To explore the problem of robust stability analysis of a distributed secondary frequency control power system model with second-order turbine-governor dynamics in the presence of heterogeneous time-varying communication delays and dynamic communication topology.

With regard to the first objective, as discussed in 1.1.2, the MG is a critical element in the next-generation power systems. Moreover, since most of the generation units in MG are inverter-based units [22], the frequency regulation has to be provided by units within the MGs in the island mode. Hence, the problems of frequency become remarkably significant in MG. In addition, the deployment of communication technology in the distributed secondary frequency control introduces new challenges such as communication delays, disturbances attenuation, and communication shape. Those challenges will be considered in the present work and extensively discussed.

Similarly, in the bulk power systems, increasing the integration of RESs complicates the operation and control of the power systems and introduced new challenges as well as the challenges coming from utilizing the communication network in the secondary frequency control. Since the SGs are the dominant units in power systems, the control design and analysis of the secondary frequency controller should take higher-order turbine-governor dynamics explicitly into consideration [23, 24]. Thus, both aspects of communication uncertainties and the higher-order model of SG will be jointly addressed and studied in the present thesis.

In order to achieve the above objectives, the load model used in the analysis presented in this thesis is the constant impedance. A simplified load model is commonly used in power system studies [1, Chapter 7] and can be described using algebraic equations. This can be justified by the fact that a constant impedance load can equivalently represent any constant power load for constant voltage amplitudes [14], i.e., $P = GV^2$ (please refer to Section2.2.1.2).

1.2 Contributions

The main contributions of the present thesis are:

i) A novel synthesis for consensus-based secondary frequency controllers in MGs is proposed in the form of a convex optimization problem with linear matrix inequality (LMI) constraints. The latter jointly considers the objectives of delay robustness, bounded L_2-gain performance for disturbance attenuation (i.e., the maximum energy amplification ratio of the system) and sparsity of the communication network. Compared to an analysis based on linearization, the proposed design criterion is equilibrium-independent (besides the usual requirement that the stationary angle differences do not exceed $|\frac{\pi}{2}|$). Thus if it is feasible, the desired performance specifications hold true in a wide range of operating conditions. The proposed design criterion is derived based on the Lyapunov-Krasovskii (LK) and descriptor methods [25, 26]. Compared to related work [14], combining the descriptor method with the LK method is essential to be able to obtain a controller synthesis in terms of linear matrix inequalitys (LMIs) which can be evaluated with efficient numerical methods [27].

ii) The derivation of sufficient delay-dependent conditions which guarantee robust stability of higher-order power system dynamics equipped with a consensus-based secondary frequency control scheme is proposed. Compared to existing work [14, 24, 28], the proposed method simultaneously accounts for second-order turbine-governor dynamics as well as time-varying communication uncertainties. Following [25, 26, 29–31], the latter are represented by heterogeneous fast-varying delays together with a dynamic communication network. The presence of higher-order (non-passive) and time-varying dynamics significantly complicates the stability analysis. However, if not accounted for in the analysis their presence may lead to instability, see, e.g., the example in [24] showing instability for power systems with non-passive second-order turbine governor dynamics. Furthermore unlike the Lyapunov functions employed in [24, 28], the present result is established by constructing a *strict* common Lyapunov-Krasovskii functional (LKF) for the nonlinear higher-order power system dynamics.

iii) For the first time, an extensive case study that evaluates the performance of a consensus-based secondary frequency control scheme on a realistic, full-detailed, medium-scale power system under the explicit consideration of communication delays are provided. Furthermore, it is empirically shown that the conditions for delay robustness established in Contribution (ii) also guarantee robust stability in the presence of additional unmodelled dynamics. Compared to the related work [18, 28], the case study not only verifies the steady-state frequency restoration with economic dispatch (where all generation units produce identical marginal costs) but, also, explores the impact of communication delays as well as the interaction of the proposed controller with unmodelled dynamics in the synthesis phase as well as unmodelled voltage phenomena. The case study are performed on the Nordic test system [32] and simulated with the software RApid Multithreaded Simulation of Electric power Systems (RAMSES) [33].

1.3 Related work

Maintaining a reliable and efficient operation of large scale power systems is becoming increasingly challenging due to the high penetration of RESs [5]. The latter leads to higher and faster varying power imbalances. Therefore, one of the most critical control challenges in next-generation power systems is frequency regulation. Since the next-generation power systems are cyber-physical systems incorporating both power systems and communication technology, this will allow developing advanced control methodology for frequency regulation [17, 19]. Thus, the main architectures for performing a secondary frequency control can either be centralized or distributed.

The function of the conventional centralized secondary frequency control termed AGC is described as follows. The area control error is transmitted to the data centre to be analyzed. Then new setpoints are broadcasted to each generator to compensate for the steady-state frequency deviation by increasing or reducing the power output [4, 34]. For a proper design of AGC and the following stability analysis, it is mandatory to take into account the communication uncertainties such as communication delays [35–38]. Stability analysis of communication delay is given in [35, 39] associated with simulation analysis in a full detailed model. Furthermore, the controller design of PID-type AGC in the deregulated system is presented in [40]. Another application of delay-robust AGC in a shipboard MG is considered in [41].

The deployment of the centralized control structure in the next-generation power system may raise concerns with regard to the scalability, flexibility and robustness of the control system [18, 19]. Besides being subjected to one point of failure, in large-scale power systems the cost and complexity associated with communication links can also become a problem. Moreover, in the MGs setting usually distributed algorithms are preferred for secondary control tasks, due to the dispersed nature of generation units [14, 17]. As a consequence, there is a need for transforming the control structure of the power system from a centralized scheme to a distributed architecture. Essentially, the available concepts of distributed frequency controller can be classified into two groups.

i) Primal-dual gradient-based algorithms [42–44]: The main advantages of primal-dual approaches are that generic convex cost functions for the generators and capacity constraints can be considered in the design. Yet, a key drawback is that exact information on the actual load demand needs to be available, which is a stringent requirement in practice (see also the discussion in [42]).

ii) Consensus-based approaches [24, 28, 45–47]: In practice, the consensus-based controller is simpler to implement than the primal-dual algorithm and also does not require prior knowledge of the actual load demand nor the generator parameters and power flows.

Furthermore, consensus-based control can guarantee an optimal steady-state resource allocation (with standard quadratic generation cost functions). The work in this thesis considers consensus-based algorithms for secondary frequency control which rely on peer-to-peer communication where each generation unit exchanges information with neighbouring participating generators [31].

Most existing results for stability of consensus-based frequency controllers are limited to generator dynamics modeled by the swing equation and assume ideal communication [45–47]. There are several exceptions, for example the work in [24, 28] where higher-order turbine-governor dynamics are considered and the work in [14] where the impact of communication uncertainties on the control performance is analysed. The latter is of paramount importance, since any distributed control scheme relies on information exchange between generators. Thus, guaranteeing robustness with respect to communication uncertainties, such as delays, message losses and link failures [20, 21], is essential to further promote a practical implementation of consensus-based control schemes in power systems. For the same reason, more realistic generator models need to be considered. Note that the inclusion of second-order turbine governor dynamics is used in many related stability studies on classical AGC [36, 40, 48–51].

In recent years, consensus-based secondary frequency control experience increasing prominence in MGs [52–57]. Delay-robustness of consensus-based secondary controllers in MGs has been investigated in [58–62], but the analysis is either limited to a linearized (small-signal) model or does not consider the electrical dynamics and is partially restricted to constant delays. In [14], stability conditions for a distributed averaging secondary frequency controller in power system have been derived under consideration of fast-varying time-delays and a dynamic communication topology, but the (nominal) communication topology is assumed to be fixed a priori and no external perturbations are considered. In addition to communication uncertainties, the electrical dynamics of the MG are also continuously exposed to perturbations, for example, load demand and renewable generations.

Bounded input-output performance of linearized models of secondary controlled MG has been considered using the $\mathcal{H}_2$-norm in [56] and the $\mathcal{H}_\infty$-norm in [63, 64]. A very similar setup for bulk power systems with distributed frequency control is employed in [55], where in addition to minimizing the $\mathcal{H}_2$-norm, the sparsity of the communication network is also promoted. The interaction between the cyber and physical layers of a related primal-dual distributed secondary control scheme has recently been explored in [65] by using a linearized power system model with uniform inertia and damping coefficients.

In summary, in the MG setting, the aspects of delay robustness, disturbance attenuation and communication topology design have to some extent been considered in the literature, but mainly on an individual basis and by using linearized MG models. In particular, there are no available approaches, which jointly address all three aspects. Yet clearly from a practical point of view, the development of holistic design criteria, which takes into account the physical and cyber layers of the system, is highly desirable to further facilitate a robust and efficient implementation of consensus-based secondary controllers in MGs. This motivates the work in Chapter 3.

Furthermore, beside the work [66] with constant delays, to the best of the author's knowledge there is no existent work on the literature that provide stability conditions for nonlinear higher-order power system dynamics in the presence of both heterogeneous time-varying communication delays and dynamic communication topology. This motivates the work in Chapters 4 and 5.

1.4 Publications

The material presented in this thesis are supported by the following publications:

- S. Alghamdi, J. Schiffer and E. Fridman, "Distributed Secondary Frequency Control Design for Microgrids: Trading Off L_2-Gain Performance and Communication Efforts under Time-Varying Delays," 2018 European Control Conference (ECC), Limassol, 2018, pp. 758-763.

- S. Alghamdi, J. Schiffer and E. Fridman, "Synthesizing Sparse and Delay-Robust Distributed Secondary Frequency Controllers for Microgrids," IEEE Transactions on Control Systems Technology.

- S. Alghamdi, J. Schiffer and E. Fridman, "Conditions for Delay-Robust Consensus-Based Frequency Control in Power Systems with Second-Order Turbine-Governor Dynamics," 2018 IEEE Conference on Decision and Control (CDC), Miami Beach, FL, 2018, pp. 786-793.

- S. Alghamdi, N. Smith, J. Schiffer and P. Aristidou, "Delay-Robust Distributed Secondary Frequency Control: A Case Study," 2019 IEEE Milan PowerTech, Milan, Italy, 2019, pp. 1-6.

1.5 Thesis Outline

- **Chapter 2:** In this chapter, the reduced model for electrical power systems used in this thesis is detailed. Furthermore, a suitable model of a MG is introduced for the purpose of designing the secondary frequency control in MGs. In addition, the mathematical background on stability analysis for the time-delay systems, used to establish most of the results in this work, is presented. Finally, some basics of algebraic graph theory, consensus protocols, and L_2-gain of dissipative systems are recalled.

- **Chapter 3:** The work in this chapter aims to provide a delay-robust design procedure for distributed secondary frequency controller in MGs. First, the consensus-based secondary control law in the MG model is introduced. Then, coordinate transformation and reduction, which are essential for the proposed controller synthesis, and the problem statement are provided. After that, the controller synthesis ensuring robustness with respect to heterogeneous fast-varying delays as well as disturbance rejection, while minimizing the number of communication links is proposed. Finally, a numerical example to demonstrate the effectiveness of the proposed approach is given.

- **Chapter 4:** This chapter is focused on the stability of the distributed secondary frequency controller in the presence of communication uncertainties in power systems. First, some preliminaries on optimal consensus-based frequency control and communication uncertainties are recalled. Next, since the turbine-governor dynamics are considered in this chapter, a novel coordinate transformation and reduction compared to [14] are proposed. Then, the robust stability analysis based on a strict LKF is presented and followed by a numerical example to demonstrate the effectiveness of the proposed approach.

- **Chapter 5:** This Chapter focuses on analysing the performance of the secondary frequency controller under communication delays in a full-detailed model using the well-known Nordic system. First, a simplified version of the delay-robust stability conditions is developed to be implemented in the case study. Next, the implementation procedure of the secondary frequency controller is proposed. Then, to evaluate the efficacy of the stability conditions and investigate the controller behavior, two scenarios are considered. Finally, a discussion about the found results is given.

- **Chapter 6:** In this chapter, the contribution of this thesis is summarized and some plans for future work are suggested.

Chapter 2

Preliminaries in power systems and control theory

This chapter is organized as follows. First, the basic notation within the thesis is introduced in Section 2.1. Then, a comprehensive overview of the employed models of power systems and MGs are given in Section 2.2. Moreover, Section 2.3 provides the required mathematical background to establish the analysis within the provide work and ease the readability of this thesis.

2.1 Notation

The set of real numbers is denoted by $\mathbb{R}$. It is convenient to define $\mathbb{R}_{\geq 0} := \{x \in \mathbb{R} | x \geq 0\}$, $\mathbb{R}_{>0} := \{x \in \mathbb{R} | x > 0\}$ and $\mathbb{R}_{<0} := \{x \in \mathbb{R} | x < 0\}$. For a set $\mathcal{V}$, $|\mathcal{V}|$ denotes its cardinality and $[\mathcal{V}]^k$ denotes the set of all subsets of $\mathcal{V}$ that contain k elements. Let $x := \mathrm{col}(x_i) \in \mathbb{R}^n$ denote a vector with entries x_i for $i = 1, \ldots, n$, $\mathbb{1}_n$ the vector with all entries equal to one, I_n the $n \times n$ identity matrix, $\mathbb{0}$ a zero matrix of appropriate dimensions and $\mathrm{diag}(a_i), i = 1, \ldots, n$, an $n \times n$ diagonal matrix with diagonal entries $a_i \in \mathbb{R}$. For $A \in \mathbb{R}^{n \times n}$, $A > 0$ $(A < 0)$ means that A is symmetric positive (negative) definite. The lower-diagonal elements of a symmetric matrix are denoted by $*$. The Euclidean norm of a vector $x \in \mathbb{R}^n$ is denoted by $\|x\|_2$. $W[-h, 0]$, $h \in \mathbb{R}_{>0}$, denotes the Banach space of absolutely continuous functions $\phi : [-h, 0] \to \mathbb{R}^n$, $h \in \mathbb{R}_{>0}$, with $\dot{\phi} \in L_2(-h, 0)^n$ and with the norms $\|\phi\|_c = \max_{\theta \in [a,b]} |\phi(\theta)|$ and $\|\phi\|_W =$

$\max_{\theta\in[a,b]}|\phi(\theta)|+\left(\int_{-h}^{0}\dot{\phi}^2 d\theta\right)^{0.5}$. Also, ∇f denotes the gradient of a function $f:\mathbb{R}^n\to\mathbb{R}$.

2.2 Preliminaries in power systems

This section describes the reduced models, used in this thesis, for both power systems and MGs. The introduced models are associated with related essential assumptions and mathematics descriptions.

2.2.1 Reduced power systems model

For the secondary frequency control development in this thesis, a reduced model of the power system, which is comprised of only SG, is introduced. The contents of the model consist of a synchronous generator model as well as a network model. The presented modeling is based on standard textbooks in power systems [1, 4, 67–69].

2.2.1.1 Modeling of synchronous generators

The considered dynamics of synchronous machines in this subsection are as follows, see also Fig 2.1. First, the electro-mechanical equation (swing equation) that describes the relationship between electrical and mechanical power is derived. Then, as the mechanical power is the output of the prime mover, the dynamics of the turbine-governor that accompanies the synchronous machine is discussed.

2.2.1.1.1 Swing equation

The main components of a SG are the stator and the rotor [1]. When the unbalance occurs between the mechanical and electromagnetic torques, the net torques leads to acceleration or deceleration of the rotor. This can be described by applying Newtons' second law on the $i-$th SG as [70]

$$M_{m_i}\ddot{\theta}+D_{d_i}\dot{\theta}=\tau_{mech_i}-\tau_{elec_i}, \tag{2.2.1}$$

where $M_{m_i}\in\mathbb{R}_{>0}$ is moment of inertia of the rotor shaft, $\theta_i:\mathbb{R}_{\geq 0}\to\mathbb{R}$ is the rotor angle, $\tau_{mech_i}\in\mathbb{R}$ and $\tau_{elec_i}\in\mathbb{R}$ are the mechanical torque and the elec-

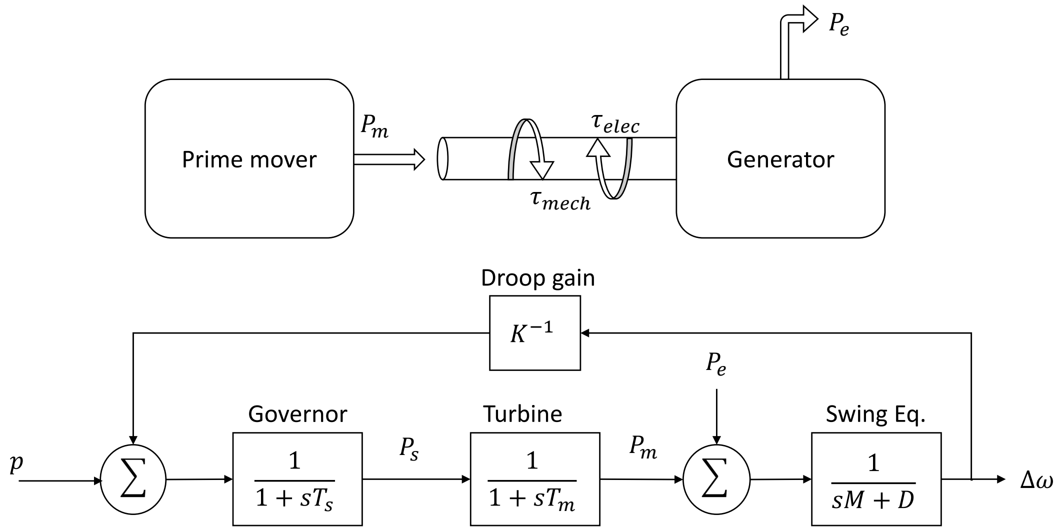

Figure 2.1: Synchronous machine model

tromagnetic torque, respectively. Moreover, $D_{d_i} \in \mathbb{R}_{>0}$ denotes the damping coefficient (accounts for the mechanical rotational loss due to windage and friction). Furthermore, the angular velocity of the rotor shaft is

$$\omega_i = \dot{\theta}_i. \tag{2.2.2}$$

Moreover, in steady-state, the angular velocity converges to the synchronous speed ω_{sm}, and the mechanical torque can be expressed as

$$\tau_{mech_i} = D_{d_i}\omega_{sm} + \tau_{elec_i}, \tag{2.2.3}$$

It is convenient to work with the power rather than the torque, therefore, by multiplying the both side of (2.2.1) by ω_{sm}, applying $P_{m_i} = \omega_{sm}\tau_{mech_i}$ and $P_i = \omega_{sm}\tau_{elec_i}$ and defining $M_i = M_{m_i}\omega_{sm}$ and $D_i = D_{d_i}\omega_{sm}$, (2.2.1) can be rewritten as follows

$$M_i\ddot{\theta} + D_i\dot{\theta} = P_{m_i} - P_i, \tag{2.2.4}$$

Finally, in standard stability analysis, it is more convenient to replace (2.2.4) by the following two first-order equations:

$$\dot{\theta}_i = \omega_i,$$

$$M_i\dot{\omega}_i = -D_i\omega_i - P_i + P_{m_i}. \tag{2.2.5}$$

Since P_{m_i} is the output of the turbine-governor system, next a standard second-order turbine-governor dynamics are introduced.

2.2.1.1.2 Turbine-governor dynamics

The speed of a synchronous generator is determined by the speed of the prime mover which directly affects the input P_{m_i}. One of the well-known prime movers used extensively throughout the world is the steam turbine. The speed of the steam turbine is controlled by the speed governor that senses the speed deviation and converts it into an appropriate valve action [68]. It is common in stability analyses to use a simplified model for the steam turbine-governor model to facilitate the stability analysis such as the TGOV1 model [71]. In the present work, a modified version of the TGOV1 [68] is used where P_m remains a state in the synchronous machine model, and P_S will become a state when the governor is added. As shown in Fig 2.1, the physical dynamics of the steam turbine-governor can be written as

$$\begin{aligned} T_{m_i}\dot{P}_{m_i} &= -P_{m_i} + P_{s_i}, \\ T_{s_i}\dot{P}_{s_i} &= -P_{s_i} - K_i^{-1}\omega_{r_i} + p_i, \end{aligned} \tag{2.2.6}$$

where $P_{s_i} : \mathbb{R}_{\geq 0} \to \mathbb{R}$ is the steam power, $\omega_{r_i} = \dot{\theta}_i - \omega^d$ is the relative frequency with $\omega^d \in \mathbb{R}_{\geq 0}$ being the desired (nominal) network frequency and $p_i : \mathbb{R}_{\geq 0} \to \mathbb{R}$ is the secondary control signal. Furthermore, $K_i \in \mathbb{R}$, $T_{m_i} \in \mathbb{R}$ and $T_{s_i} \in \mathbb{R}$ denote the droop gain, governor time and turbine time constant, respectively.

2.2.1.2 Simplified power network model

Following the typical approach in power system studies, it is assumed that the loads are constant impedences. This results in modeling the power system network as a set of Differential-Algebraic Equations (DAEs). The power network, in this thesis, is represented by using the Kron-reduction method [72] to eliminate the algebraic equations and obtain a set of differential equations.

Furthermore, the power network is described as a connected and undirected graph with a set of nodes $\mathcal{N} = \{1,2,\dots,n\}$. It is assumed that at each node a generator is connected and a phase angle $\theta_i : \mathbb{R}_{\geq 0} \to \mathbb{R}$ and ω_{r_i} are assigned to each unit $i \in \mathcal{N}$. Moreover, the following standard assumptions in secondary frequency control are made [23, 35, 73]:

i) The voltage amplitudes $V \in \mathbb{R}^n_{\geq 0}$ at all nodes are constant.

ii) The transmission line impedances are purely inductive [1].

iii) The effect of reactive power is neglected.

With these assumptions, two nodes i and k are connected via a non-zero susceptance $B_{ik} \in \mathbb{R}_{<0}$. If there is no line between i and k, then $B_{ik} = 0$. The set of neighboring nodes of node i is denoted by $\mathcal{N}_i = \{k \in \mathcal{N} | B_{ik} = 0\}$. To represent the closed-loop power system compactly, it is convenient to define the following vectors $\theta = \mathrm{col}(\theta_i)$ and $\omega = \mathrm{col}(\omega_i)$. Then, the active power flow can be written as follows $P : \mathbb{R}^n \to \mathbb{R}^n$,

$$P(\theta) = \nabla U(\theta),$$

where the potential function $U : \mathbb{R}^n \to \mathbb{R}$ is given by

$$U(\theta) = -\sum_{\{i,k\}\in[\mathcal{N}]^2} |B_{ik}| V_i V_k \cos(\theta_{ik}). \tag{2.2.7}$$

Let $P_m : \mathbb{R}_{\geq 0} \to \mathbb{R}^n$, $P_s : \mathbb{R}_{\geq 0} \to \mathbb{R}^n$ and $p : \mathbb{R}_{\geq 0} \to \mathbb{R}^n$ and, furthermore, define the diagonal and positive definite matrices $D \in \mathbb{R}^{n\times n}$, $M \in \mathbb{R}^{n\times n}$, $K \in \mathbb{R}^{n\times n}$, $T_m \in \mathbb{R}^{n\times n}$ and $T_s \in \mathbb{R}^{n\times n}$. Then, by combining (2.2.5), (2.2.6) with (2.2.7) the dynamics of the simplified power network can be compactly written as [74, Chapter 4]

$$\begin{aligned}
\dot{\theta} &= \omega_r, \\
M\dot{\omega}_r &= -D\omega_r - \nabla U(\theta) - GV^2 + P_m^d + P_m,
\end{aligned}$$

$$
\begin{aligned}
T_m \dot{P}_m &= -P_m + P_s, \\
T_s \dot{P}_s &= -P_s - K^{-1}\omega_r + p,
\end{aligned} \tag{2.2.8}
$$

where GV^2 represents (constant active power) the loads, $G = \mathrm{col}(G_{ii}) \in \mathbb{R}^n_{\geq 0}$ where $G_{ii} \in \mathbb{R}_{\geq 0}$ is the shunt conductance at the i-th node, and $P^d_m \in \mathbb{R}^n_{\geq 0}$ denotes the vector of nominal power injection setpoints.

2.2.2 Microgrid model

In the present subsection, a MG with mixed generation pool consisting of rotational and electronic interfaced units is considered. In the previous subsection, the model of the SG is introduced. Thus this subsection will focus on inverter-based generators model. Since the work in this thesis focuses on frequency control, the inverters are modeled such that they provide a synchronous frequency, i.e., a grid-forming mode. The presented modeling is based on the following references [12, 22, 75]

2.2.2.1 Grid-forming inverter model

A suitable model for the grid-forming inverter is employed to be utilized in the control design of the secondary frequency controller in MG, see Chapter 3. The dynamics model of the used grid-forming inverter can be classified as follows:

ii) The inner control loop and the output filter dynamics:

  The inner control loop consists of cascaded voltage and current controllers to generate the reference voltage signal. Let $x_{I_i} : \mathbb{R}_{\geq 0} \to \mathbb{R}^m$ be the state, denote its input signal by $v_{ref_i} : \mathbb{R}_{\geq 0} \to \mathbb{R}^3$ and suppose its output signal is v_{abc_i}. Furthermore, let the grid-side current be given by $i_{abc_i} : \mathbb{R}_{\geq 0} \to \mathbb{R}^3$. Let $f_i : \mathbb{R}^m \times \mathbb{R}^3 \times \mathbb{R}^3 \to \mathbb{R}^m$ and $h_i : \mathbb{R}^m \times \mathbb{R}^3 \to \mathbb{R}^3$ denote continuously differentiable functions and $\upsilon_i \in \mathbb{R}_{\geq 0}$ denotes a time constant of the dynamics x_{I_i}.

i) The outer control loop dynamics:

  This layer consists of active and reactive power controllers, which provide the output voltage angle and magnitude reference by adjusting the predefined setpoints according to a measured power imbalance. Let $z_{I_i} : \mathbb{R}_{\geq 0} \to \mathbb{R}^p$ denotes the state signal of outer control loop and $u_{I_i} : \mathbb{R}_{\geq 0} \to \mathbb{R}^q$ its input signal. Furthermore, let $g_i : \mathbb{R}^p \times \mathbb{R}^q \to \mathbb{R}^p$ and $w_i : \mathbb{R}^p \times \mathbb{R}^q \to \mathbb{R}^3$ be continuously differentiable functions.

Thus, the overall inverter dynamics inner control, output filter (the first line), and outer control system (the second line) can be represented as follows:

$$\begin{aligned} \dot{z}_{I_i} &= g_i(Z_I, u_I), \\ \upsilon_i \dot{x}_{I_i} &= f_i(x_{I_i}, w_i(Z_{I_i}, u_{I_i}), i_{abc_i}), \\ v_{abc_i} &= h_i(x_{I_i}, w_i(Z_{I_i}, u_{I_i})). \end{aligned} \tag{2.2.9}$$

Assumption 2.2.1. $\upsilon_i = 0$ *in* (2.2.9). *Then,* $v_{abc_i} = w_i(Z_{I_i}, u_{I_i})$.

Assumption 2.2.1 can be interpreted as the voltage and the current controllers are ideal and lead to fast and error-free tracking of the references. By using Assumption 2.2.1, the model (2.2.9) can be reduced to only outer control loop dynamics

$$\begin{aligned} \dot{z}_{I_i} &= g_i(Z_I, u_I), \\ v_{abc_i} &= h_i(Z_I, u_I). \end{aligned} \tag{2.2.10}$$

As stated in Section 2.2.2, both SGs, and inverter-based units are considered when modelling the MGs. Thus, to establish a suitable model of the inverter-based units, following [22], the subsequent model is used assuming a constant voltage, and the active power output is measured through a filter

$$\begin{aligned} \dot{\theta}_i &= \omega_i = u_{\omega_i}, \\ \tau_{p_i} \dot{P}_i^m &= -P_i^m + P_i, \end{aligned} \tag{2.2.11}$$

where $u_{\omega_i} : \mathbb{R}_{\geq 0} \to \mathbb{R}$ is control signal, P_i is the active power injection of the inverter, $P_i^m : \mathbb{R}_{\geq 0} \to \mathbb{R}$ is the measured value with $\tau_{p_i} \in \mathbb{R}_{>0}$ being the time constant of the low pass filter. With regard to primary control, it is assumed that all units are equipped with the standard frequency droop controller [1, 76, 77]. Thus, u_{ω_i} in (2.2.11) can be expressed as

$$u_{\omega_i} = \omega_i = \omega^d - k_{p_i}(P_i^m - P_i^d), \tag{2.2.12}$$

where $k_{p_i} \in \mathbb{R}_{>}0$ is the frequency droop gain, and $P_i^d \in \mathbb{R}$ is the desired setpoint. Differentiating ω_i in (2.2.12) with respect to time and using P_i^m in (2.2.12) yields

$$\begin{aligned} \dot{\omega}_i &= -k_{p_i}\dot{P}_i^m = \frac{k_{p_i}}{\tau_{p_i}}(-P_i^m + P_i), \\ \tau_{p_i}\dot{\omega} &= -(\omega - \omega^d) - k_{p_i}(P_i + P_i^d). \end{aligned} \tag{2.2.13}$$

Then by using (2.2.13) with (2.2.11) the dynamics of the i-th inverter can be introduced as follows

$$\begin{aligned} \dot{\theta}_i &= \omega_i, \\ \tau_{p_i}\dot{\omega}_i &= -(\omega_i - \omega^d) - k_{p_i}(P_i + P_i^d). \end{aligned} \tag{2.2.14}$$

Note that the dynamics of the inverter in (2.2.14) mimic the behavior of an SG [22, 78]. In practice, the implementation of droop control in the inverter-based generator experimentally does not require any mechanical devices; however, the controller is applied in digital signal processors [79].

2.2.2.2 Microgrid network model

In this section, a suitable model of MG is considered with same assumptions in section 2.2.1.2 being applied in here. As MG is small-scale power system with heterogeneous generation pool (rotational synchronous generators and inverter-interfaced units), the set of network nodes are denoted by $\mathcal{N} = N_I \cup N_{SG}$, where $\mathcal{N}_I = \{1, \ldots, n_1\}$, which represent inverter-based generators, $\mathcal{N}_{SG} = \{(n_1+1), \ldots, n\}$, which represent synchronous generators, with $n \geq 1$. The assumption of purely inductive lines is admissible in microgrid analysis, since the inverter output impedance is typically highly inductive [52, 80].

Then, the MG dynamics with considering the secondary frequency controller p are compactly given by [77, 80]

$$\begin{aligned} \dot{\theta} &= \omega, \\ M\dot{\omega} &= -D(\omega - \mathbb{1}_n \omega^d) - \nabla U(\theta) + P^{\text{net}} + p, \end{aligned} \tag{2.2.15}$$

where $D = \text{diag}(D_i) \in \mathbb{R}^n_{>0}$ is the matrix of (inverse) droop coefficients, where for any inverter-interfaced unit $D = \frac{1}{k_{p_i}}$, $\omega^d \in \mathbb{R}_{>0}$ is the reference frequency and $p : \mathbb{R}_{\geq 0} \to \mathbb{R}^n$ is the secondary frequency control input. Moreover, the matrix of (virtual) inertia coefficients is given by $M = \text{diag}(M_i) \in \mathbb{R}^n_{>0}$, where for any inverter-interfaced unit $M_i = \tau_{p_i} D_i$. In addition, P^{net} is given by $P^{\text{net}} = \text{col}(P_i^d - G_{ii} V_i^2)$, where $P_i^d \in \mathbb{R}$ denotes the active power set point and $G_{ii} V_i^2$, $G_{ii} \in \mathbb{R}_{\geq 0}$, represents the active power demand at the i-th node. Note that $P_i^d = P_m^d$ in (2.2.8). Furthermore, the turbine-governor dynamics of the SG in (2.2.8) are assumed to be ideal and represented by their corresponding steady-state equations [12, 81].

2.3 Preliminaries in control theory

This section is organized as follows. A brief introduction to the stability of time-delay systems is given in Subsection 2.3.1. Algebraic graph theory and consensus protocols are reviewed in Subsection 2.3.2 and Subsection 2.3.3, respectively. Finally, the L_2-gain of dissipative systems is recalled in Subsection 2.3.4.

2.3.1 Stability of time-delay systems

As discussed in Chapter 1, the employment of the communication network is mandatory in distributed consensus-based secondary frequency controller. Besides all the advantages of communication technology, it can introduce additional vulnerabilities to the system, one of the most prominent being communication delays. More specifically, in network-based control, sending a signal through communication channels is subject to delays. These delays are comprised of communication delays (transmission delays, propagation delays, processing delays, and queuing delays [82, 83]) and delays caused by the sample-and-hold function of control variables. In this work, the communication time-delays under consideration are the aggregation of the delays of information transmitted to the receiver and the time taken for the receiver to start acting on it. Since the presence of communication delays influences the system performance and can even lead to instability [84], taking such delays into account is necessary in order to design a well-functioning secondary frequency controller. The analysis of the time-delay systems falls into two main groups: Frequency domain analysis and time domain analysis. The frequency domain analysis is based on the eigenvalues analysis and an approximation of the solution of the characteristic equation is required [85]. This approach is not applicable to the case of time-varying delays. Yet, time-varying delays are ubiquitous in sampled data networked control systems [25, 26], such as consensus-based secondary frequency control. The reasons for this are the joint presence of digital controls and continuous physical dynamics as well as the fact that network access and propagation delays typically depend on the communication network congestion and are, hence, time-varying [30]. Therefore, following standard practice in sampled-data and networked control systems, in the present work the communication delays are represented by bounded, time-dependent functions [25, 26]. As a consequence, the resulting dynamical system is non-autonomous, which implies that an eigenvalue-based stability analysis is inconclusive [86]. The time domain analysis based on the LK theory in combination with a LMI approach [25, 26] is the alternative approach that is employed in this work.

Studying the time-delay systems has been an active topic for a long time, but a new set of significant results has been introduced in 21^{th} century such as these remarkable results [87–89]. In this subsection, the LK theorem is stated. Then, an overview of the methodology to analyze time-delay systems which will be used in this thesis is explained. The presented contents are strongly oriented on [25, 26, 90].

2.3.1.1 General Lyapunov-Krasovskii theorem

In control systems without time-delays, Lyapunov method is an efficient approach to study the stability of an equilibrium point of a dynamical system [86]. However, in the case of considering time delays, LK approach is generally used [26, 91]. Consider the following:

$$\dot{x}(t) = f(t, x_t), \quad t \geq t_0 \tag{2.3.1}$$

where $f : \mathbb{R} \times C[-h, 0] \rightarrow \mathbb{R}^n$ is continuous in both arguments and is locally Lipschitz continuous in the second argument and $x_t = x(t+\phi)$, $\phi \in [-h, 0]$ and $h \in \mathbb{R}_{>0}$. Moreover, it is assumed that $f(t, 0) = 0$ ensures that (2.3.1) possesses a trivial solution $x(t) = 0$[1].

Definition 2.3.1 ([26]). *The trivial solution of* (2.3.1) *is*

- *uniformly (in t_0) stable if, for $\forall t_0 \in \mathbb{R}$ and $\forall \epsilon > 0$, there is $\delta = \delta(\epsilon) > 0$ such that*

$$\|x_{t_o}\|_c < \delta \Rightarrow |x(t)| < \epsilon, \quad \forall t \geq t_0.$$

- *uniformly asymptotically stable if it is uniformly stable and there exists a $\delta_a > 0$ such that for any $\eta > 0$ there exists a $T(\delta_a, \eta)$ such that*

$$\|x_{t_o}\|_c < \delta_a \Rightarrow |x(t)| < \eta, \quad \forall t \geq t_0 + T(\delta_a, \eta) \quad \textit{and} \quad t_0 \in \mathbb{R}.$$

The system is uniformly asymptotically stable if its trivial solution is uniformly asymptotically stable.

Let $V : \mathbb{R} \times C[-h, 0] \rightarrow \mathbb{R}$ be a continuous functional, and let $x_\tau(t, \phi)$ be the solution of (2.3.1) at time $\tau \geq t$ with the initial condition $x_t = \phi$. The time derivative of V along (2.3.1) is given by

$$\dot{V}(t, \phi) = \lim \sup_{\Delta t \rightarrow 0^+} \frac{1}{\Delta t}[V(t + \Delta t, x_{t+\Delta t}(t, \phi)) - V(t, \phi)] \tag{2.3.2}$$

[1]Without loss of generality, by applying a change of variables, any nontrivial solution can be reduced to trivial solution.

Now, LK theorem is ready to state.

Theorem 2.3.2 (Lyaponuv-Krasovskii theorem [26]). *Suppose* $f:\mathbb{R}\times C[-h,0]\to\mathbb{R}^n$ *maps* $\mathbb{R}\times$*(bounded sets in C[-h,0]) into bounded sets of* $\mathbb{R}^n$ *and that* $u,v,w:\mathbb{R}_{\geq 0}\to\mathbb{R}_{\geq 0}$ *are continuous nondecreasing functions* $u(s)$ *and* $v(s)$ *are positive for* $s>0$, *and u(0)=v(0)=0. The trivial solution of* (2.3.1) *is uniformly stable if there exists a continuous functional* $V:\mathbb{R}\times C[-h,0]\to\mathbb{R}_{>0}$,

$$u(|\phi(0)|)\leq V(t,\phi)\leq v(\|\phi\|_c), \tag{2.3.3}$$

and such that its derivation along (2.3.1) *is non-positive in the sense that*

$$\dot{V}(t,\phi)\leq -w(|\phi(0)|) \tag{2.3.4}$$

If $w(s)>0$ *for* $s>0$, *then the trivial solution is uniformly asymptotically stable.*

Theorem 2.3.2 can be extended to involve the state derivation in the LKF, i.e, $V:\mathbb{R}\times W[-h,0]\times L_2(-h,0)\to\mathbb{R}_{\geq 0}$. Then the inequalities in Theorem 2.3.2 become

$$\begin{aligned} u(|x(t)|)&\leq V(t,x_t,\dot{x}_t)\leq v(\|x_t\|_W),\\ \dot{V}(t,x_t,\dot{x}_t)&\leq -w(|x(t)|). \end{aligned} \tag{2.3.5}$$

In the rest of this section, an overview of the methods and techniques used in this thesis to derive control design procedures or stability conditions in the thesis is provided. Consider the following general linear time-invariant system

$$\dot{x}(t)=Ax(t)+A_1x(t-\tau(t)), \tag{2.3.6}$$

where $x:\mathbb{R}_{\geq}0\to\mathbb{R}^n$ is the state vector, $A\in\mathbb{R}^{n\times n}$, $A_1\in\mathbb{R}^{n\times n}$ are constant matrices and $\tau:\mathbb{R}_{\geq 0}\to[0,h]$, $h\in\mathbb{R}_{\geq 0}$, denotes the time delay. The reason for using the linear system (2.3.6) is to focus on the part with time delay and using a quadratic term to the non-delayed part, see (2.3.7). The subsequent content will be focusing on the two main aspects of the time-delay system analysis which are choosing the appropriate LKF and the used bounding techniques.

2.3.1.2 Choosing an appropriate Lyapunov-Krasovskii functional

Different LKF forms will be briefly discussed. In the beginning, a well-known LKF that will be used in the subsequent analysis is given by [90, 92–94]:

$$\begin{aligned} V(t) =& x^\top(t)Px(t) + \int_{t-\tau(t)}^{t} x^\top(s)Qx(s)ds + \int_{t-h}^{t} x^\top(s)Sx(s)ds \\ &+ h\int_{-h}^{0}\int_{t+\theta}^{t} \dot{x}^\top(s)R\dot{x}(s)dsd\theta \end{aligned} \tag{2.3.7}$$

where $P \in \mathbb{R}^{n\times n}$, $S \in \mathbb{R}^{n\times n}$, $R \in \mathbb{R}^{n\times n}$, $Q \in \mathbb{R}^{n\times n}$ are positive definite matrices.

Remark 2.3.3. *Setting $S = R = 0$ in (2.3.7) leads to delay-independent stability conditions. However, this analysis is very conservative, especially with small delays, and will not be considered in this thesis [26].*

Remark 2.3.4. *The functional (2.3.7) with $Q = 0$ results in delay-dependent conditions for systems with fast-varying delays, i.e., there are no restrictions on the properties of the time derivative of $\tau(t)$ [25, 26].*

2.3.1.2.1 Interval time-varying delay

The previous analyses are accounted only for the delay with $\tau \in [0,h]$. However, in some scenarios, the communication delays are modeled as interval delays where a lower bound for the delay is $h_0 \neq 0$, i.e, $\tau \in [h_0,h_1]$, and $0 \leq h_0 \leq h_1$. In order to account for the interval delays, the LKF will be modified as follows [26]:

$$\begin{aligned} &V(t) = V_1 + V_2 + V_3, \\ &V_1 = x^\top(t)Px, \\ &V_2 = \int_{t-h_0}^{t} x^\top(s)S_0x(s)ds + \int_{t-h_1}^{t-h_0} x^\top(s)S_1x(s)ds, \\ &V_3 = h_0\int_{-h_0}^{0}\int_{t+\theta}^{t} \dot{x}^\top(s)R_0\dot{x}(s)dsd\theta + (h_1-h_0)\int_{-h_1}^{-h_0}\int_{t+\theta}^{t} \dot{x}^\top(s)R_1\dot{x}(s)dsd\theta \end{aligned} \tag{2.3.8}$$

where $P \in \mathbb{R}^{n\times n}$, $S_1 \in \mathbb{R}^{n\times n}$, $S_2 \in \mathbb{R}^{n\times n}$, $R_1 \in \mathbb{R}^{n\times n}$, $R_2 \in \mathbb{R}^{n\times n}$, are positive definite matrices. As will be shown in Chapter3 2 and 3, considering the interval delay leads to less conservative results.

2.3.1.3 Bounded techniques

The result of the derivative of the LKF (2.3.7) by using the Leibniz integral rule [1] is

$$\begin{aligned}\dot{V} &= 2x^\top(t)Px(t) + x^\top(t)Sx(t) - x^\top(t-h)Sx(t-h) + h^2\dot{x}(t)R\dot{x}(t) \\ &- h\int_{t-h}^{t} \dot{x}^\top(s)R\dot{x}(s)ds\end{aligned} \tag{2.3.10}$$

In order to convert the integral parts

$$-h\int_{t-h}^{t} \dot{x}^\top(s)R\dot{x}(s)ds = -h\int_{t-\tau(t)}^{t} \dot{x}^\top(s)R\dot{x}(s)ds - h\int_{t-h}^{t-\tau(t)} \dot{x}^\top(s)R\dot{x}(s)ds \tag{2.3.11}$$

into suitable LMI, various bounding techniques are utilized to reduce the conservatism of the resulting conditions. The following techniques are used in this work.

2.3.1.3.1 Jensen's Inequality

Proposition 2.3.5 (Jensen's Inequality [26]). *For any matrix $R = R^\top \in \mathbb{R}^{n\times n}$, $h \in \mathbb{R}$, and a vector function $x : [-h, 0] \to \mathbb{R}^n$ such that the integrations concerned are well-defined, the following holds:*

$$\int_{-h}^{0} x^\top(u)Rx(u)du \geq \frac{1}{h}\int_{-h}^{0} x(u)^\top du R \int_{-h}^{0} x(u)du. \tag{2.3.12}$$

Applying the inequality in (2.3.12) to the terms in (2.3.11) yields

$$-h\int_{t-\tau(t)}^{t} \dot{x}^\top(s)R\dot{x}(s)ds \leq \frac{-h}{\tau(t)}\left[x(t) - x(t-\tau(t))\right]^\top R\left[x(t) - x(t-\tau(t))\right],$$

[1]**Leibniz's rule**

$$\frac{d}{dx}\left(\int_{a(x)}^{b(x)} f(x,t)dt\right) = f(x,b(x))\frac{d}{dx}b(x) - f(x,a(x))\frac{d}{dx}a(x) + \int_{a(x)}^{b(x)} \frac{\partial}{\partial x}f(x,t)dt \tag{2.3.9}$$

$$-h\int_{t-h}^{t-\tau(t)}\dot{x}^\top(s)R\dot{x}(s)ds \leq \frac{-h}{h-\tau(t)}$$
$$\Big[x(t-\tau(t))-x(t-h)\Big]^\top R\Big[x(t-\tau(t))-x(t-h)\Big]. \tag{2.3.13}$$

Then, the value of the term $-h\int_{t-h}^{t}\dot{x}(s)^\top R\dot{x}(s)ds$ can be written as follows

$$-h\int_{t-h}^{t}\dot{x}^\top(s)R\dot{x}(s)ds = \bar{\eta}^\top\begin{bmatrix}\frac{-h}{\tau}R & 0\\ 0 & \frac{-h}{h-\tau(t)}R\end{bmatrix}\bar{\eta}, \tag{2.3.14}$$

where

$$\bar{\eta} = \mathrm{col}\left(x(t)-x(t-\tau(t)), x(t-\tau(t))-x(t-h)\right).$$

The above leads to non-convex conditions and conservative results. To overcome such results, the following technique will be implemented.

2.3.1.3.2 A reciprocally convex approach

Lemma 2.3.6. *[26] For any positive definite matrices $R_{1\ldots n}\in\mathbb{R}^{n\times n}$, $e_{1\ldots n}\in\mathbb{R}^n$, and $S_{ij}\in\mathbb{R}^{n\times n}$ and positive α_i where $\sum\alpha_i = 1$ such that*

$$\begin{bmatrix}R_i & S_{ij}\\ * & Rj\end{bmatrix}\geq 0, \tag{2.3.15}$$

the following inequality holds

$$\sum_{i=1}^{N}\frac{1}{\alpha_i}e_i^T R_i e_i \geq \begin{bmatrix}e_1\\ e_2\\ \vdots\\ e_N\end{bmatrix}^T\begin{bmatrix}R_1 & S_{12} & \ldots & S_{1N}\\ * & R_2 & \ldots & S_{1N}\\ * & * & \ddots & \vdots\\ * & * & \ldots & R_N\end{bmatrix}\begin{bmatrix}e_1\\ e_2\\ \vdots\\ e_N\end{bmatrix}. \tag{2.3.16}$$

Now, define $e_1 = x(t)-x(t-\tau)$, $e_2 = x(t-\tau)-x(t-h)$, $\alpha_1 = \frac{-\tau}{h}$, and $\alpha_2 = \frac{-h+\tau}{h}$. The expression in (2.3.14) can be rewritten using (2.3.16) as follow

$$-h\int_{t-h}^{t}\dot{x}^\top(s)R\dot{x}(s)ds \leq -\bar{\eta}^\top\begin{bmatrix}R & S_{12}\\ * & R\end{bmatrix}\bar{\eta}, \tag{2.3.17}$$

2.3.1.4 The descriptor method

The descriptor method is an efficient tool to perform a stability analysis of the time-delay system [88]. Consider the following model transformation

$$\dot{x}(t) = z(t), \qquad 0 = -z(t) + Ax(t) + A_1 x(t-\tau). \tag{2.3.18}$$

Thus, the system in (2.3.6) can be rewritten as

$$E\dot{\bar{x}}(t) = \bar{A}\bar{x}(t) + \bar{A}_1 \bar{x}(t-\tau), \tag{2.3.19}$$

where

$$\bar{x} = \begin{bmatrix} x(t) \\ z(t) \end{bmatrix}, \quad E = \begin{bmatrix} I & 0 \\ 0 & 0 \end{bmatrix}, \quad \bar{A} = \begin{bmatrix} 0 & I \\ A & -I \end{bmatrix}, \bar{A}_1 = \begin{bmatrix} 0 & 0 \\ 0 & A_1 \end{bmatrix}, \\ \text{and} \quad \bar{x}(t-\tau) = \begin{bmatrix} 0 \\ x(t-\tau) \end{bmatrix}. \tag{2.3.20}$$

Then, the used LKF in (2.3.7) is modified as follows

$$\begin{aligned} V(t) &= \bar{x}^\top(t) EP\bar{x}(t) + \int_{t-\tau(t)}^{t} x^\top(s) Q x(s) ds + \int_{t-h}^{t} x^\top(s) S x(s) ds \\ &+ h\int_{-h}^{0}\int_{t+\theta}^{t} \dot{x}^\top(s) R \dot{x}(s) ds d\theta. \end{aligned} \tag{2.3.21}$$

The P matrix in (2.3.21) is defined as $P = \begin{bmatrix} P & \mathbb{0} \\ P_2 & P_3 \end{bmatrix}$, where $P_2 \in \mathbb{R}^{n\times n}$ and $P_3 \in \mathbb{R}^{n\times n}$ are slack variables. Then, the time derivative of the first part of (2.3.21) yields

$$\frac{d}{dt}\bar{x}^\top(t) EP\bar{x}(t) = 2x^\top P x + 2[x^\top P_2^\top + \dot{x}^\top P_3^\top][Ax + A_1 x(t-\tau) - \dot{x}]. \tag{2.3.22}$$

By choosing $P_3 = \epsilon P_2$ where $\epsilon \in \mathbb{R}_{>}0$ is a tuning parameter and considering $\dot{x}$ as a state, we can obtain an efficient control design tool, see Chapter 3.

2.3.2 Algebraic graph theory

A communication network is essential for the implementation of the distributed frequency controller. The standard modeling approach for communication-based networks in the control community is through algebraic graph theory [31, 53]. Therefore, some notation and fundamentals information about algebraic graph theory are recalled in this subsection.

An undirected weighted graph of order n is a triple $\mathcal{G} = (\mathcal{V}, \mathcal{E}, z)$, with set of nodes $\mathcal{V} = \{1, \ldots, n\}$, set of undirected edges $\mathcal{E} \subseteq [\mathcal{V}]^2$, $\mathcal{E} = \{e_1, \ldots, e_m\}$, $m = |\mathcal{E}|$ and weight function $z : \mathcal{E} \to \mathbb{R}_{\geq 0}$. In the present thesis, two approaches are employed to define the Laplacian matrix as follows.

i) By associating an arbitrary ordering to the edges, the node-edge incidence matrix $\mathcal{B} \in \mathbb{R}^{|\mathcal{V}| \times |\mathcal{E}|}$ of an undirected graph is defined element-wise as $b_{il} = 1$, if node i is the source of the l-th edge e_l, $b_{il} = -1$, if i is the sink of e_l and $b_{il} = 0$ otherwise. The Laplacian matrix of an undirected weighted graph is given by [95, 96]

$$\mathcal{L} = \mathcal{B}\mathcal{Z}\mathcal{B}^\top, \quad \mathcal{Z} = \operatorname{diag}(z_l), \tag{2.3.23}$$

where $z_l \geq 0$ is the weight of the l-th edge, $l = 1, \ldots, m$.

The definition in (2.3.23) will be employed for the design of a distributed secondary frequency controller in MGs where the weights of the edge are treated as variables, for more information see Chapter 3.

ii) The entries of the adjacency matrix $\mathcal{A} \in \mathbb{R}^{|\mathcal{N}| \times |\mathcal{N}|}$ are defined as $a_{ik} = 1$ if there is an edge between nodes i and k and $a_{ik} = 0$ otherwise. The degree of a node is given by $d_i = \sum_{k=1}^{|\mathcal{N}|} a_{ik}$. With $\mathcal{D} = \operatorname{diag}(d_i) \in \mathbb{R}^{|\mathcal{N}| \times |\mathcal{N}|}$, the Laplacian matrix of an undirected graph is defined as

$$\mathcal{L} = \mathcal{D} - \mathcal{A}. \tag{2.3.24}$$

The formula of the Laplacina matrix in (2.3.24) will be utilized for the stability analysis of distributed secondary frequency controller in power systems, for more information see Chapter 4.

An ordered sequence of nodes such that any pair of consecutive nodes in the sequence is connected by an edge is called a path. An undirected graph $\mathcal{G}$ is called connected if for all pairs $\{i,k\} \in [\mathcal{V}]^2$ there exists a path from i to k. The Laplacian matrix $\mathcal{L}$ of an undirected graph is positive semidefinite with a simple zero eigenvalue if and only if the graph is connected. The corresponding right eigenvector to this simple zero eigenvalue is $\mathbb{1}_n$, i.e., $\mathcal{L}\mathbb{1}_n = \mathbb{0}_n$ [96]. We refer the reader to [95, 96] for further information on graph theory.

2.3.3 Consensus protocol

Consensus algorithms are promising control schemes for secondary control tasks in next-generation power systems, as discussed in Chapter 1. Thus, this subsection is devoted to introducing the consensus protocol. To achieve consensus in network systems means that all agents reach an agreement upon a certain quantity of interest that depends on the state of all agents [31]. Moreover, the consensus protocol (or algorithm) is characterized as a process that specifies the information exchange between the agent and all of its neighbors on the network [31]. A crucial feature of consensus protocols is that they are distributed protocols where a central communication is not required.

Consider an undirected weighted network topology represented by $\mathcal{G} = (\mathcal{V}, \mathcal{E}, z)$. Moreover, suppose that the graph is connected. Then the typical continuous consensus algorithm of the $i-$th agent with $x_i : \mathbb{R}_{\geq 0} \to \mathbb{R}$ being the state of the agent is described by [31]

$$\dot{x} = \sum_{j=1}^{n} a_{ij}(x_j - x_i), \tag{2.3.25}$$

where a_{ij} is the (j,i)-th entry of the adjacency matrix $\mathcal{A}$. Furthermore, the dynamics in (2.3.25) can be compactly written in matrix form as

$$\dot{x} = -\mathcal{L}x, \tag{2.3.26}$$

where $x = \mathrm{col}(x_i) \in \mathbb{R}^n$ and $\mathcal{L}$ is the Laplacian matrix of the graph. Moreover, let $x(t, x_0)$ denote the solution of (2.3.26) with initial condition $x_0 \in \mathbb{R}^n$. Then, the algorithm (2.3.26) asymptotically solves an average-consensus problem [31], i.e.,

$$\lim_{t\to\infty} x(t,x_0) = \alpha \mathbb{1}_n, \quad \alpha = \frac{1}{|n|}\sum_{i\sim n} x_i(0). \tag{2.3.27}$$

In the present work, an extension of the protocol (2.3.26) is the weighted average consensus protocol given by [31]

$$\dot{x} = -K\mathcal{L}x, \tag{2.3.28}$$

where $K \in \mathbb{R}^{n\times n}$ is a positive definite diagonal matrix.

Consensus protocols are distributed protocols, and peer-to-peer communication between participating units is essential for their implementation [31]. In any real-world setting, the information is not propagating through the network under ideal conditions. Therefore in any practical situation, the information exchange between agent i and its neighbour agent j will be affected by communication delay τ. Consequently, the consensus algorithm is modified to incorporate the communication delay as follows [31]

$$\dot{x} = -K\mathcal{L}x(t-\tau). \tag{2.3.29}$$

The loss of information, e.g., due to package losses or link failures, is modeled via a dynamic communication network with switched communication topology $\mathcal{G}_\sigma(t)$ [29–31, 97]. Here, $\sigma : \mathbb{R}_{\geq 0} \to \mathcal{M}$ is a switching signal, $\mathcal{M} = \{1, 2, \ldots, \nu\}$, $\nu \in \mathbb{R}_{>0}$, is an index set and $\{\mathcal{G}_1, \mathcal{G}_2, \ldots, \mathcal{G}_\nu\}$ denotes the set of finite network topologies. We denote by $\mathcal{L}_\ell = \mathcal{L}(\mathcal{G}_\ell)$ the Laplacian matrix corresponding to the index $\ell = \sigma(t) \in \mathcal{M}$ and by $\mathcal{E}_\ell$ the corresponding set of edges. As done in [14, 29, 31, 97], we assume that the communication topology $\mathcal{G}_{\sigma(t)}$ is undirected and connected for all $t \in \mathbb{R}_{\geq 0}$. The consensus algorithm with switched communication topology is given by

$$\dot{x} = -K\mathcal{L}_{\ell}x(t). \tag{2.3.30}$$

2.3.4 L_2-Gain of dissipative systems

The content of this subsection briefly recalls some standard results on dissipative systems based on [86, 98]. Consider the state space system

$$\Sigma : \begin{cases} \dot{x} &= f(x,u), \\ y &= h(x,u) \end{cases}, \tag{2.3.31}$$

with $x \in \mathbb{R}^n$, $u \in \mathbb{R}^m$ and $y \in \mathbb{R}^p$.

A signal $u : \mathbb{R}_{\geq 0} \to \mathbb{R}^m$ is in L_2 if its L_2-norm $\|u\|_{L_2}$, given by

$$\|u\|_{L_2} = \sqrt{\int_0^{\infty} u^{\top}(t)u(t)dt},$$

is finite. The extended L_2-space L_{2e} is defined by

$$L_{2e} = \{u \,|\, u_{\tau_e} \in L_2 \, \forall \tau_e \in [0,\infty)\},$$

where u_{τ_e}, $\tau_e \in [0,\infty)$, is the truncation of u defined by

$$u_{\tau_e} = \begin{cases} u(t), & 0 \leq t \leq \tau_e \\ 0, & t > \tau_e \end{cases}.$$

The following notions are employed in this thesis.

Definition 2.3.7. *The state space system Σ is said to have finite L_2-gain if there exist finite nonnegative constants γ and b, such that for all $\tau_e \geq 0$ and for all $u \in L_{2e}$,*

$$\|y_{\tau_e}\|_{L_2} \leq \gamma \|u_{\tau_e}\|_{L_2} + b.$$

Definition 2.3.8. *The state space system Σ is dissipative with respect to the* *supply rate* $s : \mathbb{R}^m \times \mathbb{R}^q \to \mathbb{R}$ *if there exists a function* $\mathcal{S} : \mathbb{R}^n \to \mathbb{R}_{\geq 0}$*, called the storage function, such that for all* $t_1 \geq t_0$ *and all input functions* u*,*

$$\mathcal{S}(x(t_1)) \leq \mathcal{S}(x(t_0)) + \int_{t_0}^{t_1} s(u(t), y(t))dt.$$

Definition 2.3.9. *The state space system* Σ *has a* L_2*-gain less than or equal to* γ *if it is dissipative with respect to the supply rate* $s(u,y) = \frac{1}{2}(\gamma^2\|u\|_2^2 - \|y\|_2^2)$*. The* L_2*-gain of* Σ *is defined as* $\gamma(\Sigma) = \inf\{\gamma \,|\, \Sigma \text{ has } L_2\text{-gain} \leq \gamma\}$*.*

Based on [86, Definition 6.2], differently from the above definition, the following notion of a *small-signal* L_2-gain with $u \in L_{2_e}$ is employed.

Definition 2.3.10. *The state space system* Σ *has a small-signal* L_2*-gain less than or equal to* γ *if it is dissipative with respect to the supply rate* $s(u,y) = \frac{1}{2}(\gamma^2\|u\|_2^2 - \|y\|_2^2)$ *for all* $u \in L_2^m$ *with* $\sup_{0 \leq t \leq \tau_e} \|u_{\tau_e}\|_2 \leq r$ *for some positive real constant* r*.*

Chapter 3

Delay-robust distributed secondary frequency control design for microgrids

3.1 Introduction

As discussed in Chapter 1, one of the main objectives of the present thesis is a synthesis of distributed secondary frequency controllers in MGs. A suitable model of MG, to be used in this Chapter, has been developed in Chapter 2. Build upon this model, a control design is proposed such that delay robustness, disturbance attenuation, and communication topology design are addressed. The work of this Chapter is motivated by the fact that the development of holistic design criteria, which takes into account the physical and cyber layers of the system, is highly desirable to further facilitate a robust and efficient implementation of consensus-based secondary controllers in MGs.

3.2 Distributed secondary frequency control in microgrid

3.2.1 Objectives and distributed control scheme

Suppose that the solutions of the system (2.2.15) evolve along a motion with constant frequency $\omega^s = \mathbb{1}_n \omega^*$, $\omega^* \in \mathbb{R}$. Then,

$$\mathbb{1}_n^\top M \dot{\omega}^s = 0 \quad \Rightarrow \quad \omega^* = \omega^d + \frac{\mathbb{1}_n^\top P^{\text{net}} + \mathbb{1}_n^\top u^*}{\mathbb{1}_n^\top D \mathbb{1}_n}, \tag{3.2.1}$$

where the fact that $\mathbb{1}_n^\top \nabla U(\theta) = 0$ has been used. A standard requirement in power system operation is that in steady-state $\omega^* = \omega^d$, i.e., the network synchronizes to the nominal frequency [1, 76]. However, in practice, the load demands $G_{ii}V_i^2$ contained in P^{net} in (2.2.15) are unknown and thus, typically, $\mathbb{1}_n^\top P^{\text{net}} \neq 0$. Therefore, the control inputs u^* have the task to compensate this power imbalance such that indeed $\omega^* = \omega^d$, see (3.2.1). This task is termed secondary frequency control [1, 76].

The work in the present chapter aims at achieving this classical secondary control objective by simultaneously allocating the stationary secondary control injections in an optimal fashion, i.e. by solving an economic dispatch problem online. Therefore, the following optimization problem [45] is introduced:

$$\begin{aligned} &\min_{u^*} \frac{1}{2}(u^*)^\top A u^*, \\ &\text{subject to } \mathbb{1}_n^\top P^{\text{net}} + \mathbb{1}_n^\top u^* = 0, \end{aligned} \tag{3.2.2}$$

where $A = \text{diag}(A_{ii}) \in \mathbb{R}^{n \times n}$ is a diagonal positive definite weighting matrix. Hence, the cost function is quadratic and strictly convex. It can be seen from (3.2.1) that satisfying the constraint in (3.2.2) guarantees steady-state frequency restoration.

Let $K \in \mathbb{R}^{n\times n}_{>0}$ be a diagonal feedback gain matrix and $\mathcal{L} \in \mathbb{R}^{n\times n}$ be the Laplacian matrix of an undirected and connected graph with incidence matrix

$\mathcal{B}$ and diagonal matrix of nonnegative edge weights $\mathcal{Z}$, see (2.3.23). Consider the distributed secondary frequency control [14, 52, 99]

$$\begin{aligned} u &= -p, \\ \dot{p} &= K(\omega - \mathbb{1}_n \omega^d) - KA\mathcal{L}Ap. \end{aligned} \tag{3.2.3}$$

It has been shown in [46, 47], that the control (3.2.3) restores the frequency to its nominal value, while ensuring economic optimality in a synchronized state if A is formulated by economic considerations., i.e.,

$$A_{ii}u_i^s = A_{kk}u_k^s \quad \forall i \in \mathcal{N}, \quad \forall k \in \mathcal{N}.$$

As discussed in Chapter 2, there will always be a certain minimum communication delay between different agents, i.e., in the present case generation units [100]. As a consequence, the information sent from node i to node k over the edge $\{i,k\}$ is affected by communication delay that is modeled by an interval (or non-small) delay [26]

$$\tau_{ik} : \mathbb{R}_{\geq 0} \to [h_{0_{ik}}, h_{1_{ik}}],$$

with upper and lower bounds $0 \leq h_{0_{ik}} \leq h_{1_{ik}}$. In addition, the subsequent analysis also accounts for asymmetric delays, i.e., $\tau_{ik} \neq \tau_{ki}$. The corresponding control error e_{ik} is then computed as [29, 31]

$$e_{ik}(t) = A_{ii}p_i(t - \tau_{ik}(t)) - A_{kk}p_k(t - \tau_{ik}(t)). \tag{3.2.4}$$

To obtain a compact representation of the closed-loop system, the matrices $\bar{\mathcal{B}}_r \in \mathbb{R}^{|\mathcal{V}|\times|\mathcal{E}|}$, $r = 1,\dots,2m$ are introduced, where $m = |\mathcal{E}|$ is the number of edges of the undirected graph. Since it is allowed for $\tau_{ik}(t) \neq \tau_{ki}(t)$, $2m$ matrices $\bar{\mathcal{B}}_r$ are required to represent all delayed information flows in the network. The matrices $\bar{\mathcal{B}}_r$ are defined as follows. If node i is the source of the r-th edge $\{i,k\}$ and the information flow is affected by the delay $\tau_r(t) = \tau_{ik}(t)$,

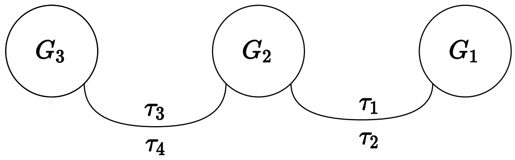

Figure 3.1: Example of undirected connected graph

then $\bar{b}_{ir} = 1$ and all other entries of $\bar{\mathcal{B}}_r$ are zero. If node i is the sink of the r-th edge $\{i,k\}$ and the information flow is affected by the delay $\tau_r(t) = \tau_{ik}(t)$, then $\bar{b}_{ir} = -1$ and all other entries of $\bar{\mathcal{B}}_r$ are zero. Hence, the Laplacian matrix can be obtained by

$$\sum_{r=1}^{2m} \bar{\mathcal{B}}_r \mathcal{Z} \mathcal{B}^\top = \mathcal{L},$$

and by introducing

$$\mathcal{T}_r = \bar{\mathcal{B}}_r \mathcal{Z} \mathcal{B}^\top, \tag{3.2.5}$$

the control law in (3.2.3) can be written compactly as

$$\dot{p} = K(\omega - \mathbb{1}_n \omega^d) - KA\left(\sum_{r=1}^{2m} \mathcal{T}_r A p(t - \tau_r)\right). \tag{3.2.6}$$

Hence, given (3.2.3), the distributed secondary control design problem requires determining the matrices K and $\mathcal{Z}$. This problem is addressed in the present Chapter.

As the term $\mathcal{T}_r$ is playing an important rule in the controller low (3.2.6), the following example serves to help to understand how to construct this term.

Example 3.2.1. *Consider an undirected and connected graph with 3 nodes, 2 undirected edges and a weighting matrix $\mathcal{Z} = diag(1,1,1)$, as shown in figure 3.1. Moreover, consider 4 different delays τ_r, $r = 1,\ldots,4$. Then, the matrices $\bar{\mathcal{B}}_r$ and $\mathcal{B}$ can be represented as*

$$\mathcal{B} = \begin{bmatrix} 1 & -1 & 0 \\ 0 & 1 & -1 \end{bmatrix}^\top, \quad \bar{\mathcal{B}}_1 = \begin{bmatrix} 1 & 0 & 0 \\ 0 & 0 & 0 \end{bmatrix}^\top, \quad \bar{\mathcal{B}}_2 = \begin{bmatrix} 0 & -1 & 0 \\ 0 & 0 & 0 \end{bmatrix}^\top,$$

$$\bar{\mathcal{B}}_3 = \begin{bmatrix} 0 & 0 & 0 \\ 0 & 1 & 0 \end{bmatrix}^\top, \quad \bar{\mathcal{B}}_4 = \begin{bmatrix} 0 & 0 & 0 \\ 0 & 0 & -1 \end{bmatrix}^\top,$$

Using (3.2.5) *leads to*

$$\mathcal{T}_1 = \begin{bmatrix} 1 & -1 & 0 \\ 0 & 0 & 0 \\ 0 & 0 & 0 \end{bmatrix} \quad \mathcal{T}_2 = \begin{bmatrix} 0 & 0 & 0 \\ -1 & 1 & 0 \\ 0 & 0 & 0 \end{bmatrix} \quad \mathcal{T}_3 = \begin{bmatrix} 0 & 0 & 0 \\ 0 & 1 & -1 \\ 0 & 0 & 0 \end{bmatrix} \quad \mathcal{T}_4 = \begin{bmatrix} 0 & 0 & 0 \\ 0 & 0 & 0 \\ 0 & -1 & 1 \end{bmatrix}$$

By using $\sum_{r=1}^{2m} \mathcal{B}_r = \mathcal{B}$, *tha Laplacian matrix can be obtained as follows*

$$\sum_{r=1}^{2m} \bar{\mathcal{B}}_r \mathcal{Z} \mathcal{B}^\top = \sum_{r=1}^{2m} \bar{\mathcal{T}}_r = \mathcal{L} = \begin{bmatrix} 1 & -1 & 0 \\ -1 & 2 & -1 \\ 0 & -1 & 1 \end{bmatrix}$$

3.2.2 Closed-loop system

Combining (2.2.15) with (3.2.3) yields

$$\begin{aligned} \dot{\theta} &= \omega, \\ M\dot{\omega} &= -D(\omega - \mathbb{1}_n \omega^d) - \nabla U(\theta) + P^{\text{net}} - p, \\ \dot{p} &= K(\omega - \mathbb{1}_n \omega^d) - KA\left(\sum_{r=1}^{2m} \mathcal{T}_r A p(t-\tau_r)\right). \end{aligned} \tag{3.2.7}$$

For the subsequent controller synthesis, the following notion is useful, see also [14, 80].

Definition 3.2.2. *The system* (3.2.7) *admits a synchronized motion if it has a solution for all* $t \geq 0$ *of the form*

$$\theta^s(t) = \theta_0^s + \omega^s t, \quad \omega^s = \omega^* \mathbb{1}_n, \quad p^s \in \mathbb{R}^n,$$

where $\omega^* \in \mathbb{R}$ *and* $\theta_0^s \in \mathbb{R}^n$ *are such that*

$$|\theta_{0,i}^s - \theta_{0,k}^s| < \frac{\pi}{2} \quad \forall i \in \mathcal{N}, \forall k \in \mathcal{N}_i.$$

It has been shown in [46, 47, 99] that the system (3.2.7) possesses at most one synchronized motion $\mathrm{col}(\theta^s, \omega^s, p^s)$ which is not affected by the existence of time-delay. This motion also fulfills the identical marginal cost requirement (3.2.4) and is described by

$$u^s = -p^s, \quad p^s = \lambda A^{-1}\mathbb{1}_n, \quad \lambda = \frac{\mathbb{1}_n^\top p^{\mathrm{net}}}{\mathbb{1}_n^\top A^{-1}\mathbb{1}_n}. \tag{3.2.8}$$

The objective of this Chapter is to develop a design procedure for the consensus-based secondary frequency controller (3.2.6) that ensures robustness with respect to heterogeneous fast-varying communication delays. Meanwhile, the proposed synthesis provides the option to achieve a trade-off between the L_2-gain performance and the number of required communication links.

3.3 Controller synthesis

3.3.1 Coordinate transformation and error system

Following the approach in [14], a coordinate transformation and reduction are performed that are instrumental to the proposed synthesis. Let $K = \kappa\mathcal{K}$, where $\mathcal{K} \in \mathbb{R}^{n\times n}$ is a diagonal matrix with positive diagonal entries and $\kappa > 0$ is a parameter. Note that the fact that $\sum_{r=1}^{2m} \mathcal{T}_r \mathbb{1}_n = \mathcal{L}\mathbb{1}_n = \mathbb{0}_n$ leads to an invariant subspace in the p-variables, which highly complicates the design of a strict LKF for the dynamics (3.2.7). Thus, to develop the controller synthesis in the presence of heterogeneous fast-varying delays the following coordinate transformation with $\bar{p} \in \mathbb{R}^{n-1}$ and $\zeta \in \mathbb{R}$ is employed to eliminate this invariant subspace

$$\begin{bmatrix} \bar{p} \\ \zeta \end{bmatrix} = \mathcal{W}^\top (\kappa\mathcal{K})^{-\frac{1}{2}} p, \; \mathcal{W} = \begin{bmatrix} W & \frac{1}{\sqrt{\mu}}\mathcal{K}^{-\frac{1}{2}} A^{-1}\mathbb{1}_n \end{bmatrix}, \tag{3.3.1}$$

where $W \in \mathbb{R}^{n\times(n-1)}$ is chosen such that $W^\top \mathcal{K}^{-\frac{1}{2}} A^{-1}\mathbb{1}_n = \mathbb{0}_{n-1}$ and $\mu = \|\mathcal{K}^{-\frac{1}{2}} A^{-1}\mathbb{1}_n\|_2^2$. Hence, the column vectors of W form an orthonormal basis that is orthogonal to $\mathcal{K}^{-\frac{1}{2}} A^{-1}\mathbb{1}_n$. Thus, the transformation matrix $\mathcal{W} \in \mathbb{R}^{n\times n}$

is orthogonal, i.e.,

$$\mathcal{W}\mathcal{W}^\top = WW^\top + \frac{1}{\mu}\mathcal{K}^{-\frac{1}{2}}A^{-1}\mathbb{1}_n\mathbb{1}_n^\top\mathcal{K}^{-\frac{1}{2}}A^{-1} = I_n. \tag{3.3.2}$$

From (3.3.1) ζ is given by

$$\zeta = \frac{\kappa^{-\frac{1}{2}}}{\sqrt{\mu}}\mathbb{1}_n^\top A^{-1}\mathcal{K}^{-1}p. \tag{3.3.3}$$

By using (3.2.7) together with the fact $\sum_{r=1}^{2m}\mathcal{T}_r\mathbb{1}_n = \mathbb{0}_n$, the following is obtained

$$\dot{\zeta} = \frac{\kappa^{\frac{1}{2}}}{\sqrt{\mu}}\mathbb{1}_n^\top A^{-1}(\omega - \mathbb{1}_n\omega^d),$$

which by integrating with respect to time and recalling (3.3.3) yields

$$\zeta = \frac{\kappa^{\frac{1}{2}}}{\sqrt{\mu}}\mathbb{1}_n^\top A^{-1}(\theta - \theta_0 - \mathbb{1}_n\omega^d t + \kappa^{-1}\mathcal{K}^{-1}p_0) = \frac{\kappa^{\frac{1}{2}}}{\sqrt{\mu}}\mathbb{1}_n^\top A^{-1}\left(\theta - \mathbb{1}_n\omega^d t\right) + \bar{\zeta}_0, \tag{3.3.4}$$

where

$$\bar{\zeta}_0 = \frac{\kappa^{\frac{1}{2}}}{\sqrt{\mu}}\mathbb{1}_n^\top A^{-1}\left(\kappa^{-1}\mathcal{K}^{-1}p_0 - \theta_0\right). \tag{3.3.5}$$

Thus,

$$\begin{aligned} p &= (\kappa\mathcal{K})^{\frac{1}{2}}W\bar{p} + \frac{1}{\sqrt{\mu}}(\kappa\mathcal{K})^{\frac{1}{2}}\mathcal{K}^{-\frac{1}{2}}A^{-1}\mathbb{1}_n\zeta, \\ &= (\kappa\mathcal{K})^{\frac{1}{2}}W\bar{p} + \frac{\kappa}{\mu}A^{-1}\mathbb{1}_n\mathbb{1}_n^\top A^{-1}(\theta - \mathbb{1}_n\omega^d t) + \frac{\kappa^{\frac{1}{2}}}{\sqrt{\mu}}A^{-1}\mathbb{1}_n\bar{\zeta}_0, \end{aligned}$$

and

$$p(t-\tau_r) = (\kappa\mathcal{K})^{\frac{1}{2}}W\bar{p}(t-\tau_r) + \frac{1}{\sqrt{\mu}}(\kappa\mathcal{K})^{\frac{1}{2}}\mathcal{K}^{-\frac{1}{2}}A^{-1}\mathbb{1}_n\zeta(t-\tau_r),$$

$r = 1, \ldots, 2m$. By using (3.3.1) and following the procedure in [14, Section 3.2], the closed-loop system (3.2.7) in new reduced order coordinates can be represented by

$$
\begin{aligned}
\dot{\theta} =& \omega, \\
M\dot{\omega} =& -D(\omega - \mathbb{1}_n\omega^d) + P^{\text{net}} - \nabla U(\theta) - (\kappa\mathcal{K})^{\frac{1}{2}} W\bar{p} \\
& -\frac{\kappa}{\mu}A^{-1}\mathbb{1}_n\mathbb{1}_n^\top A^{-1}(\theta - \mathbb{1}_n\omega^d t) - \frac{\kappa^{\frac{1}{2}}}{\sqrt{\mu}}A^{-1}\mathbb{1}_n\bar{\zeta}_0, \\
\dot{\bar{p}} =& \kappa^{\frac{1}{2}}W^\top\mathcal{K}^{\frac{1}{2}}(\omega - \mathbb{1}_n\omega^d) - \kappa W^\top\mathcal{K}^{\frac{1}{2}}A\left(\sum_{r=1}^{2m}\mathcal{T}_r A\mathcal{K}^{\frac{1}{2}}W\bar{p}(t-\tau_r)\right),
\end{aligned} \tag{3.3.6}
$$

where the variable ζ in (3.3.1) has been expressed in terms of θ, ω^d, θ_0 and p_0, see (3.3.4). The following assumption is made [14, 80].

Assumption 3.3.1. *The system* (3.3.6) *possesses a synchronized motion.*

With Assumption 3.3.1, the error states are defined as follows

$$
\begin{aligned}
&\tilde{\omega} = \omega - \omega^s, \quad \tilde{\theta} = \left(\theta_0 - \theta_0^s + \int_0^t \tilde{\omega}(\tau)d\tau\right), \\
&\tilde{p} = \bar{p} - \bar{p}^s, \quad x = \text{col}(\tilde{\theta}, \tilde{\omega}, \tilde{p}).
\end{aligned}
$$

Since one of the key contributions of this Chapter is to provide a controller synthesis that is explicitly robust with respect to exogenous perturbations (in terms of the system's L_2-gain), the output performance is stated before representing the closed-loop system in the reduced error coordinate. It is assumed that both the communication and electrical layers are exposed to disturbances $d_\omega : \mathbb{R}_{\geq 0} \to \mathbb{R}^n$, $d_\omega \in L_{2e}^n$, $d_p : \mathbb{R}_{\geq 0} \to \mathbb{R}^{n-1}$, $d_p \in L_{2e}^{n-1}$, respectively. Inspired by [55], the performance output of the closed-loop system is defined as

$$
y = \begin{bmatrix} W_1^{\frac{1}{2}}\tilde{\omega} \\ W_2^{\frac{1}{2}}\tilde{p} \end{bmatrix},
$$

where the weighting matrix

$$
W_1 = M > 0, \tag{3.3.7}
$$

accounts for the system's kinetic energy and the matrix

$$W_2 = W^\top \mathcal{K}^{\frac{1}{2}} \bar{W}_2 \mathcal{K}^{\frac{1}{2}} W, \quad \bar{W}_2 = I_n - \frac{1}{\mathbb{1}_n^\top A^{-1} \mathbb{1}_n} A^{-\frac{1}{2}} \mathbb{1}_n \mathbb{1}_n^\top A^{-\frac{1}{2}}, \tag{3.3.8}$$

quantifies the deviation of the controller states (in error coordinates) from their average (scaled by $\kappa^{-1} A^{\frac{1}{2}}$).

Then, the error system corresponding to (3.3.6) is given by

$$\begin{aligned}
\dot{\tilde{\theta}} =& \tilde{\omega}, \\
M\dot{\tilde{\omega}} =& -D\tilde{\omega} - \nabla U(\tilde{\theta} + \theta^s) + \nabla U(\theta^s) - (\kappa \mathcal{K})^{\frac{1}{2}} W \tilde{p} - \frac{1}{\mu} \kappa A^{-1} \mathbb{1}_n \mathbb{1}_n^\top A^{-1} \tilde{\theta} + d_\omega, \\
\dot{\tilde{p}} =& \kappa^{\frac{1}{2}} W^\top \mathcal{K}^{\frac{1}{2}} \tilde{\omega} - \kappa W^\top \mathcal{K}^{\frac{1}{2}} A \left(\sum_{r=1}^{2m} \mathcal{T}_r A \mathcal{K}^{\frac{1}{2}} W \tilde{p}(t - \tau_r) \right) + d_p, \\
y =& \begin{bmatrix} W_1^{\frac{1}{2}} \tilde{\omega} \\ W_2^{\frac{1}{2}} \tilde{p} \end{bmatrix}, \quad d = \begin{bmatrix} d_\omega \\ d_p \end{bmatrix}.
\end{aligned} \tag{3.3.9}$$

Moreover, with Assumption 3.3.1, the system (3.3.9) has an equilibrium point $x^s = \mathrm{col}(\tilde{\theta}^s, \tilde{\omega}^s, \tilde{p}^s)$ at the origin. Recall that ω^s and p^s are uniquely given by (3.2.8). Hence, for any fixed $\bar{\zeta}_0$ asymptotic stability of x^s implies that any solution $\mathrm{col}(\theta, \omega, p)$ of the original system (3.2.7) with an initial condition that satisfies

$$\bar{\zeta}_0 = \frac{\kappa^{\frac{1}{2}}}{\sqrt{\mu}} \mathbb{1}_n^\top A^{-1} \left(\kappa^{-1} \mathcal{K}^{-1} p_0 - \theta_0 \right),$$

converges to a synchronized motion $\mathrm{col}(\theta^s, \omega^s, p^s)$ with initial angles satisfying

$$\bar{\zeta}_0 = \frac{\kappa^{\frac{1}{2}}}{\sqrt{\mu}} \mathbb{1}_n^\top A^{-1} \left(\kappa^{-1} \mathcal{K}^{-1} p^s - \theta_0^s \right).$$

This applies for any value of $\bar{\zeta}_0$. Moreover, the dynamics in (3.3.9) are independent of $\bar{\zeta}_0$. Consequently, x^s being asymptotically stable implies that all solutions of the original system (3.2.7) converge to a synchronized motion.

3.3.2 Problem statement

The desired robustness properties are accounted for in our approach by using the LK and descriptor methods together with a L_2-gain dissipation inequality for time-delay systems, see Definition 2.3.8 and [Chapters 4 and 5][26]. Compared to [26] these methods applied to the nonlinear system (3.3.9).

The number of communication links could be minimized by means of the 0-norm of the vector $\mathcal{Z}\mathbb{1}_m$, i.e., $\|\mathcal{Z}\mathbb{1}_m\|_0 = \{\text{number of}\, z_i |\, z_i \neq 0\}$ (recall from (2.3.23) that $\mathcal{Z} \geq 0$ is a diagonal matrix). Yet, the difficulty in using this approach is that the problem is non-convex. Hence, to overcome the non-convexity, the ℓ_1-norm $\|\mathcal{Z}\mathbb{1}_m\|_1 = \sum_{i=1}^{m} |z_i|$ is often used as a convex relaxation of the 0-norm [101–104]. This is motivated by the fact the ℓ_1-norm is the convex envelope of the 0-norm and therefore its best convex relaxation [103, 104]. To further improve this relaxation, the reweighted ℓ_1-norm $\|W_{\mathcal{Z}}\mathcal{Z}\mathbb{1}_m\|_1$ can be used [104], where the entries of the diagonal matrix $W_{\mathcal{Z}}$ are chosen as

$$w_{\mathcal{Z},i} = (z_i + \upsilon)^{-1}, \quad i = 1, \ldots, m, \tag{3.3.10}$$

with υ being a small positive number. This, however, implies that an iterative scheme is needed, since the assigned values of the weighting matrix $W_{\mathcal{Z}}$ depend on the solution of the optimization problem.

The above discussion leads to the following problem formulation.

Problem 3.3.2. *Consider the system* (3.3.9) *with Assumption 3.3.1. Determine κ and $\mathcal{Z}$, such that given $h_{0_r} \in \mathbb{R}_{>0}$, $h_{1_r} \in \mathbb{R}_{>0}$ with $h_{0_r} \leq \tau_r(t) \leq h_{1_r}$, $r = 1, \ldots, 2m$,*

- *$x^s = \mathbb{0}_{3n-1}$ is a uniformly asymptotically stable equilibrium point of the system* (3.3.9)*,*
- *the system* (3.3.9) *is dissipative with respect to the supply rate $s(d,y) = \frac{1}{2}(\gamma^2\|d\|_2^2 - \|y\|_2^2)$, where d and y are given in* (3.3.9)*,*
- *and the number of communication links is minimized, i.e.,* $\min_{\mathcal{Z}\geq 0}$ *trace*$(\mathcal{Z})$.

3.3.3 Main result

To present the main result, it is convenient to introduce the scaled matrix of edge weights and the corresponding scaled interconnection matrices of the communication network, i.e.,

$$\bar{\mathcal{Z}} = \kappa \mathcal{Z}, \qquad \bar{\mathcal{T}}_r = W^\top \mathcal{K}^{\frac{1}{2}} A \bar{\mathcal{B}}_r \bar{\mathcal{Z}} \mathcal{B}^\top A \mathcal{K}^{\frac{1}{2}} W. \tag{3.3.11}$$

Proposition 3.3.3. *Consider the system* (3.3.9) *with Assumption 3.3.1. Recall the weighting matrices* W_1 *and* W_2 *given in* (3.3.7) *and* (3.3.8)*, respectively. Fix constants* $0 \leq h_{0_r} \leq h_{1_r}$*,* $r = 1, \ldots, 2m$*,* $\mathcal{K} > 0$ *and* $\varepsilon > 0$ *as well as weighting parameters* $\alpha > 0$*,* $\beta > 0$ *and a diagonal weighting matrix* $W_{\mathcal{Z}} > 0$*. Suppose that there exist parameters* $\bar{\gamma} > 0$ *and* $\bar{\kappa} > 0$ *and matrices* $\bar{\mathcal{Z}} \geq 0$*,* $P > 0$*,* $R_{0_r} > 0$*,* $R_{1_r} > 0$*,* $S_{0_r} > 0$*,* $S_{1_r} > 0$ *and* S_{12_r}*, such that the following optimization problem is feasible:*

$$\begin{aligned} &\min_{\bar{\gamma}, \bar{\kappa}, \bar{\mathcal{Z}}} \alpha \bar{\gamma} - \beta \bar{\kappa} + \mathit{trace}\big(W_{\mathcal{Z}} \bar{\mathcal{Z}}\big) \\ &\textit{subject to} \\ &Q_H = \begin{bmatrix} Q_{H_1} & Q_{H_2} \\ * & Q_{H_3} \end{bmatrix} < 0, \end{aligned} \tag{3.3.12}$$

where

$$Q_{H_1} = \begin{bmatrix} -D + \frac{1}{2} W_1 & \mathbb{0} & \frac{1}{2} \varepsilon \bar{\kappa} \mathcal{K}^{\frac{1}{2}} W & \mathbb{0} & \mathbb{0} & \mathbb{0} \\ * & Q_{h_{22}} & P - \frac{1}{2} I_{n-1} & Q_{h_{24}} & Q_{h_{25}} & \mathbb{0} \\ * & * & Q_{h_{33}} & \mathbb{0} & Q_{h_{35}} & \mathbb{0} \\ * & * & * & Q_{h_{44}} & Q_{h_{45}} & S_{12} \\ * & * & * & * & Q_{h_{55}} & Q_{h_{56}} \\ * & * & * & * & * & Q_{h_{66}} \end{bmatrix},$$

$$Q_{H_2} = \begin{bmatrix} \frac{1}{2} I_n & \mathbb{0} & \mathbb{0} & \mathbb{0} & \mathbb{0} & \mathbb{0} \\ \mathbb{0} & \frac{1}{2} I_{n-1} & \frac{\varepsilon}{2} I_{n-1} & \mathbb{0} & \mathbb{0} & \mathbb{0} \end{bmatrix}^\top,$$

$$Q_{H_3} = \begin{bmatrix} -\frac{1}{2}\bar{\gamma}I_n & \mathbb{0} \\ * & -\frac{1}{2}\bar{\gamma}I_{n-1} \end{bmatrix}$$

$S_0 = blockdiag(S_{0_r}), \quad R_0 = blockdiag(R_{0_r}), \quad S_1 = blockdiag(S_{1_r}),$

$R_1 = blockdiag(R_{1_r}), \quad S_{12} = blockdiag(S_{12_r}),$

$$Q_{h_{22}} = \sum_{r=1}^{2m} S_{0_r} - \sum_{r=1}^{2m} R_{0_r} + \frac{1}{2}W_2, \quad Q_{h_{24}} = \left[R_{0_1} \dots R_{0_{2m}}\right],$$

$$Q_{h_{25}} = \left[-\frac{1}{2}\bar{\mathfrak{T}}_1, \dots, -\frac{1}{2}\bar{\mathfrak{T}}_{2m}\right], \quad Q_{h_{33}} = -\varepsilon I_{n-1} + \sum_{r=1}^{2m} h_{0_r}^2 R_{0_r} + \sum_{r=1}^{2m} (h_{1_r} - h_{0_r})^2 R_{1_r},$$

$$Q_{h_{35}} = \left[-\frac{\varepsilon}{2}\bar{\mathfrak{T}}_1, \dots, -\frac{\varepsilon}{2}\bar{\mathfrak{T}}_{2m}\right] \quad Q_{h_{44}} = -S_0 + S_1 - R_0 - R_1,$$

$$Q_{h_{45}} = Q_{h_{56}} = R_1 - S_{12}, \quad Q_{H_{55}} = -2R_1 + S_{12} + S_{12}^\top, \quad Q_{h_{66}} = -R_1 - S_1,$$

with $\bar{\mathfrak{T}}_r$ *being defined in* (3.3.11) *and*

$$\begin{bmatrix} R_1 & S_{12} \\ * & R_1 \end{bmatrix} \geq 0. \tag{3.3.13}$$

Choose the controller parameters as

$$\kappa = \bar{\kappa}^2, \quad \mathfrak{T}_r = \frac{1}{\kappa}\bar{\mathcal{B}}_r \mathcal{Z} \mathcal{B}^\top. \tag{3.3.14}$$

Then, for all $\tau_r(t) \in [h_{0_r}, h_{1_r}]$, *the origin is a locally uniformly asymptotically stable equilibrium point of the system* (3.3.9) *and the system has a small-signal* L_2*-gain less than or equal to* $\gamma = \sqrt{\bar{\gamma}}$ *with respect to the supply rate* $s(d,y) = \frac{1}{2}\left(\gamma^2\|d\|_2^2 - \|y\|_2^2\right)$, *where* d *and* y *are given in* (3.3.9).

Proof. The proof is established by combining ideas of the related stability analysis conducted in [14] with the control design approach using the descriptor method, which has been applied previously to linear time-delay systems, see, e.g., [26]. By noting that the delay appears only in $\tilde{p}$, consider the LKF

$$V(x, \dot{x}, t) = V_1 + \sum_{r=1}^{2m} V_{2_r},$$

$$
\begin{aligned}
V_1 &= \frac{1}{2}\tilde{\omega}^\top(t)M\tilde{\omega}(t) + U(\tilde{\theta}(t)+\theta^s) - \nabla U(\theta^s)^\top\tilde{\theta}(t) + \tilde{p}^\top(t)P\tilde{p}(t) \\
&+ \frac{\kappa}{2\mu}(\mathbb{1}_n^\top A^{-1}\tilde{\theta}(t))^2 + \epsilon\tilde{\omega}^\top(t)M\mathbb{1}_n\mathbb{1}_n^\top A^{-1}\tilde{\theta}(t) \\
&+ \epsilon\tilde{\omega}^\top(t)AM\left(\nabla U(\tilde{\theta}(t)+\theta^s) - \nabla U(\theta^s)\right), \\
V_{2_r} &= \int_{t-h_{0_r}}^{t}\tilde{p}^\top(s)S_{0_r}\tilde{p}(s)ds + \int_{t-h_{1_r}}^{t-h_{0_r}}\tilde{p}^\top(s)S_{1_r}\tilde{p}(s)ds \\
&+ h_{0_r}\int_{-h_{0_r}}^{0}\int_{t+\phi}^{t}\dot{\tilde{p}}^\top(s)R_{0_r}\dot{\tilde{p}}(s)dsd\phi + (h_{1_r}-h_{0_r})\int_{-h_{1_r}}^{-h_{0_r}}\int_{t+\phi}^{t}\dot{\tilde{p}}^\top(s)R_{1r}\dot{\tilde{p}}(s)dsd\phi,
\end{aligned}
\tag{3.3.15}
$$

where $\epsilon > 0$, $P > 0$, $S_{0_r} > 0$, $S_{1_r} > 0$, $R_{0_r} > 0$, and $R_{1_r} > 0$.

The function V_1 consists of the traditional kinetic and potential energy terms $\tilde{\omega}^\top M\tilde{\omega}$ and $U(\tilde{\theta}(t)+\theta^s)$, respectively, together with a Bregman term to center the Lyapunov function [54] as well as a quadratic term in the reduced controller states $\tilde{p}$. Furthermore, a Chetaev-type cross term between $\tilde{\omega}$ and $\tilde{\theta}$ is added, which - as shown in the sequel - is essential to ensure that $\dot{V}$ is strictly negative definite. The function V_{2_r} are designed to account for the presence of interval fast-varying communication delays [26].

The first step is to show that V in (3.3.15) is strict locally positive definite. The gradient of V_1 is given by

$$
\nabla V_1 = \begin{bmatrix} v_1 \\ M\tilde{\omega} + \epsilon AM(\nabla U(\tilde{\theta}+\theta^s) - \nabla U(\theta^s)) + \epsilon M\mathbb{1}_n\mathbb{1}_n^\top A^{-1}\tilde{\theta} \\ 2P\tilde{p} \end{bmatrix}, \tag{3.3.16}
$$

with

$$
\begin{aligned}
v_1 =& \nabla U(\tilde{\theta}+\theta^s) - \nabla U(\theta^s) + \epsilon\nabla^2 U(\tilde{\theta}+\theta^s)^\top MA\tilde{\omega} + \frac{\kappa}{\mu}(A^{-1}\mathbb{1}_n\mathbb{1}_n^\top A^{-1})\tilde{\theta} \\
&+ \epsilon A^{-1}\mathbb{1}_n\mathbb{1}_n^\top M\tilde{\omega},
\end{aligned}
$$

Clearly, at the equilibrium point $x^s = \mathbb{0}_{3n-1}$, $\nabla V_1 = \mathbb{0}_{3n-1}$. Moreover the

Hessian of V_1 evaluated at x^s is given by

$$\nabla^2 V_1|_{x^s} = \begin{bmatrix} \nabla^2 U(\theta^s) + \frac{\kappa}{\mu} A^{-1}\mathbb{1}_n \mathbb{1}_n^\top A^{-1} & v_{12} & 0 \\ * & M & 0 \\ * & * & \frac{1}{2} I_{n-1} \end{bmatrix}, \tag{3.3.17}$$

where

$$v_{12} = \epsilon A M \nabla^2 U(\theta^s) + \epsilon M \mathbb{1}_n \mathbb{1}_n^\top A^{-1}. \tag{3.3.18}$$

It is known that with Assumption 3.3.1, $\nabla^2 U(\theta^s)$ is a Laplacian matrix with $\ker(\nabla^2 U(\theta^s)) = \mathrm{span}(\mathbb{1}_n)$ [14, 80]. Furthermore, $A^{-1}\mathbb{1}_n\mathbb{1}_n^\top A^{-1}$ is a positive semidefinite matrix and $\ker(A^{-1}\mathbb{1}_n\mathbb{1}_n^\top A^{-1}) \cap \ker(\nabla^2 U(\theta^s)) = \mathbb{0}_n$. In addition, M is a diagonal matrix with positive diagonal entries. Thus, all block-diagonal entries of $\nabla^2 V_1|_{x^s}$ are positive definite. This implies that there is a sufficiently small $\epsilon^* > 0$ such that for all $\epsilon \in]0, \epsilon^*]$, $\nabla^2 V_1|_{x^s} > 0$. Furthermore, S_{0_r}, S_{1r}, R_{0_r}, and R_{1_r} in V_{2_r} are positive definite matrices. Therefore, x^s is a strict minimum of V.

Recall that the objective here is to design controller gains, such that the L_2-gain of the system (3.3.9) is minimized while also ensuring delay robustness. By using [26, Lemma 4.3], this translates to the following constrained optimization problem

$$\begin{aligned} &\min \gamma \\ &\text{subject to} \\ &\dot{V}(x, \dot{x}, t) - \frac{1}{2}\left(\gamma^2 \|d(t)\|_2^2 - \|y(t)\|_2^2\right) \leq -\varrho\left(\|x(t)\|_2^2 + \|d(t)\|_2^2\right), \end{aligned}$$

where $\dot{V}$ denotes the time-derivative of the LKF V in (3.3.15) and ϱ is some positive constant. Differentiating V yields

$$\dot{V} = \dot{V}_1 + \sum_{r=1}^{2m} \dot{V}_{2_r},$$

$$
\begin{aligned}
\dot{V}_1 =& -\tilde{\omega}^\top D\tilde{\omega} - \kappa^{\frac{1}{2}}\tilde{\omega}^\top \mathcal{K}^{\frac{1}{2}} W\tilde{p} + \tilde{\omega}^\top d_\omega + \tilde{p}^\top P\dot{\tilde{p}} + \dot{\tilde{p}}^\top P\tilde{p} + \epsilon\tilde{\omega}^\top AM\nabla^2 U(\tilde{\theta}+\theta^s)\tilde{\omega} \\
& - \epsilon\tilde{\omega}^\top DA\left(\nabla U(\tilde{\theta}+\theta^s) - \nabla U(\theta^s)\right) + \epsilon d_\omega^\top A\left(\nabla U(\tilde{\theta}+\theta^s) - \nabla U(\theta^s)\right) \\
& - \epsilon\tilde{p}^\top W^\top(\kappa\mathcal{K})^{\frac{1}{2}} A\left(\nabla U(\tilde{\theta}+\theta^s) - \nabla U(\theta^s)\right) \\
& - \epsilon\left(\nabla U(\tilde{\theta}+\theta^*) - \nabla U(\theta^s)\right)^\top A\left(\nabla U(\tilde{\theta}+\theta^s) - \nabla U(\theta^s)\right) \\
& + \epsilon\tilde{\omega}^\top M\mathbb{1}_n\mathbb{1}_n^\top A^{-1}\tilde{\omega} - \epsilon\tilde{\omega}^\top D\mathbb{1}_n\mathbb{1}_n^\top A^{-1}\tilde{\theta} - \epsilon\tilde{p}^\top W^\top(\kappa\mathcal{K})^{\frac{1}{2}}\mathbb{1}_n\mathbb{1}_n^\top A^{-1}\tilde{\theta} \\
& + \epsilon d_\omega^\top\mathbb{1}_n\mathbb{1}_n^\top A^{-1}\tilde{\theta} - \epsilon\frac{\kappa}{\mu}\tilde{\theta}^\top A^{-1}\mathbb{1}_n\mathbb{1}_n^\top A^{-1}\mathbb{1}_n\mathbb{1}_n^\top A^{-1}\tilde{\theta}, \\
\dot{V}_{2_r} =& \tilde{p}^\top(t)S_{0_r}\tilde{p}(t) - \tilde{p}^\top(t-h_{0_r})\left(S_{0_r} - S_{1_r}\right)\tilde{p}(t-h_{0_r}) - \tilde{p}^\top(t-h_{1_r})S_{1_r}\tilde{p}(t-h_{1_r}) \\
& + \dot{\tilde{p}}^\top(t)\left(h_{0_r}^2 R_{0_r} + (h_{1_r}-h_{0_r})^2 R_{1_r}\right)\dot{\tilde{p}}(t) \\
& - h_{0_r}\int_{t-h_{0_r}}^{t}\dot{\tilde{p}}^\top(s)R_{0_r}\dot{\tilde{p}}(s)ds - (h_{1_r}-h_{0_r})\int_{t-h_{1_r}}^{t-h_{0_r}}\dot{\tilde{p}}^\top(s)R_{1_r}\dot{\tilde{p}}(s)ds.
\end{aligned}
\tag{3.3.19}
$$

Since under the conditions of the proposition 3.3.3, the second LMI in (3.3.12) is feasible, applying Jensen's inequality together with Lemma 3.3 in [26], see also [105], gives

$$
-h_{0_r}\int_{t-h_{0_r}}^{t}\dot{\tilde{p}}^\top(s)R_{0_r}\dot{\tilde{p}}(s)ds \le -\left[\tilde{p}(t) - \tilde{p}(t-h_{0_r})\right]^\top R_{0_r}\left[\tilde{p}(t) - \tilde{p}(t-h_{0_r})\right],
$$

and, likewise,

$$
\begin{aligned}
& -(h_{1_r}-h_{0_r})\int_{t-h_{1_r}}^{t-h_{0_r}}\dot{\tilde{p}}^\top(s)R_{1_r}\dot{\tilde{p}}(s)ds \\
& \le -\begin{bmatrix}\tilde{p}(t-h_{0_r}) - \tilde{p}(t-\tau_r(t)) \\ \tilde{p}(t-\tau_r(t)) - \tilde{p}(t-h_{1_r})\end{bmatrix}^\top \begin{bmatrix} R_{1_r} & S_{12_r} \\ * & R_{1_r}\end{bmatrix}\begin{bmatrix}\tilde{p}(t-h_{0_r}) - \tilde{p}(t-\tau_r(t)) \\ \tilde{p}(t-\tau_r(t)) - \tilde{p}(t-h_{1_r})\end{bmatrix},
\end{aligned}
$$

Next, the descriptor method is applied, see [26, Chapter 3] and 2.3.1.4. Let P_2 and P_3 be matrix variables and add the expression

$$
0 = 2\left[\tilde{p}^\top P_2^\top + \dot{\tilde{p}}^\top P_3^\top\right]\left[\kappa^{\frac{1}{2}} W^\top \mathcal{K}^{\frac{1}{2}}\tilde{\omega}\right.
$$

$$-\kappa W^\top \mathcal{K}^{\frac{1}{2}} A \left(\sum_{r=1}^{2m} \mathcal{T}_r A \mathcal{K}^{\frac{1}{2}} W \tilde{p}(t-\tau_r(t)) \right) + d_p - \dot{\tilde{p}} \Bigg],$$

to (3.3.3). Furthermore, by defining

$$\begin{aligned}
\xi =& \mathrm{col}\Big(\left(\nabla U(\tilde{\theta}+\theta^s) - \nabla U(\theta^s)\right), \left(\mathbb{1}_n \mathbb{1}_n^\top A^{-1}\tilde{\theta}\right), \tilde{\omega}, \tilde{p}, \dot{\tilde{p}}, \xi_1, \xi_2, \xi_3, d_\omega, d_p \Big),\\
\xi_1 =& \mathrm{col}\left(\tilde{p}(t-h_{0_1}), \dots, \tilde{p}\left(t-h_{0_{2m}}\right)\right),\\
\xi_2 =& \mathrm{col}\left(\tilde{p}(t-\tau_1(t)), \dots, \tilde{p}(t-\tau_{2m}(t))\right),\\
\xi_3 =& \mathrm{col}\left(\tilde{p}(t-h_{1_1}), \dots, \tilde{p}\left(t-h_{1_{2m}}\right)\right),
\end{aligned}$$

selecting $P_2 = \frac{1}{2} I_{n-1}$ and $P_3 = \epsilon P_2 = \frac{\epsilon}{2} I_{n-1}$ with $\varepsilon > 0$, recalling $\bar{\mathcal{T}}_r$ in (3.3.11) and defining $\bar{\kappa} = \kappa^{\frac{1}{2}}$ and $\bar{\gamma} = \gamma^2$, The following can be obtained

$$\dot{V} - \frac{1}{2}\left(\gamma^2 \|d\|_2^2 - \|y\|_2^2\right) \le \xi^\top \left(\begin{bmatrix} \mathbb{0} & \mathbb{0} \\ * & \mathcal{Q}_H \end{bmatrix} + \epsilon \Xi_H \right) \xi, \tag{3.3.20}$$

where

$$\mathcal{Q}_H = \begin{bmatrix} \mathcal{Q}_{H_1} & \mathcal{Q}_{H_2} \\ * & \mathcal{Q}_{H_3} \end{bmatrix} \tag{3.3.21}$$

$$\begin{aligned}
\mathcal{Q}_{H_1} =& \begin{bmatrix} -D + 0.5W_1 & \frac{1}{2}(\kappa\mathcal{K})^{\frac{1}{2}}(-W + 2WP_2) & (\kappa\mathcal{K})^{\frac{1}{2}} W P_3 & \mathbb{0} & \mathbb{0} & \mathbb{0} \\ * & Q_{h_{22}} & P - P_2^\top & \mathcal{Q}_{h_{24}} & \mathcal{Q}_{h_{25}} & \mathbb{0} \\ * & * & \mathcal{Q}_{h_{33}} & \mathbb{0} & \mathcal{Q}_{h_{35}} & \mathbb{0} \\ * & * & * & \mathcal{Q}_{h_{44}} & \mathcal{Q}_{h_{45}} & S_{12} \\ * & * & * & * & \mathcal{Q}_{h_{55}} & \mathcal{Q}_{h_{56}} \\ * & * & * & * & * & \mathcal{Q}_{h_{66}} \end{bmatrix},\\
\mathcal{Q}_{H_2} =& \begin{bmatrix} \frac{1}{2} I_n & \mathbb{0} & \mathbb{0} & \mathbb{0} & \mathbb{0} & \mathbb{0} \\ \mathbb{0} & P_2^\top & P_3^\top & \mathbb{0} & \mathbb{0} & \mathbb{0} \end{bmatrix}^\top,\\
\mathcal{Q}_{H_3} =& \begin{bmatrix} -\frac{1}{2}\bar{\gamma} I_n & \mathbb{0} \\ * & -\frac{1}{2}\bar{\gamma} I_{n-1} \end{bmatrix}
\end{aligned} \tag{3.3.22}$$

with

$$
\begin{aligned}
&S_0 = \mathrm{blockdiag}(S_{0_r}), \quad R_0 = \mathrm{blockdiag}(R_{0_r}), \quad S_1 = \mathrm{blockdiag}(S_{1_r}),\\
&R_1 = \mathrm{blockdiag}(R_{1_r}), \quad S_{12} = \mathrm{blockdiag}(S_{12_r}),\\
&\mathcal{Q}_{h_{22}} = \sum_{r=1}^{2m} S_{0_r} - \sum_{r=1}^{2m} R_{0_r} + \frac{1}{2}W_2, \quad \mathcal{Q}_{h_{24}} = \left[R_{0_1} \dots R_{0_{2m}}\right],\\
&\mathcal{Q}_{h_{25}} = \left[\bar{\mathcal{Q}}_{h_{25,1}}, \dots, \bar{\mathcal{Q}}_{h_{25,2m}}\right], \quad \bar{\mathcal{Q}}_{h_{25,r}} = -\kappa P_2^\top W^\top \mathcal{K}^{\frac{1}{2}} A \mathcal{T}_r A \mathcal{K}^{\frac{1}{2}} W,\\
&\mathcal{Q}_{h_{33}} = -P_3^\top - P_3 + \sum_{r=1}^{2m} \left(h_{0_r}^2 R_{0_r} + (h_{1_r} - h_{0_r})^2 R_{1_r}\right),\\
&\mathcal{Q}_{h_{35}} = \left[\bar{\mathcal{Q}}_{h_{35,1}}, \dots, \bar{\mathcal{Q}}_{h_{35,2m}}\right], \quad \bar{\mathcal{Q}}_{h_{35,r}} = -\kappa P_3^\top W^\top \mathcal{K}^{\frac{1}{2}} A \mathcal{T}_r A \mathcal{K}^{\frac{1}{2}} W,\\
&\mathcal{Q}_{h_{44}} = -S_0 + S_1 - R_0 - R_1, \quad \mathcal{Q}_{H_{45}} = \mathcal{Q}_{h_{56}} = R_1 - S_{12},\\
&\mathcal{Q}_{h_{66}} = -S_1 - R_1
\end{aligned}
$$

and

$$
\Xi_H = \begin{bmatrix}
-A & \mathbb{0} & -\frac{1}{2}AD & -\frac{1}{2}A(\kappa\mathcal{K})^{\frac{1}{2}}W & \mathbb{0} & \mathbb{0} & \mathbb{0} & \mathbb{0} & \frac{1}{2}A & \mathbb{0}\\
* & -\frac{\kappa}{\mu}A^{-1} & -\frac{1}{2}D & -\frac{1}{2}(\kappa\mathcal{K})^{\frac{1}{2}}W & \mathbb{0} & \mathbb{0} & \mathbb{0} & \mathbb{0} & \frac{1}{2}I_n & \mathbb{0}\\
* & * & \frac{1}{2}E_{33} & \mathbb{0} & \mathbb{0} & \mathbb{0} & \mathbb{0} & \mathbb{0} & \mathbb{0} & \mathbb{0}\\
* & * & * & \mathbb{0} & \mathbb{0} & \mathbb{0} & \mathbb{0} & \mathbb{0} & \mathbb{0} & \mathbb{0}\\
* & * & * & * & \mathbb{0} & \mathbb{0} & \mathbb{0} & \mathbb{0} & \mathbb{0} & \mathbb{0}\\
* & * & * & * & * & \mathbb{0} & \mathbb{0} & \mathbb{0} & \mathbb{0} & \mathbb{0}\\
* & * & * & * & * & * & \mathbb{0} & \mathbb{0} & \mathbb{0} & \mathbb{0}\\
* & * & * & * & * & * & * & \mathbb{0} & \mathbb{0} & \mathbb{0}\\
* & * & * & * & * & * & * & * & \mathbb{0} & \mathbb{0}\\
* & * & * & * & * & * & * & * & * & \mathbb{0}
\end{bmatrix},
$$

where

$$
E_{33} = AM\nabla^2 U(\tilde{\theta} + \theta^s) + \nabla^2 U(\tilde{\theta} + \theta^s)MA + M\mathbb{1}_n\mathbb{1}_n^\top A^{-1} + A^{-1}\mathbb{1}_n\mathbb{1}_n^\top M.
$$

Under the standing assumptions, $Q_H < 0$. Furthermore, the upper 2×2 block of Ξ_H is negative definite. Thus, by invoking [14, Lemma 11], it is concluded that the matrix sum in (3.3.20) is negative definite for some small $\epsilon > 0$. Consequently,

$$\dot{V}(x,\dot{x},t) - \frac{1}{2}\left(\gamma^2 \|d(t)\|^2 - \|y(t)\|^2\right) \leq -\varrho\left(\|x(t)\|_2^2 + \|d(t)\|_2^2\right),$$

for some $\epsilon \in \mathbb{R}_{>0}$ and $\varrho \in \mathbb{R}_{>0}$. By invoking [26, Lemma 4.3] it is concluded that the origin of the system (3.3.9) is locally uniformly asymptotically stable and that the system has a small-signal L_2-gain less than or equal to $\gamma = \sqrt{\bar{\gamma}}$.

To conclude the proof, note that the matrix Q_H in (3.3.12) is a LMI in the controller variables $\bar{\kappa}$ and $\bar{\mathcal{L}}$ as well as in the auxiliary variables $\bar{\gamma}$, R, S_{12} and S with additional (fixed) tuning parameter ε. The matrix Q_{H_1} in the LMI in (3.3.12) corresponds to the delay-robustness and the shape of the communication network, while the rest are for including L_2-gain performance. Therefore, sparsity of the communication network can be included in the control design by augmenting the cost function in the optimization problem (3.3.12) with the term trace$\left(\bar{\mathcal{Z}}\right)$. This yields the convex optimization problem (3.3.12), where additional weighting factors have been included to trade off L_2-gain performance (α) against frequency error convergence[1] (β) and communication efforts ($W_{\mathcal{Z}}$). □□□

Remark 3.3.4. The proposed control synthesis in Proposition 3.3.3 is stated in the form of a standard optimization problem, i.e.

$$\begin{aligned} &\min_x f(x) \\ &\text{subject to } A(x,y) < 0, \end{aligned}$$

[1]In the author's experience, with $\beta = 0$ the numerical value of $\bar{\kappa}$ resulting from the optimization problem is typically very small. This is explained by the fact that $\bar{\kappa}$ only appears in a positive off-diagonal term in Q_H in (3.3.12). Yet, when tested in simulations it turns out that a minimum value of $\bar{\kappa}$ is required to drive the frequency error to zero, thus justifying the choice $\beta > 0$.

with decision variables x and y and A represents a linear matrix inequality in x and y. Moreover, the subjected LMIs in (3.3.12) result in controller parameters to ensure delay-robust stability and disturbance attenuation and minimize the number of communication links. The influence of parameters in the cost function is shown in the numerical example.

Remark 3.3.5. With regard to the feasibility of the optimization problem (3.3.12) we see from the definition of the matrix Q_H in (3.3.12) that for any given h_{0_r}, h_{1_r}, $r=1,\ldots,2m$, choosing $\varepsilon \gg 0$, $\bar{\kappa} \ll 1$ (positive off-diagonal term) and $\|\bar{Z}\| \ll 1$ (positive off-diagonal term), ensures that there always exists $\bar{\gamma} \gg 1$ (positive on-diagonal term with negative sign) such that $Q_H < 0$. Hence, the optimization problem can always be parametrized, such that a feasible solution exists. However, we can also see from (3.3.12) that with increasing value of h_{1_r}, the achievable L_2-gain performance is likely to deteriorate, which is to be expected (as in the considered system (3.3.9) delays deteriorate the performance).

Remark 3.3.6. The optimization problem (3.3.12) has been derived such that it is linear and convex in both the objective function and the constraints. Hence, it can be solved efficiently using standard numerical methods [106, 107], also for large-scale problems.

Remark 3.3.7. In order to obtain the minimum number of communication links, the optimization problem (3.3.12) is solved for a number of iterations, in each of which the weight matrix $W_{\mathcal{Z}}$ is updated. Hence, in each of these iterations the conditions of Proposition 3.3.3 are satisfied, see the numerical example for more details.

The proposed control design in (3.3.12) can be further reduced and introduced in a simpler way, if a uniform delay is considered, i.e., $h_{0_r} = 0$, $\tau_r(t) = \tau(t) \in [0,h]$, $h_{1_r} = h$, $r = 1,\ldots,2m$. This leads to representing the closed-loop system (3.3.9) as follows

$$\dot{\tilde{\theta}} = \tilde{\omega},$$

$$
\begin{aligned}
M\dot{\tilde{\omega}} &= -D\tilde{\omega} - \nabla U(\tilde{\theta}+\theta^s) + \nabla U(\theta^s) - (\kappa\mathcal{K})^{\frac{1}{2}} W\tilde{p} - \frac{1}{\mu}\kappa A^{-1}\mathbb{1}_n\mathbb{1}_n^\top A^{-1}\tilde{\theta} + d_\omega,\\
\dot{\tilde{p}} &= \kappa^{\frac{1}{2}} W^\top \mathcal{K}^{\frac{1}{2}}\tilde{\omega} - \kappa W^\top \mathcal{K}^{\frac{1}{2}} A\mathcal{L}A\mathcal{K}^{\frac{1}{2}} W\tilde{p}(t-\tau) + d_p,\\
y &= \begin{bmatrix} W_1^{\frac{1}{2}}\tilde{\omega} \\ W_2^{\frac{1}{2}}\tilde{p} \end{bmatrix}, \quad d = \begin{bmatrix} d_\omega \\ d_p \end{bmatrix}.
\end{aligned} \tag{3.3.23}
$$

Furthermore, the terms in (3.3.11) can also be rewritten as

$$
\bar{\mathcal{Z}} = \kappa\mathcal{Z}, \qquad \bar{\mathcal{L}} = \mathcal{K}^{\frac{1}{2}} A\mathcal{B}\bar{\mathcal{Z}}\mathcal{B}^\top A\mathcal{K}^{\frac{1}{2}}. \tag{3.3.24}
$$

The subsequent corollary provides a design criterion in the case of uniform communication delay.

Corollary 3.3.8 (Uniform communication delay)**.** *Consider the system* (3.3.23) *with Assumption 3.3.1. Recall the weighting matrices W_1 and W_2 given in* (3.3.7) *and* (3.3.8)*. Fix $h \geq 0$, $\mathcal{K} > 0$ and $\varepsilon > 0$ as well as weighting parameters $\alpha > 0$, $\beta > 0$ and a diagonal weighting matrix $W_{\mathcal{Z}} > 0$. Suppose that there exist parameters $\bar{\kappa} > 0$ and matrices $\bar{\mathcal{Z}} \geq 0$, $R > 0$, $S > 0$ and S_{12}, such that the following optimization problem is feasible:*

$$
\min_{\bar{\gamma},\bar{\kappa},\bar{\mathcal{Z}}} \alpha\bar{\gamma} - \beta\bar{\kappa} + \mathit{trace}\big(W_{\mathcal{Z}}\bar{\mathcal{Z}}\big)
$$

subject to

$$
\begin{aligned}
Q_u &= \begin{bmatrix}
-D+\frac{1}{2}W_1 & \mathbb{0} & Q_{u13} & \mathbb{0} & \mathbb{0} & \frac{1}{2}I_n & \mathbb{0}\\
* & Q_{u22} & -\frac{1}{4}I_{n-1} & S_{12} & Q_{u25} & \mathbb{0} & \frac{1}{2}I_{n-1}\\
* & * & Q_{u33} & \mathbb{0} & Q_{u35} & \mathbb{0} & \frac{1}{4}\varepsilon I_{n-1}\\
* & * & * & -S-R & R-S_{12}^\top & \mathbb{0} & \mathbb{0}\\
* & * & * & * & Q_{u55} & \mathbb{0} & \mathbb{0}\\
* & * & * & * & * & -\frac{1}{2}\bar{\gamma}I_n & \mathbb{0}\\
* & * & * & * & * & * & -\frac{1}{2}\bar{\gamma}I_{n-1}
\end{bmatrix} < 0,\\
&\begin{bmatrix} R & S_{12} \\ * & R \end{bmatrix} \geq 0,
\end{aligned} \tag{3.3.25}
$$

where

$$Q_{u13} = \frac{1}{4}\varepsilon\bar{\kappa}\mathcal{K}^{\frac{1}{2}}W, \quad Q_{u22} = S - R + \frac{1}{2}W_2, \quad Q_{u25} = R - S_{12} - \frac{1}{2}W^\top\bar{\mathcal{L}}W,$$
$$Q_{u33} = -\frac{1}{2}\varepsilon I_{n-1} + h^2 R, \quad Q_{u35} = -\frac{1}{4}\varepsilon W^\top\bar{\mathcal{L}}W, \quad Q_{u55} = -2R + S_{12} + S_{12}^\top.$$

Choose the controller parameters as

$$\kappa = \bar{\kappa}^2, \quad \mathcal{L} = \frac{1}{\kappa}\mathcal{B}\bar{\mathcal{Z}}\mathcal{B}^\top. \tag{3.3.26}$$

Then, for all $\tau(t) \in [0,h]$, the origin is a locally uniformly asymptotically stable equilibrium point of the system (3.3.23) *and the system has a small-signal L_2-gain less than or equal to $\gamma = \sqrt{\bar{\gamma}}$ with respect to the supply rate $s(d,y) = \frac{1}{2}\left(\gamma^2\|d\|_2^2 - \|y\|_2^2\right)$, where d and y are given in* (3.3.23).

Proof. The same approach as the proof of Proposition 3.3.3 is used expect the communication delay is model as a uniform delay with $h_{0_r} = 0$. Consequently, set $h_{1_r} = h$, $\tau_r(t) = \tau(t) \in [0,h]$, and accordingly let $S_0 = 0$, $R_0 = 0$, $S_1 = S$, $R_1 = R$, and $P = I_n$ in (3.3.15). Then, setting $\epsilon = 0$ in (3.3.15) and differentiating V yields

$$\begin{aligned}\dot{V} =& -\tilde{\omega}^\top(t)D\tilde{\omega}(t) - \frac{1}{2}\kappa^{\frac{1}{2}}\tilde{\omega}^\top(t)\mathcal{K}^{\frac{1}{2}}W\tilde{p}(t) + \tilde{\omega}^\top(t)d_\omega(t) + \frac{1}{2}\tilde{p}^\top(t)d_p(t)\\ &+ h^2\dot{\tilde{p}}^\top(t)R\dot{\tilde{p}}(t) + \tilde{p}^\top(t)S\tilde{p}(t) - \frac{\kappa}{2}\tilde{p}^\top(t)W^\top\mathcal{K}^{\frac{1}{2}}A\mathcal{L}A\mathcal{K}^{\frac{1}{2}}W\tilde{p}(t-\tau)\\ &- h\int_{t-h}^{t}\dot{\tilde{p}}^\top(s)R\dot{\tilde{p}}(s)ds - \tilde{p}^\top(t-h)S\tilde{p}(t-h).\end{aligned} \tag{3.3.27}$$

Then, apply Jensen's inequality (2.3.12) together with (2.3.17) and add the expression

$$\begin{aligned}0 = 0.5&\left[\tilde{p}(t)^\top + \varepsilon\dot{\tilde{p}}^\top(t)\right]\left[\kappa^{\frac{1}{2}}W^\top\mathcal{K}^{\frac{1}{2}}\tilde{\omega}(t)\right.\\ &\left.-\kappa W^\top\mathcal{K}^{\frac{1}{2}}A\mathcal{L}A\mathcal{K}^{\frac{1}{2}}W\tilde{p}(t-\tau(t)) + d_p(t) - \dot{\tilde{p}}(t)\right]\end{aligned}$$

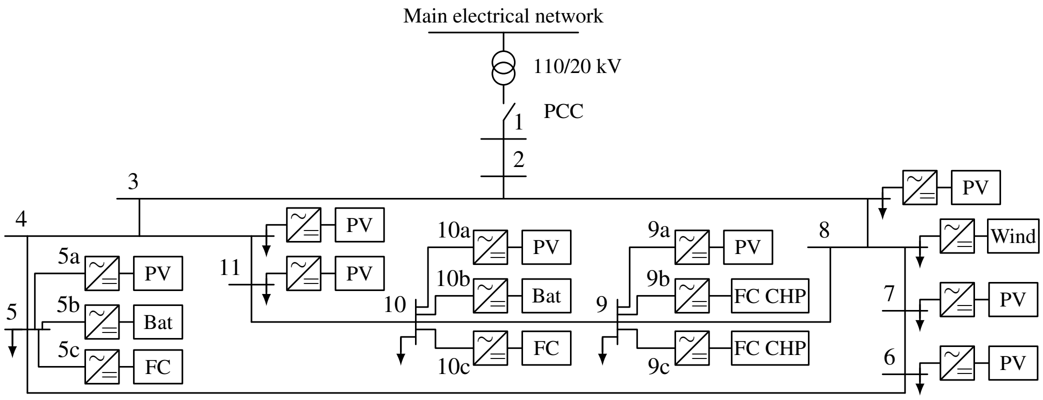

Figure 3.2: 20kV MV CIGRE benchmark microgrid with 11 main buses and inverter-interfaced units of type: photovoltaic (PV), fuel cell (FC), battery, combined heat and power (CHP) FC, and wind turbine. The controlled units are located at buses 4, 5b, 5c, 6, 7, 9b, 9c, 10b, 10c and 11. PCC denotes the point of common coupling to the main grid.

to (3.3.27). Furthermore, by recalling $\bar{\mathcal{L}}$ in (3.3.24) and defining

$$\bar{\kappa} = \kappa^{\frac{1}{2}}, \quad \bar{\gamma} = \gamma^2,$$

the matrix Q_u in (3.3.8) can be obtained. Following the Proposition 3.3.3 proof, for some $\epsilon \in \mathbb{R}_{>0}$, it is straightforward to show that the origin of the system (3.3.23) is locally uniformly asymptotically stable and that the system has a small-signal L_2-gain less than or equal to $\gamma = \sqrt{\bar{\gamma}}$.

□□□

3.4 Numerical example

The performance of the proposed controller synthesis and the inherent design trade-off between the maximum guaranteed L_2-gain and the sparsity of the communication network are illustrated via numerical experiments on the three-phase islanded Subnetwork 1 of the CIGRE benchmark MV network [108, 109] shown in Fig. 3.2.

3.4.1 System description

The system contains 11 main buses and a total of 15 distributed generation units. The values of the network parameters are mainly taken from [108, 109].

Similarly to [80], the following modifications are made compared to the original system in [109]. At bus 9b, an inverter-interfaced combined heat and power (CHP) fuel cell (FC) is used instead of the CHP diesel generator. Moreover, the power ratings of the controllable generation units (CHPs, batteries, FC, PVs) are scaled by a factor 4 to be able to meet the load demand of the system in islanded mode. To integrate the PV units at buses 4, 6, 7 and 11 in the frequency control, it is assumed that they are operated at 70% of their actual maximum power point and, thus, can increase or decrease their generation. Hence, the system in Fig. 3.2 has a total of ten controllable generation units of which four are PVs at buses 4 ($i = 1$), 6 ($i = 4$), 7 ($i = 5$)and 11 ($i = 10$), two are batteries at buses 5b ($i = 2$) and 10b ($i = 8$), two are FCs in households at buses 5c ($i = 3$) and 10c ($i = 9$) and two are FC CHPs at buses 9b ($i = 6$) and 9c ($i = 7$). The power ratings of the inverters in per unit (pu) are $S_i^N = [0.0168, 0.5053, 0.0278, 0.0253, 0.0253, 0.2611, 0.1785, 0.1684, 0.0118,$ $0.0084]$. It is also assumed that all controllable units are equipped with frequency droop control and the network is modelled by (3.2.7). We set $K = \kappa D$ where $D =$ diag(0.084, 2.526, 0.139, 0.126, 0.126, 1.305, 0.893, 0.842, 0.059, 0.042).

Non-controlled generation units are connected at buses 3 and 8. The loads in the network represent industrial and household loads. Their data is specified in [109, Table 1]. Moreover, the largest R/X ratio in the reduced admittance matrix is less than 0.3. Thus, the assumption of dominantly inductive admittances is satisfied. The numerical implementation is conducted on a machine featuring an Intel Core i5-6400 with 16GB of RAM and using Matlab (R2018b), Yalmip (version 09-02-2018) [107] and the solver Mosek (version 8.1.0.51) [110]. For the present simulations, the fast-varying delays are generated by using the rate transition and variable time delay blocks in Matlab/Simulink with a sampling time $T_{sam} = 2$ms.

3.4.2 Scenario 1: Heterogeneous communication delays

To carry out the secondary control design, i.e., to solve the optimization problem (3.3.12) and following the associated analysis, it is assumed that the communication between different units is affected by heterogenous fast-varying delays. To this end, the network is divided into four different groups of generation units based on the geographical distances between them, see Fig. 3.2. Then it is assumed that the communication amongst units within the same group is affected by a lower time delay than that between units from different groups (since these are located further apart). Thus, we consider delays $h_{0_1} = 150\text{ms} \leq \tau_1(t) \leq h_{1_1} = 200\text{ms}$ between the generators 4, 5b, 5c, 11, $h_{0_2} = 200\text{ms} \leq \tau_2(t) \leq h_{1_2} = 250\text{ms}$ between 9b, 9c, 10b, 10c, $h_{0_3} = 100\text{ms} \leq \tau_3(t) \leq h_{1_3} = 150\text{ms}$ between the generators 6 and 7. Moreover, the maximum delay between the remaining nodes in the network is $h_{0_4} = 450\text{ms} \leq \tau_4(t) \leq h_{1_4} = 500\text{ms}$. Furthermore, the matrix A is chosen as $A = \text{diag}(S_i^N)^{-1}$ and $\varepsilon = 0.3$.

Recall that the objective function of the proposed controller synthesis in (3.3.12) is parametrized in terms of the weightings α, β and $\mathcal{W}_{\mathcal{Z}}$. To illustrate the effects which these different weighting parameters have on the resulting secondary frequency controller and on the closed-loop performance, a two-step case study is pursued. In the first design step, the influence of α and β is illustrated on the relation of the feedback gain κ and the estimated L_2-gain γ. This is done without enforcing any additional sparsity requirements on the communication topology (i.e., $\mathcal{W}_{\mathcal{Z}} = \mathbb{0}$). As a result of this first design step, a nominal controller parametrization along with a nominal estimate for the L_2-gain is identified. These nominal values are then used as references for the second design step, which explores the impact of reducing the number of communication links on the L_2-gain performance. Remark that during all design steps, robustness with respect to the specified heterogeneous fast-varying delays $\tau_1(t), \ldots, \tau_4(t)$ is guaranteed (as long as the optimization problem (3.3.12) is feasible).

Design step 1. In the first step, different values of α and β with $W_{\mathcal{Z}} = \mathbb{0}$ are considered. The main purpose of this stage is to illustrate the necessity to include $\beta \neq 0$ in the problem (3.3.12). Hence, to start with, set $\beta = 0$ and solve

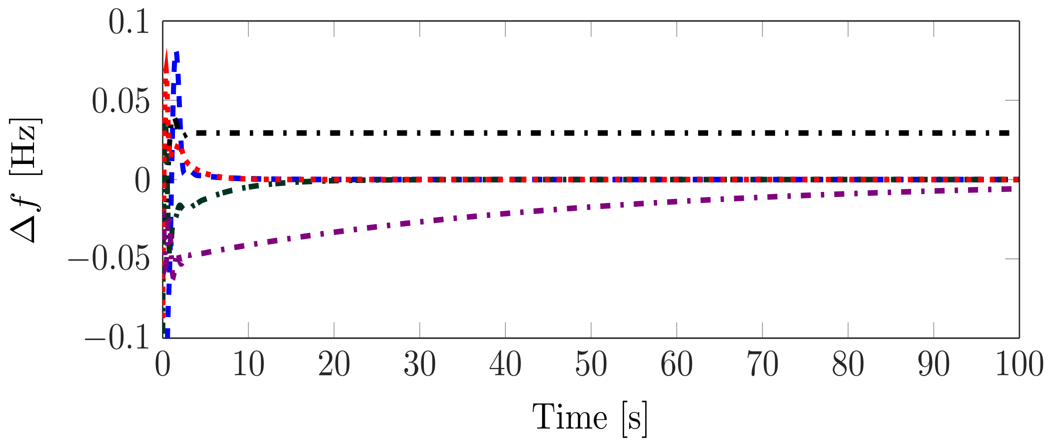

Figure 3.3: Frequency convergence at bus 9b for different values of κ. The lines correspond to: $\kappa = 1.122 \times 10^{-9}$ '– .', $\kappa = 1.1676$ ' –', $\kappa = 0.1844$ '···', $\kappa = 0.0217$ '–.', $\kappa = 0.4656$ '- -'

the optimization problem (3.3.12). The design problem is feasible, but yields a value for κ close to zero, which leads to a rather slow convergence of the frequency to its nominal value, see Fig. 3.3. This undesired behavior can be alleviated by setting $\beta > 0$, when solving (3.3.12). Furthermore, on the other extreme, setting $\alpha = 0$ leads to a higher value of κ, but a much larger upper estimate of the L_2-gain γ, which indicates a degradation of the robustness properties of the closed-loop system with respect to external perturbations. Consequently, in order to obtain a controller parametrization, which simultaneously yields fast frequency convergence and robustness $\alpha > 0$ and $\beta > 0$ have to be chosen. Further results for κ and γ are given in Table 3.1 for different values of α and β. The frequency convergence for the different cases in Table 3.1 is shown for the unit at bus 9b in Fig. 3.3.

Since all scenarios in Table 3.1 with $\alpha \neq 0$ and $\beta \neq 0$ have very similar L_2-gain performances, the closed-loop system is simulated by using the largest feedback gain, i.e., $\kappa = 0.4656$ and $\gamma = 3.7092$, for two disturbance scenarios. In the first scenario, the system is being subjected to sinusoidal disturbances $d_\omega = d_p = 0.2\sin(12.57t)$ [pu] in both the electrical and communication layers for $t \in [1, 2]$, which can be interpreted as possible oscillations due to harmonics or load variations. The resulting system trajectories are shown in Fig. 3.4,

Table 3.1: Results for κ and γ obtained from solving the optimization problem (3.3.12) in 'Design step 1' for different values of α and β

α	1	0	1	3	1
β	0	1	1	1	3
γ	3.6325	123.598	3.6614	3.6358	3.7092
κ	1.12×10^{-9}	1.1676	0.1844	0.0217	0.4656
Number of communication links (with $\mathcal{W}_{\mathcal{Z}} = \mathbb{0}$)	45	27	28	37	21

from which it can be seen that the system returns to the original equilibrium point after the disturbances vanish. In the second disturbance scenario, a step disturbance in active power of magnitude 0.1 [pu] starting at $t = 1$s and lasting until $t = 3$s is applied to the electrical layer, while simultaneously a white noise disturbance signal is applied to the communication layer. The behavior of the system trajectories is depicted in Fig. 3.5. Also in this case, the system trajectories remain bounded and converge to the equilibrium after the disturbances have vanished.

The number of required communication links is also given in Table 3.1. It can be seen that with increasing magnitude of κ, the number of required links tends to decrease from 45 to around 21. Since the shape of the communication topology is a very important aspect when implementing the secondary control law (3.2.6), the next design step seeks to further explore its impact on the closed-loop performance.

Design step 2. In light of the above observations, we select $\gamma^* = 3.7092$ and $\kappa^* = 0.4656$ as a benchmark. Then, the controller is redesigned with the aim of minimizing the number of communication links while preserving robustness with respect to heterogeneous time-varying delays. Fixing κ^* and γ^* corresponds to setting $\alpha = \beta = 0$ in (3.3.12). The weighting matrix $W_{\mathcal{Z}}$ is determined by using the reweighted ℓ_1-norm approach [104], see also (3.3.10). After solving the optimization problem (3.3.12) for up to 10 iterations, in each

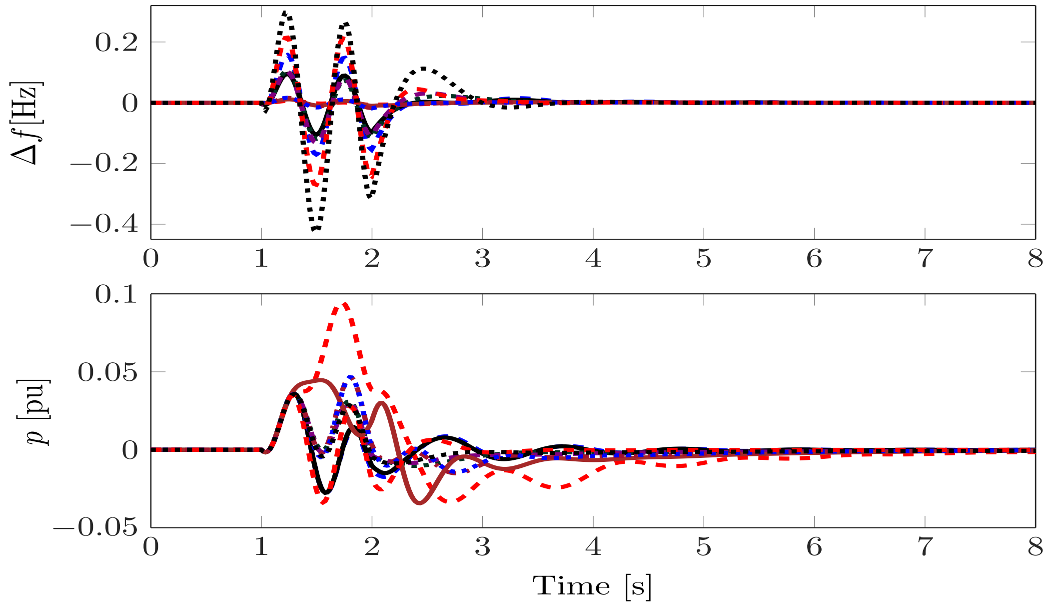

Figure 3.4: Simulation results of the system (3.3.9) with $\kappa = 0.4656$ and $\gamma = 3.7092$, after being subjected to sinusoidal disturbances: $d_\omega = d_p = 0.2\sin(12.57t)$ [pu] for $t \in [1,2]$.

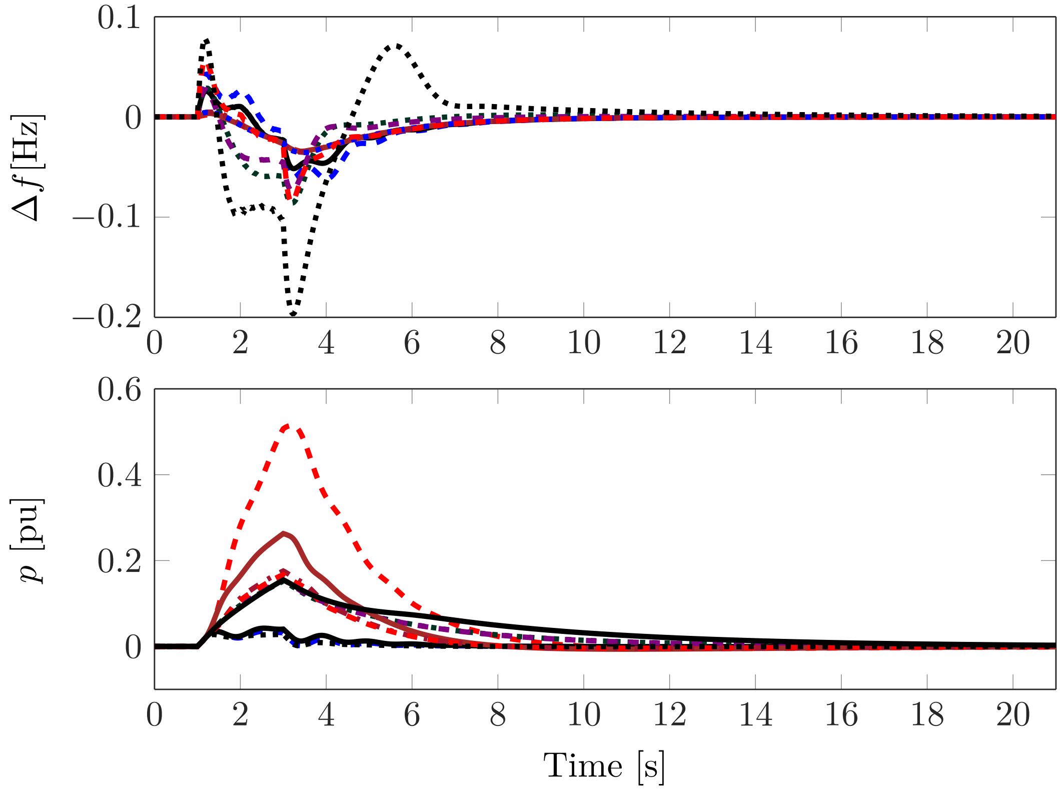

Figure 3.5: Simulation results of the system (3.3.9) with $\kappa = 0.4656$ and $\gamma = 3.7092$, after being subjected to disturbances: a step disturbance of magnitude 0.1 [pu] is applied to the electrical layer, while white noise is applied in the communication layer for $t \in [1,3]$.

of which the weight matrix $W_{\mathcal{Z}}$ is updated, we obtain a controller with 17 communication links with the same L_2-gain performance as in the case of 21 communication links.

To further investigate the trade-off between the L_2-gain performance and the required communication efforts, we successively degrade the required L_2-performance (by increasing the value of γ^*) and then compute the necessary number of communication links by solving the optimization problem (3.3.12). It is found that by increasing the value of the performance index γ by less than 10% of γ^*, the number of communication links is further reduced from 17 to 12, see Fig. 3.6, which are only 3 more links than the 9 required to ensure connectivity of the communication network. Hence, it is concluded that the proposed controller synthesis (3.3.12) is well-suited to obtain practical parametrizations of the control law (3.2.3) that exhibit both good robustness properties and low communication requirements.

By evaluating the evolution of the non-zero entries in the Laplacian matrix $\mathcal{L}$, illustrated in the plots in Fig. 3.6, it is found that the controller weighting matrix A seems to have a significant impact on the sparsity pattern. Namely, the unit at node 5b ($i=2$) with the smallest entry a_{ii} (largest power S_i^N) has the largest initial degree[1] and also preserves that degree with increasing weight on the sparsity. Compared to this, the generation unit $i=10$, which has the largest weight a_{ii}, has from the start only a degree of 1. Meanwhile, the degree of the remaining nodes is being reduced with increasing weight on the sparsity. Thereby, it is observed that the communication links between generation units with larger weights a_{ii} ($i=1,3,5,9,10$) disappear first. Hence, with $A=\mathrm{diag}(S_i^N)^{-1}$ this implies that the larger generation units tend to have a higher degree of connectivity.

The subsequent analysis is directed to further investigate how the controller parameters affect the convergence speed of the closed-loop system (3.3.9). To do so, the analysis focuses on the behavior of the controller state p. Since A

[1] In an unweighted graph without self-loops, the degree of a node corresponds to the number of edges attached to it.

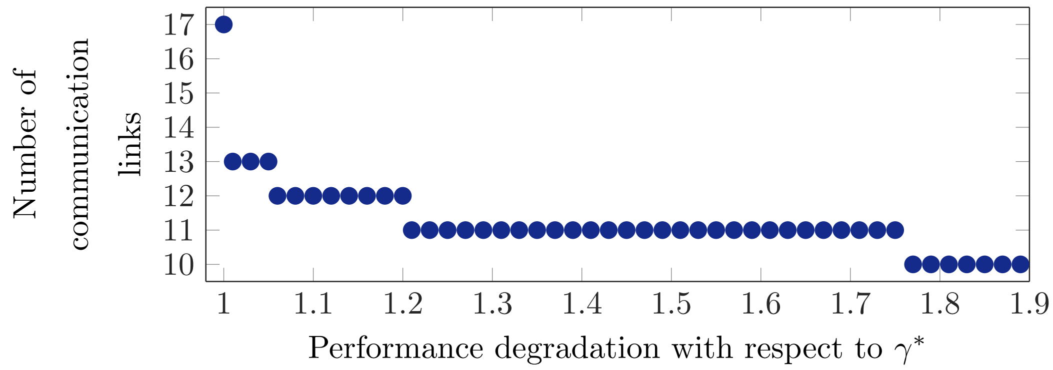

Figure 3.6: Number of non-zero elements of $\mathcal{Z}$ for different values of γ. The number of required communication links in the case of $\gamma^* = 3.7092$ is 17.

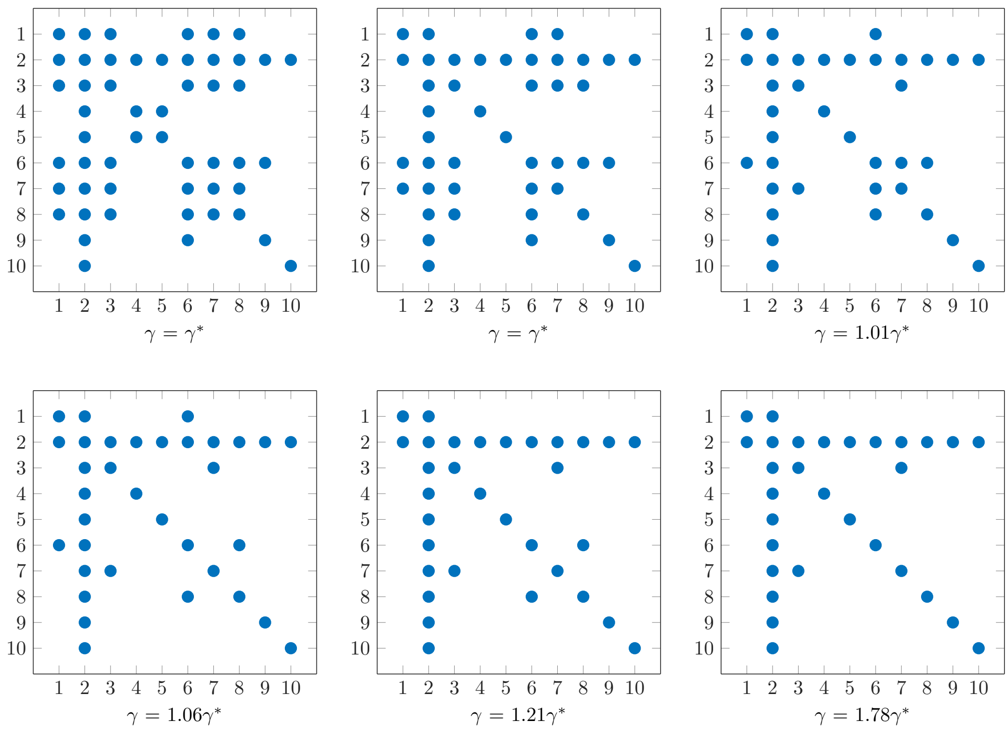

Figure 3.7: Sparsity pattern of $\mathcal{L}$ for different values of γ. The figure represent units at buses 4 ($i = 1$), 5b ($i = 2$), 5c ($i = 3$), 6 ($i = 4$), 7 ($i = 5$), 9b ($i = 6$), 9c ($i = 7$), 10b ($i = 8$), 10c ($i = 9$) and 11 ($i = 10$).

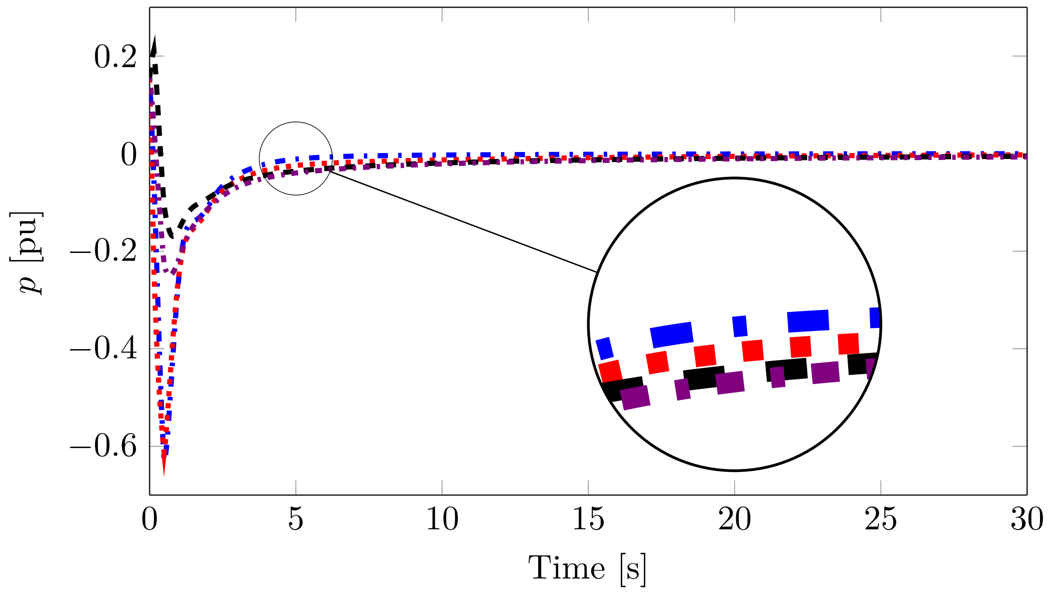

Figure 3.8: The convergence of the state p for generation unit $9b$ ($i = 6$) with different numbers of communication links. The lines correspond to: No. comm. links=6 '– .', No. comm. links=4 '···', No. comm. links=3 '- -'and No. comm. links=1 '– .'.

is fixed by economic considerations and $K = \kappa\mathcal{K}$ where $\mathcal{K}$ is fixed, the remaining degrees of freedom in the control design are κ and $\mathcal{L}$. The effect of κ on the convergence speed has already been studied in design step 1 (see Table 3.1 and Fig 3.3). Thus, it is now investigated how the sparsity of $\mathcal{L}$ affects the convergence speed. Based on the present numerical experiments, the controller states of all generation units exhibit a very similar behavior with regard to the convergence speed in dependency of the sparsity of $\mathcal{L}$. Therefore, generation unit 9b ($i = 6$) used as an illustrative example, since as shown in Fig. 3.8, that unit has access to different numbers of communication links in the different topologies obtained during the design. From simulations (with the same initial condition), it is observed that the convergence speed is only slightly reduced with increasing sparsity of $\mathcal{L}$, see Fig. 3.8. Based on the author experience, the magnitude of κ has a more significant influence on the convergence speed than the shape of the communication network. This also motivated the inclusion of κ in the cost function of the optimization problem (3.3.12).

3.4.3 Scenario 2: Uniform communication delay ($\tau_r = \tau$ and $h_0 = 0$)

In this simulation scenario, the design procedure for the distributed secondary frequency controller (3.3.8) is evaluated. The matrix A is chosen as $A = \text{diag}(a_i)$ where $a = \text{col}(0.21, 0.28, 0.56, 0.18, 0.18,\ 0.26, 0.4, 0.19, 0.3, 0.24)$ (per unit values). The same two design steps in scenario 1 are performed. In the first step with setting $\alpha = \beta = 1$, a nominal feedback gain of $\kappa = 2.6792$ and a nominal bound for the L_2-gain of $\gamma^* = 0.9637$ are obtained. The results in Fig. 3.9 illustrate the convergence of the system trajectories to a synchronized motion after being subjected to external perturbations. Furthermore, after performing the second design step and as expected, the obtained results show a trade-off between the value of γ and the number of non-zero off-diagonal entries of the matrix $\mathcal{Z}$, see Fig. 3.10. Note that in all cases, robustness with respect to fast-varying delays $\tau(t) \leq h$ is guaranteed.

Recall that the design approach leading to (3.3.8) is based on the descriptor method with fixed tuning parameter ε. The latter could potentially introduce some conservativeness. Thus to improve the estimation of the L_2-gain, the optimization problem (3.3.8) is solved, and the obtained values for κ and $\mathcal{L}$ are implemented in a modified version of the conditions for stability *analysis* derived in [14] that incorporates the L_2-gain performance. The resulting performance index γ with the analysis conditions in [14] is only 9.5% lower than the γ^* obtained via (3.3.8). Hence, in the present case the descriptor method does not introduce significantly more conservativeness, while providing the advantage that κ and $\mathcal{L}$ are free design variables (in the analysis in [14] they are treated as constant parameters).

Finally, the conditions proposed in (3.3.12) are compared with those derived in (3.3.8). To this end, the same parameters as in 3.4.3 are used, considering a uniform fast-varying delay $\tau_r(t) = \tau(t)$ with the difference of setting set $h_0 \leq \tau(t) \leq h_1$ and $h_0 = 50\text{ms}$ instead of $h_0 = 0$ as in (3.3.8). By employing the values of κ and γ as used in 3.4.3 and solving the optimization problem (3.3.12),

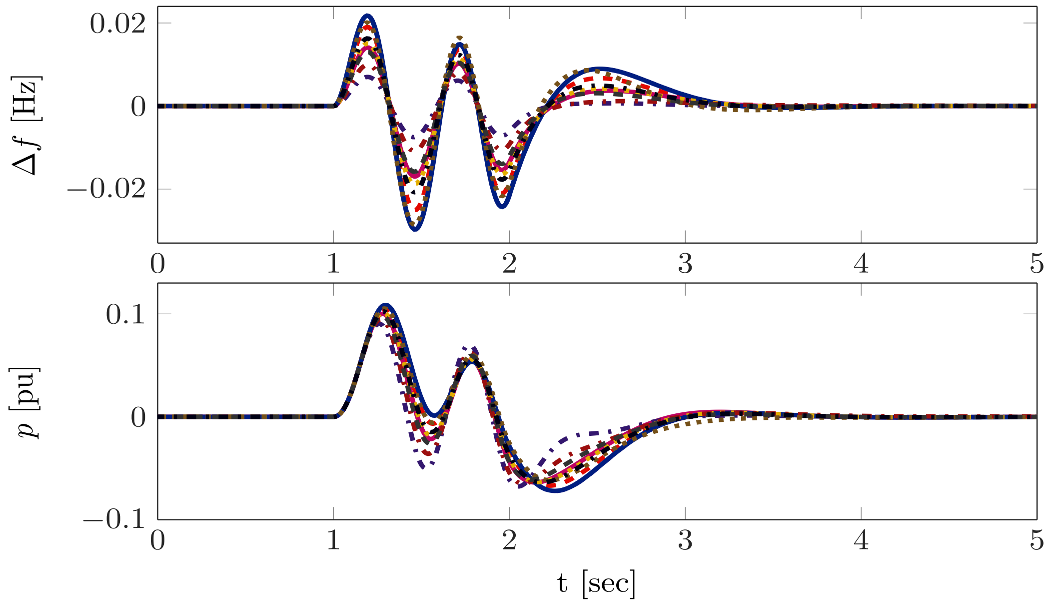

Figure 3.9: Simulation results with $\kappa = 2.6792$, $\gamma = 0.9637$, and $h = 100$ms

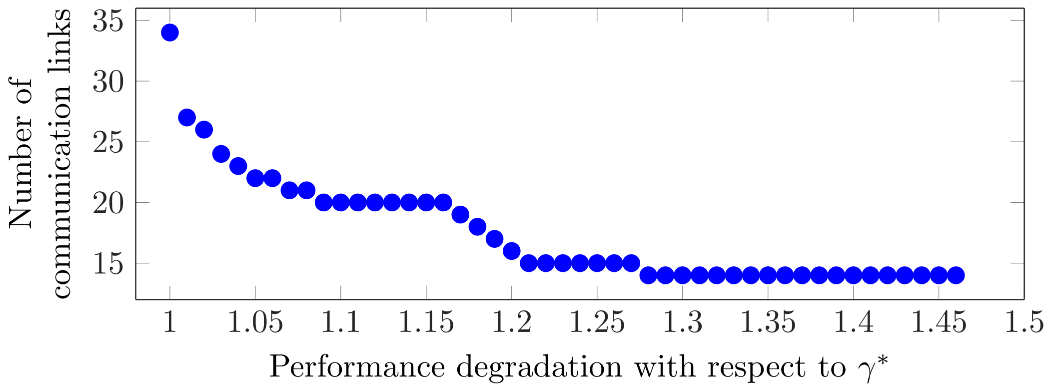

Figure 3.10: Number of non-zero elements of $\mathcal{Z}$ for different values of γ. The number of required communication links in the case of $\gamma^* = 0.9637$ is 34.

the obtained result is an admissible upper bound for the communication delay of $h_{1_{\text{new}}} = 134$ ms, which corresponds to $1.34h_1$ with h_1 being the maximum admissible delay obtained in 3.4.3. This shows that the proposed control synthesis with interval time-varying delays derived in (3.3.12) permits to obtain significantly improved stability guarantees.

3.5 Summary

Consensus algorithms are promising control schemes for secondary control in MGs. Since consensus algorithms are distributed protocols, communication efforts, disturbance attenuation and robustness with respect to time delays are significant factors for the control design and closed-loop performance. The work in this chapter has jointly addressed these three challenges by proposing a design approach for a consensus-based secondary frequency controller in MGs that guarantees robustness with respect to uniform and heterogeneous fast-varying delays and simultaneously permits to trade off finite L_2-gain performance against the sparsity of the required communication network. More precisely, both the LKF and the descriptor methods have been applied to develop a controller synthesis in the form of a constraint convex optimization problem. The proposed synthesis guarantees uniform local asymptotic stability for any operating point satisfying the usual safety requirement of the equilibrium phase angle differences being contained in an arc of length $\frac{\pi}{2}$.

Furthermore, the relevance of the provided weighting parameters on the resulting closed-loop behavior has been illustrated via a two-step design case study based on the CIGRE benchmark MV distribution network. The numerical results show that the proposed approach can be used to identify minimal communication topologies, while at the same time guaranteeing desired delay robustness and disturbance attenuation properties. In addition, it has been shown how the weighting factors have to be chosen to facilitate a trade-off between the L_2-performance and the required communication efforts.

Chapter 4

Conditions for delay-robust consensus-based frequency control in power systems

4.1 Introduction

This Chapter focuses on the stability of the power system operated with the consensus-based distributed secondary frequency controller in the presence of the communication uncertainties. In the previous Chapter, for the purpose of the controller synthesis in MG, a reduced-order model (limited to the swing equation) was used to represent a heterogeneous generation pool containing rotational synchronous generators and inverter-interfaced units. The previous model fits precisely in the case of MGs to provide a sufficient design procedure for the controller gain and the communication topology. Furthermore, a more realistic higher-order generator model with second-order turbine-governor dynamics is considered in this Chapter. The presence of higher-order and time-varying dynamics significantly complicates the stability analysis, and if they are not accounted for in the stability analysis, their presence may lead to instability [24]. Therefore, the work in this Chapter is devoted to addressing the previous challenges.

4.2 Optimal consensus-based frequency control in power systems

Differently from the previous Chapter, the model in this Chapter focuses on the stability conditions for power system where the majority of the generation units are SGs. To motivate the need for a consensus-based secondary control law, the steady-state frequency deviation of the system (2.2.8) will be studied. Similar to (3.2.1), suppose the solution of the system (2.2.8) converges to a synchronous motion with $\omega_r^s = \mathbb{1}_n \omega_r^*$ and constants ω_r^*, P_m^s and P_s^s. Then, ω_r^* is obtained from

$$\mathbb{1}_n^\top M \dot{\omega}^s = \mathbb{1}_n^\top T_m \dot{P}_m^s = \mathbb{1}_n^\top T_s \dot{P}_s^s = 0$$

as

$$\omega_r^* = \frac{-\mathbb{1}_n^\top G V^2 + \mathbb{1}_n^\top P_m^d + \mathbb{1}_n^\top p^s}{\mathbb{1}_n^\top D \mathbb{1}_n + \mathbb{1}_n^\top K^{-1} \mathbb{1}_n},$$

Recall that in order to achieve a zero frequency deviation, the following should be hold $-\mathbb{1}_n^\top G V^2 + \mathbb{1}_n^\top P_m^d + \mathbb{1}_n^\top p^s = 0$. Thus, The objective of the the controller p is to perform classical secondary control task and meanwhile ensuring the economic dispatch, see section 3.2.1.

As discussed in 2.2.1.1.2, P_m is controlled via a turbine-governor system. Thus, a suitable distributed consensus-based secondary frequency controller, such that the stationary solutions P_m^s of the closed-loop power system correspond to optimal solutions of (3.2.2) is introduced. Inspired by [24, 28], the following consensus-based secondary frequency control scheme is considered

$$T_p \dot{p} = -p + P_m - (I_n - K^{-1})\omega_r - A\mathcal{L}Ap, \tag{4.2.1}$$

where the controller (4.2.1) is associated with an undirected connected communication network represented by the Laplacian matrix $\mathcal{L} \in \mathbb{R}^{n\times n}$ enabling distributed information exchange between the generators. Furthermore, the diagonal positive definite matrix $T_p \in \mathbb{R}^{n\times n}$ denotes the controller time constants. It has been shown in [24, 28, 45], that - if appropriately tuned - the control (4.2.1) is able to restore the frequency to its nominal value, that is, $\lim_{t\to\infty}\|\omega_i - \omega^d\| = 0$ for all $i \in \mathcal{N}$. In addition, it was shown in [28, 45] that in steady-state $P_m^s = p^s$ and that the power injections of all generation units satisfy the identical marginal cost requirement, i.e.,

$$A_{ii}P^s_{m,i} = A_{kk}P^s_{m,k} \quad \forall i \in \mathcal{N}, \quad \forall k \in \mathcal{N}. \tag{4.2.2}$$

Remark 4.2.1. *The controller* (3.2.3) *is simpler to implement than the controller in* (4.2.1) *since it only requires local frequency and exchanged marginal cost. However, the controller* (4.2.1) *has the advantage of inclusive higher-order dynamics by employing additional generation output information.*

4.2.1 Communication uncertainties: Time-varying delays and dynamic communication network

In this Chapter, conditions under which the closed-loop power system dynamics are robust with respect to the practically most relevant communication uncertainties, namely message delays, and information loss [20, 21] are derived. With regard to communication delays, similar to Chapter 3, a time-varying bounded communication delay $\tau_{ik} : \mathbb{R}_{\geq 0} \to [h_{0_{ik}}, h_{1_{ik}}]$, $h_{0_{ik}} \in \mathbb{R}_{\geq 0}$, $h_{1_{ik}} \in \mathbb{R}_{\geq 0}$, affects the information flow from node i to node k is assumed. Furthermore, the loss of information, e.g., due to package losses or link failures, is modeled via a dynamic communication network with switched communication topology, where $\mathcal{L}_\ell = \mathcal{L}(\mathcal{G}_\ell)$, see 2.3.3. It is also assumed that the delays between two connected nodes are not affected by the switches in topology.

To derive the closed-loop system representation of (2.2.8) and (4.2.1) with communication uncertainties, following [14], the matrices $L_{\ell,m}$, $m = 1,\ldots,2\bar{\mathcal{E}}$, $\bar{\mathcal{E}} = \max_{\ell=\sigma(t)\in\mathcal{M}} |\mathcal{E}_\ell|$, is introduced with nonzero entries $l_{\ell,m,ii} = 1$, $l_{\ell,m,ik} = -1$, if in the ℓ-th communication topology node i is connected to node k and all other entries are zero. Hence,

$$\mathcal{L}_\ell = \sum_{m=1}^{2\bar{\mathcal{E}}} L_{\ell,m}.$$

Furthermore, the vector $x = \mathrm{col}(P_m, P_s, p) \in \mathbb{R}^{3n}$ is defined as well as the matrices

$$T = \mathrm{blkdiag}(T_m, T_s, T_p), \quad \bar{A} = \mathrm{blkdiag}(A, A, A), \tag{4.2.3}$$

$$\Phi = \begin{bmatrix} I_n & -I_n & \mathbb{0} \\ \mathbb{0} & I_n & -I_n \\ -I_n & \mathbb{0} & I_n \end{bmatrix} \tag{4.2.4}$$

and

$$\Psi_{\ell,m} = \bar{A}\,\mathrm{blkdiag}\left(\mathbb{0}, \mathbb{0}, L_{\ell,m}\right)\bar{A}. \tag{4.2.5}$$

Then, by combining (2.2.8) with (4.2.1), the closed-loop dynamics with delays and dynamic communication network can be compactly written as

$$\begin{aligned}
\dot{\theta} &= \omega_r, \\
M\dot{\omega}_r &= -D\omega_r - \nabla U(\theta) - GV^2 + P_m^d + \begin{bmatrix} I_n & \mathbb{0}_{n\times 2n} \end{bmatrix} x, \\
T\dot{x} &= -\Phi x - \left(\sum_{m=1}^{2\bar{\mathcal{E}}} \Psi_{\ell,m} x(t-\tau_m)\right) - \begin{bmatrix} \mathbb{0} \\ K^{-1} \\ I_n - K^{-1} \end{bmatrix} \omega_r.
\end{aligned} \tag{4.2.6}$$

Remark 4.2.2. *The power system model employed in the related work [14] is derived under the assumptions that $\|T_m\|_p \ll \|M\|_p$ and $\|T_s\|_p \ll \|M\|_p$, see also* (4.2.3), *where $\|\cdot\|_p$ denotes a matrix p-norm. Then, by invoking singular perturbation arguments the slow dynamics corresponding to the turbine-governor system in* (4.2.6) *can be represented by their corresponding steady-state equations [12, 81]. However, even though these parameter assumptions are prevalent in the control community, for many practical power plants they are not satisfied, see, e.g., the examples in [24, 40] and in Section 4.4. As a consequence, the turbine-governor dynamics are usually modeled explicitly in* *the related power systems literature on load frequency control [36, 40, 48–51]. These facts are the main motivation to extend the analysis in [14] to the model* (4.2.6) *in the present work. Due to the resulting higher-order dynamics different coordinate transformation and reduction steps than those employed in [14] are required to construct a* strict *LKF for the system* (4.2.6)*. This problem is addressed in the next section.*

4.3 Robust stability in the presence of communication uncertainties

4.3.1 Coordinate transformation and reduction

In order to establish the main stability result, a coordinate transformation and reduction that are essential to construct the proposed strict LKF in Section 4.3.3 is introduced. This step is motivated by the following property of the matrix family

$$\Phi + \sum_{m=1}^{2\bar{\mathcal{E}}} \Psi_{\ell,m}, \quad \ell = \sigma(t) \in \mathcal{M},$$

which reveals an invariant subspace in the x-dynamics of the closed-loop power system model (4.2.6).

Lemma 4.3.1. *Consider the matrices* $\bar{A}$ *in* (4.2.3), Φ *in* (4.2.4) *and* $\Psi_{\ell,m}$ *in* (4.2.5)*. For any* $v \in \mathbb{R}^{3n} \setminus \{\alpha \bar{A}^{-1} \mathbb{1}_{3n}\}$, $\alpha \in \mathbb{R}$,

$$v^\top \left(\frac{1}{2} \left(\Phi + \Phi^\top \right) + \sum_{m=1}^{2\bar{\mathcal{E}}} \Psi_{\ell,m} \right) v > 0. \tag{4.3.1}$$

Proof. To establish the claim, it is convenient to write the symmetric part of Φ as

$$\begin{bmatrix} \tilde{\Phi}_{11} & \tilde{\Phi}_{12} \\ * & I_n \end{bmatrix} = \frac{1}{2} \left(\Phi + \Phi^\top \right),$$

with

$$\tilde{\Phi}_{11} = \begin{bmatrix} I_n & -\frac{1}{2}I_n \\ -\frac{1}{2}I_n & I_n \end{bmatrix}, \qquad \tilde{\Phi}_{12} = -\frac{1}{2}\begin{bmatrix} I_n \\ I_n \end{bmatrix}.$$

Clearly, $\tilde{\Phi}_{11} > 0$ and

$$I_n - \tilde{\Phi}_{12}^{\top}\tilde{\Phi}_{11}^{-1}\tilde{\Phi}_{12} = \mathbb{0}.$$

Hence, the Schur complement implies that $\frac{1}{2}\left(\Phi + \Phi^{\top}\right) \geq 0$ and since $\tilde{\Phi}_{11} > 0$, in addition, $v^{\top}\frac{1}{2}\left(\Phi + \Phi^{\top}\right)v > 0$ for all $v = \mathrm{col}(v_1, v_2, \mathbb{0}_n)$, $v_1 \in \mathbb{R}^n$, $v_2 \in \mathbb{R}^n$, $v \neq \mathbb{0}_{3n}$. Moreover, for any $\ell = \sigma(t) \in \mathcal{M}$, $\mathcal{L}_\ell$ is a Laplacian matrix of an undirected and connected graph. Hence,

$$v_3^{\top} A\mathcal{L}_\ell A v_3 > 0 \quad \forall\, v_3 \in \mathbb{R}^n \setminus \{\alpha A^{-1}\mathbb{1}_n\}, \quad \alpha \in \mathbb{R}.$$

The established facts imply that for any $\ell = \sigma(t) \in \mathcal{M}$, the matrix sum

$$\frac{1}{2}\left(\Phi + \Phi^{\top}\right) + \sum_{m=1}^{2\bar{\mathcal{E}}} \Psi_{\ell,m}$$

is positive semidefinite and that (4.3.1) is satisfied with equality if and only if $v_3 = \alpha A^{-1}\mathbb{1}_n$. In order for

$$\left(\frac{1}{2}\left(\Phi + \Phi^{\top}\right) + \sum_{m=1}^{2\bar{\mathcal{E}}} \Psi_{\ell,m}\right) v = \mathbb{0}_{3n}$$

to be satisfied for some $v = \mathrm{col}(v_1, v_2, v_3)$ with $v_3 = \alpha A^{-1}\mathbb{1}_n$, then v_1 and v_2 have to satisfy

$$\begin{aligned} v_1 - \frac{1}{2}v_2 - \alpha\frac{1}{2}A^{-1}\mathbb{1}_n &= \mathbb{0}_n, \\ -\frac{1}{2}v_1 + v_2 - \alpha\frac{1}{2}A^{-1}\mathbb{1}_n &= \mathbb{0}_n, \\ -\frac{1}{2}v_1 - \frac{1}{2}v_2 + \alpha A^{-1}\mathbb{1}_n &= \mathbb{0}_n. \end{aligned}$$

By using the second equation, v_2 can be expressed as

$$v_2 = \frac{1}{2}v_1 + \alpha\frac{1}{2}A^{-1}\mathbb{1}_n.$$

Moreover, by substituting the value of v_2 in the third equation, $v_1 = \alpha A^{-1}\mathbb{1}_n$ is obtained, which gives $v_2 = \alpha A^{-1}\mathbb{1}_n$, completing the proof. □□□

In light of Lemma 4.3.1 and inspired by [14, 29, 97], consider the change of coordinates

$$\begin{bmatrix} \bar{x} \\ \zeta_d \end{bmatrix} = \mathcal{W}_d^\top T^{\frac{1}{2}} x, \quad \mathcal{W}_d = \begin{bmatrix} W_d & \frac{1}{\sqrt{\mu}} T^{\frac{1}{2}} \bar{A}^{-1}\mathbb{1}_{3n} \end{bmatrix}, \tag{4.3.2}$$

where $W_d \in \mathbb{R}^{3n\times 3n-1}$, $\bar{A}$ is given in (4.2.3), $\mu_d = \|T^{\frac{1}{2}}\bar{A}^{-1}\mathbb{1}_{3n}\|_2^2$, W_d is chosen such that $W_d^\top T^{\frac{1}{2}}\bar{A}^{-1}\mathbb{1}_{3n} = \mathbb{0}_{3n-1}$ and the transformation matrix $\mathcal{W}_d \in \mathbb{R}^{3n\times 3n}$ is orthogonal, i.e., $\mathcal{W}_d\mathcal{W}_d^\top = I_{3n}$. Thus, $\bar{x}$ is a projection of x on the subspace orthogonal to $T^{\frac{1}{2}}\bar{A}^{-1}\mathbb{1}_{3n}$ scaled by $T^{\frac{1}{2}}$. The proposed change of coordinate in (4.3.2) has an advantage over the one in (3.3.1) that it permits the incorporation of higher-order dynamics.

From (4.3.2) we have that

$$\zeta_d(x) = \frac{1}{\sqrt{\mu_d}}\mathbb{1}_{3n}^\top \bar{A}^{-1} T^{\frac{1}{2}} T^{\frac{1}{2}} x = \frac{1}{\sqrt{\mu_d}}\mathbb{1}_{3n}^\top \bar{A}^{-1} T x. \tag{4.3.3}$$

Using (4.2.6) together with the fact $\mathbb{1}_{3n}^\top \bar{A}^{-1}\Phi_{\ell,m} = \mathbb{0}_{3n}$ leads to

$$\dot{\zeta}_d(x) = \frac{1}{\sqrt{\mu_d}}\mathbb{1}_{3n}^\top \bar{A}^{-1} T\dot{x} = -\frac{1}{\sqrt{\mu_d}}\mathbb{1}_n^\top A^{-1}\omega_r,$$

which by integrating with respect to time and recalling (4.2.6) and (4.3.3) yields

$$\zeta_d(x) = -\frac{1}{\sqrt{\mu_d}}\mathbb{1}_n^\top A^{-1}\theta + \zeta_{d_0}, \tag{4.3.4}$$

where

$$\zeta_{d_0} = \frac{1}{\sqrt{\mu_d}}\mathbb{1}_n^\top A^{-1}\theta_0 + \frac{1}{\sqrt{\mu_d}}\mathbb{1}_{3n}^\top \bar{A}^{-1}Tx_0.$$

Furthermore,

$$x = T^{-\frac{1}{2}}\mathcal{W}_d \begin{bmatrix} \bar{x} \\ \zeta_d \end{bmatrix} = T^{-\frac{1}{2}}W_d\bar{x} - \frac{1}{\mu_d}\bar{A}^{-1}\mathbb{1}_{3n}\left(\mathbb{1}_n^\top A^{-1}\theta - \mu_d\zeta_{d_0}\right).$$

Hence,

$$\dot{\bar{x}} = W_d^\top T^{\frac{1}{2}}\dot{x} = -W_d^\top T^{-\frac{1}{2}}\Phi T^{-\frac{1}{2}}W_d\bar{x} - W_d^\top T^{-\frac{1}{2}}\left(\sum_{m=1}^{2\bar{\mathcal{E}}}\Psi_{\ell,m}T^{-\frac{1}{2}}W_d\bar{x}(t-\tau_m)\right)$$
$$-W_d^\top T^{-\frac{1}{2}}\begin{bmatrix} \mathbb{0} \\ K^{-1} \\ I_n - K^{-1}\end{bmatrix}\omega_r,$$

where the facts $\Phi\bar{A}^{-1}\mathbb{1}_{3n} = \mathbb{0}_{3n}$ and $\Psi_{\ell,m}\bar{A}^{-1}\mathbb{1}_{3n} = \mathbb{0}_{3n}$ has been used.

By substituting ζ_d by (4.3.4), the overall closed loop system (4.2.6) can be expressed in the reduced order coordinates as

$$\begin{aligned}
\dot{\theta} =& \omega_r, \\
M\dot{\omega}_r =& -D\omega_r - \nabla U(\theta) - GV^2 + P_m^d + \begin{bmatrix} I_n & \mathbb{0}_{n\times 2n}\end{bmatrix}T^{-\frac{1}{2}}W_d\bar{x} \\
& -\frac{1}{\mu}A^{-1}\mathbb{1}_n(\mathbb{1}_n^\top A^{-1}\theta - \mu_d\zeta_{d_0}), \\
\dot{\bar{x}} =& -W_d^\top T^{-\frac{1}{2}}\Phi T^{-\frac{1}{2}}W_d\bar{x} - W_d^\top T^{-\frac{1}{2}}\begin{bmatrix} \mathbb{0} \\ K^{-1} \\ I_n - K^{-1}\end{bmatrix}\omega_r \\
& -W_d^\top T^{-\frac{1}{2}}\left(\sum_{m=1}^{2\bar{\mathcal{E}}}\Psi_{\ell,m}T^{-\frac{1}{2}}W_d\bar{x}(t-\tau_m)\right).
\end{aligned} \tag{4.3.5}$$

4.3.2 Error system

The following standard assumption is made on existence of a synchronous motion satisfying the usual security constraint on the stationary phase angle differences [14, 24, 28].

Assumption 4.3.2. *The system* (4.3.1) *possesses a synchronous motion* $col(\theta^s, \mathbb{0}_n, \bar{x}^s) \in \mathbb{R}^{5n-1}$, *such that*

$$|\theta_i^s - \theta_k^s| < \frac{\pi}{2} \quad \forall i \in \mathcal{N},\, \forall k \in \mathcal{N}_i.$$

With Assumption 4.3.2, the error states are defined as follows,

$$\tilde{\theta} = \theta - \theta^s, \quad \tilde{x} = \bar{x} - \bar{x}^s, \quad z = \mathrm{col}(\tilde{\theta}, \omega_r, \tilde{x}) \in \mathbb{R}^{5n-1}.$$

The dynamics (4.3.1) expressed in the error coordinates are given by

$$\begin{aligned}
\dot{\tilde{\theta}} &= \omega_r, \\
M\dot{\omega}_r &= -D\omega_r - \nabla U(\tilde{\theta}+\theta^s) + \nabla U(\theta^s) + \begin{bmatrix} I_n & \mathbb{0}_{n\times 2n} \end{bmatrix} T^{-\frac{1}{2}} W_d \tilde{x} - \frac{1}{\mu} A^{-1}\mathbb{1}_n^\top \mathbb{1}_n A^{-1}\tilde{\theta}, \\
\dot{\tilde{x}} &= -W_d^\top T^{-\frac{1}{2}} \Phi T^{-\frac{1}{2}} W_d \tilde{x} - W_d^\top T^{-\frac{1}{2}} \begin{bmatrix} \mathbb{0} \\ K^{-1} \\ I_n - K^{-1} \end{bmatrix} \omega_r \\
&\quad - W_d^\top T^{-\frac{1}{2}} \left(\sum_{m=1}^{2\bar{\mathcal{E}}} \Psi_{\ell,m} T^{-\frac{1}{2}} W_d \tilde{x}(t-\tau_m) \right).
\end{aligned} \tag{4.3.6}$$

Following the analysis in Chapter 3 and with Assumption 4.3.2, the system (4.3.6) has an equilibrium point z^s at the origin. Furthermore, asymptotic stability of z^s implies that any solution $\mathrm{col}(\theta, \omega_r, x)$ of the original system

(4.2.6) with an initial condition that satisfies

$$\zeta_{d_0} = \frac{1}{\sqrt{\mu_d}} \mathbb{1}_n^\top A^{-1} \theta_0 + \frac{1}{\sqrt{\mu_d}} \mathbb{1}_{3n}^\top \bar{A}^{-1} T x_0$$

converges to an equilibrium $\mathrm{col}(\theta^s, \mathbb{0}_n, x^s)$. This applies for any value of ζ_{d_0}. Moreover, the dynamics in (4.3.6) are independent of ζ_d. Consequently, z^s being asymptotically stable implies that all solutions of the original system (4.2.6) converge to an equilibrium point.

4.3.3 Main result

To present the main result, it is convenient to define the following two matrices

$$\bar{\Phi} = W_d^\top T^{-\frac{1}{2}} \Phi T^{-\frac{1}{2}} W_d, \tag{4.3.7}$$

$$\bar{\Psi}_{\ell,m} = W_d^\top T^{-\frac{1}{2}} \Psi_{\ell,m} T^{-\frac{1}{2}} W_d. \tag{4.3.8}$$

Note that Lemma 4.3.1 implies that $\bar{\Phi} + \sum_{m=1}^{2\bar{\mathcal{E}}} \bar{\Psi}_{\ell,m} > 0$, which is essential to derive a strict LKF for the dynamics (4.3.6) and, thus, establish the result below.

Proposition 4.3.3. *Consider the system* (4.3.6) *with Assumption 4.3.2. Fix A, K, $\mathcal{L}$, T and D as well as $h_{0_m} \in \mathbb{R}_{>0}$, $h_{1_m} \in \mathbb{R}_{>0}$, $m = 1, \ldots, 2\bar{\mathcal{E}}$. Suppose that for all $\Psi_{\ell,m}$ defined in* (4.3.8), *$\ell = 1, \ldots, |\mathcal{M}|$, there exist matrices $R_{1_m} > 0 \in \mathbb{R}^{(3n-1)\times(3n-1)}$, $S_{1_m} > 0 \in \mathbb{R}^{(3n-1)\times(3n-1)}$, $R_{2_m} > 0 \in \mathbb{R}^{(3n-1)\times(3n-1)}$, $S_{2_m} > 0 \in \mathbb{R}^{(3n-1)\times(3n-1)}$, $P > 0 \in \mathbb{R}^{(3n-1)\times(3n-1)}$, $P_2 \in \mathbb{R}^{(3n-1)\times(3n-1)}$, $P_3 \in \mathbb{R}^{(3n-1)\times(3n-1)}$, and $S_{12,m} \in \mathbb{R}^{(3n-1)\times(3n-1)}$ satisfying*

$$\mathcal{Q} = \begin{bmatrix} -D & \mathcal{Q}_{12} & \mathcal{Q}_{13} & \mathbb{0}_{n\times(3n-1)} & \mathbb{0}_{n\times(3n-1)} & \mathbb{0}_{n\times(3n-1)} \\ * & \mathcal{Q}_{22} & \mathcal{Q}_{23} & \mathcal{Q}_{24} & \mathcal{Q}_{25} & \mathbb{0}_{n\times(3n-1)} \\ * & * & \mathcal{Q}_{33} & \mathbb{0} & \mathcal{Q}_{35} & \mathbb{0}_{n\times(3n-1)} \\ * & * & * & \mathcal{Q}_{44} & R_2 - S_{12} & S_{12} \\ * & * & * & * & \mathcal{Q}_{55} & R_2 - S_{12} \\ * & * & * & * & * & -S_2 - R_2 \end{bmatrix} < 0, \tag{4.3.9}$$

where

$$
\begin{aligned}
&S_1 = blockdiag(S_{1_m}), \quad R_1 = blockdiag(R_{1_m}), \quad S_2 = blockdiag(S_{2_m}),\\
&R_2 = blockdiag(R_{2_m}), \quad S_{12} = blockdiag(S_{12_m}),\\
&\mathcal{Q}_{12} = \frac{1}{2}\begin{bmatrix} I_n & \mathbb{0}_{n\times 2n}\end{bmatrix} T^{-\frac{1}{2}}W_d - \begin{bmatrix}\mathbb{0} & K^{-1} & I_n - K^{-1}\end{bmatrix} T^{-\frac{1}{2}}W_d P_2,\\
&\mathcal{Q}_{13} = -\begin{bmatrix}\mathbb{0} & K^{-1} & I_n - K^{-1}\end{bmatrix} T^{-\frac{1}{2}}W_d P_3,\\
&\mathcal{Q}_{22} = -P_2^\top \bar{\Phi} - \bar{\Phi}^\top P_2 + \sum_{k=1}^{2\bar{\mathcal{E}}} S_{1_k} - \sum_{k=1}^{2\bar{\mathcal{E}}} R_{1_k},\\
&\mathcal{Q}_{23} = -\bar{\Phi}^\top P_3 + P - P_2^\top, \quad \mathcal{Q}_{24} = \begin{bmatrix} R_{0_1} \dots R_{0_{2m}}\end{bmatrix} \quad \mathcal{Q}_{25} = \begin{bmatrix}\bar{\mathcal{Q}}_{25,1} \dots \bar{\mathcal{Q}}_{25,2\bar{\mathcal{E}}}\end{bmatrix},\\
&\bar{\mathcal{Q}}_{25,m} = -P_2^\top \bar{\Psi}_{\ell,m}, \quad \mathcal{Q}_{33} = -P_3 - P_3^\top + \sum_{k=1}^{2\bar{\mathcal{E}}} h_{0_k}^2 R_{1_k} + \sum_{k=1}^{2\bar{\mathcal{E}}} (h_{1_k} - h_{0_k})^2 R_{2_k},\\
&\mathcal{Q}_{35} = \begin{bmatrix}\bar{\mathcal{Q}}_{35,1} \dots \bar{\mathcal{Q}}_{35,2\bar{\mathcal{E}}}\end{bmatrix}, \quad \bar{\mathcal{Q}}_{35,m} = -P_3^\top \bar{\Psi}_{\ell,m}, \quad \mathcal{Q}_{44} = -S_1 + S_2 - R_1 - R_2\\
&\mathcal{Q}_{55} = -2R_2 + S_{12} + S_{12}^\top
\end{aligned}
$$

as well as

$$
\begin{bmatrix} R_2 & S_{12} \\ * & R_2 \end{bmatrix} \geq 0. \tag{4.3.10}
$$

Then, for all $\tau_m(t) \in [h_{0_m}, h_{1_m}]$ *the origin is a locally uniformly asymptotically stable equilibrium point of the system* (4.3.6).

Proof. By noting that the delay only appears in $\tilde{x}$ and inspired by [14, 24, 26] consider the LKF with $\epsilon \in \mathbb{R}_{>0}$,

$$
\begin{aligned}
V &= V_1 + \sum_{m=1}^{2\bar{\mathcal{E}}} V_{2m},\\
V_1 &= \frac{1}{2}\omega_r^\top M \omega_r + U(\tilde{\theta} + \theta^s) - \nabla U(\theta^s)^\top \tilde{\theta} + \tilde{x}^\top P \tilde{x} + \epsilon \omega_r^\top M \mathbb{1}_n \mathbb{1}_n^\top A^{-1} \tilde{\theta}\\
&\quad + \frac{1}{2\mu}(\mathbb{1}_n^\top A^{-1}\tilde{\theta})^2 + \epsilon \omega_r^\top A M \left(\nabla U(\tilde{\theta} + \theta^s) - \nabla U(\theta^s)\right),\\
V_{2m} &= \int_{t-h_{0_m}}^{t} \tilde{x}^\top(s) S_{0_m} \tilde{x}(s) ds + \int_{t-h_{1_m}}^{t-h_{0_m}} \tilde{x}^\top(s) S_{1_m} \tilde{x}(s) ds\\
&\quad + h_{0_m} \int_{-h_{0_m}}^{0} \int_{t+\phi}^{t} \dot{\tilde{x}}^\top(s) R_{0_m} \dot{\tilde{x}}(s) ds d\phi
\end{aligned}
$$

$$+(h_{1_m}-h_{0_m})\int_{-h_{1_m}}^{-h_{0_m}}\int_{t+\phi}^{t}\dot{\tilde{x}}^\top(s)R_{1_m}\dot{\tilde{x}}(s)dsd\phi. \tag{4.3.11}$$

To establish the claim, it is first shown that the above LKF is locally positive definite. The gradient function of V_1 is given by

$$\nabla V_1=\begin{bmatrix}\nabla v_1\\ M\omega_r+\epsilon AM(\nabla U(\tilde{\theta}+\theta^s)-\nabla U(\theta^s))+\epsilon M\mathbb{1}_n\mathbb{1}_n^\top A^{-1}\tilde{\theta}\\ 2P\tilde{x}\end{bmatrix},$$

where

$$\nabla v_1=\nabla U(\tilde{\theta}+\theta^s)-\nabla U(\theta^s)+\epsilon\nabla^2U(\tilde{\theta}+\theta^s)^\top MA\omega_r+\frac{1}{\mu}(A^{-1}\mathbb{1}_n\mathbb{1}_n^\top A^{-1})\tilde{\theta}$$
$$+\epsilon A^{-1}\mathbb{1}_n\mathbb{1}_n^\top M\omega_r.$$

Clearly, at the origin $\nabla V_1|_{z^s}=\mathbb{0}_{5n-1}$. Moreover the Hessian of V_1 evaluated at z^s is given by

$$\nabla^2V_1|_{z^s}=\begin{bmatrix}\nabla^2v_{11} & \nabla^2v_{12} & \mathbb{0}_{n\times(3n-1)}\\ * & M & \mathbb{0}_{n\times(3n-1)}\\ * & * & 2P\end{bmatrix},$$

where

$$\nabla^2v_{11}=\nabla^2U(\theta^s)+\frac{1}{\mu}A^{-1}\mathbb{1}_n\mathbb{1}_n^\top A^{-1},$$
$$\nabla^2v_{12}=\epsilon AM\nabla^2U(\theta^s)+\epsilon M\mathbb{1}_n\mathbb{1}_n^\top A^{-1}.$$

Similar to the approach in the proof of the proposition 3.3.8, it is easy to show that all block-diagonal entries of $\nabla^2V_1|_{z^s}$ are positive definite. Moreover, S_{0_m}, S_{1_m}, R_{0_m} and R_{1_m} in V_{2m} are positive definite matrices. Therefore, z^s is a strict minimum of V.

Then the time derivatives of V_1 and V_{2m} are given by

$$\begin{aligned}
\dot{V}_1 =& -\omega_r^\top D\omega_r + \omega_r^\top \begin{bmatrix} I_n & \mathbb{0}_{n\times 2n} \end{bmatrix} T^{-\frac{1}{2}} W_d \tilde{x} + 2\dot{\tilde{x}}^\top P \tilde{x} + \epsilon\tilde{\omega}_r^\top AM\nabla^2 U(\tilde{\theta}+\theta^s)\tilde{\omega}_r \\
& - \epsilon\tilde{\omega}_r^\top DA\left(\nabla U(\tilde{\theta}+\theta^s) - \nabla U(\theta^s)\right) + \epsilon\tilde{\omega}_r^\top M\mathbb{1}_n\mathbb{1}_n^\top A^{-1}\tilde{\omega}_r \\
& - \epsilon\tilde{x}^\top W_d^\top T^{-\frac{1}{2}} \begin{bmatrix} I_n \\ \mathbb{0}_{2n\times n} \end{bmatrix} A\left(\nabla U(\tilde{\theta}+\theta^s) - \nabla U(\theta^s)\right) \\
& - \epsilon\left(\nabla U(\tilde{\theta}+\theta^*) - \nabla U(\theta^s)\right)^\top A\left(\nabla U(\tilde{\theta}+\theta^s) - \nabla U(\theta^s)\right) \\
& - \epsilon\tilde{\omega}_r^\top D\mathbb{1}_n\mathbb{1}_n^\top A^{-1}\tilde{\theta} - \epsilon\tilde{x}^\top W_d^\top T^{-\frac{1}{2}} \begin{bmatrix} I_n \\ \mathbb{0}_{2n\times n} \end{bmatrix} \mathbb{1}_n\mathbb{1}_n^\top A^{-1}\tilde{\theta} \\
& - \frac{\epsilon}{\mu}\tilde{\theta}^\top A^{-1}\mathbb{1}_n\mathbb{1}_n^\top A^{-1}\mathbb{1}_n\mathbb{1}_n^\top A^{-1}\tilde{\theta}, \\
\dot{V}_{2m} =& \tilde{x}^\top S_{0_m}\tilde{x} - \tilde{x}^\top(t-h_{0_m})(S_{0_m} - S_{1_m})\tilde{x}(t-h_{0_m}) - \tilde{x}^\top(t-h_{1_m})S_{1_m}\tilde{x}(t-h_{1_m}) \\
& + \dot{\tilde{x}}^\top\left(h_{0_m}^2 R_{0_m} + (h_m - h_{0_m})^2 R_{1_m}\right)\dot{\tilde{x}} - h_{0_m}\int_{t-h_{0_m}}^{t} \dot{\tilde{x}}^\top(s)R_{0_m}\dot{\tilde{x}}(s)ds \\
& - (h_{1_m} - h_{0_m})\int_{t-h_{1_m}}^{t-h_{0_m}} \dot{\tilde{x}}^\top(s)R_{1_m}\dot{\tilde{x}}(s)ds.
\end{aligned} \tag{4.3.12}$$

Furthermore, since (4.3.10) is satisfied by assumption, applying Jensen's inequality together with [26, Lemma 3.3], see 2.3.1.3, yields

$$\begin{aligned}
&-h_{0_m}\int_{t-h_{0_m}}^{t} \dot{\tilde{x}}^\top(s)R_{0_m}\dot{\tilde{x}}(s)ds \leq -\left[\tilde{x}(t) - \tilde{x}(t-h_{0_m})\right]^\top R_{0_m}\left[\tilde{x}(t) - \tilde{x}(t-h_{0_m})\right], \\
&-(h_{1_m} - h_{0_m})\int_{t-h_{1_m}}^{t-h_{0_m}} \dot{\tilde{x}}(s)^\top R_{1_m}\dot{\tilde{x}}(s)ds \leq -\eta_m^\top \begin{bmatrix} R_{1_m} & S_{12,m} \\ * & R_{1_m} \end{bmatrix} \eta_m,
\end{aligned} \tag{4.3.13}$$

where $\eta_m = \mathrm{col}(\tilde{x}(t-h_{0_m}) - \tilde{x}(t-\tau_m), \tilde{x}(t-\tau_m) - \tilde{x}(t-h_{1_m}))$
Next, the descriptor method is applied, see 2.3.1.4, i.e.,

$$0 = 2\left[\tilde{x}^\top P_2^\top + \dot{\tilde{x}}^\top P_3^\top\right] \left[-W_d^\top T^{-\frac{1}{2}} \begin{bmatrix} \mathbb{0} \\ K^{-1} \\ I_n - K^{-1} \end{bmatrix} \omega_r - W_d^\top T^{-\frac{1}{2}}\Phi T^{-\frac{1}{2}} W_d\tilde{x} \right.$$

$$-W_d^\top T^{-\frac{1}{2}}\left(\sum_{m=1}^{2\bar{\mathcal{E}}}\Psi_{\ell,m}T^{-\frac{1}{2}}W_d\tilde{x}(t-\tau_m)\right)-\dot{\tilde{x}}\Bigg]. \tag{4.3.14}$$

By summing over (4.3.13), adding (4.3.14) together with (4.3.12), and recalling $\bar{\Phi}$ in (4.3.7) and $\bar{\Psi}_{\ell,m}$ in (4.3.8), the following is obtained

$$\dot{V}\leq\xi^\top\left(\begin{bmatrix}\mathbb{0} & \mathbb{0}\\ * & \mathcal{Q}\end{bmatrix}+\epsilon\Xi_d\right)\xi, \tag{4.3.15}$$

where

$$\begin{aligned}&\xi=\mathrm{col}\left(\omega_r,\tilde{x},\dot{\tilde{x}},\xi_1,\xi_2\right),\quad \xi_1=\mathrm{col}\left(\tilde{x}(t-h_{0_1}),\ldots,\tilde{x}(t-h_{0_{2\bar{\mathcal{E}}}})\right),\\ &\xi_2=\mathrm{col}\left(\tilde{x}(t-\tau_1),\ldots,\tilde{x}(t-\tau_{2\bar{\mathcal{E}}})\right),\quad \xi_3=\mathrm{col}\left(\tilde{x}(t-h_{1_1}),\ldots,\tilde{x}(t-h_{1_{2\bar{\mathcal{E}}}})\right),\end{aligned}$$

$$\Xi_d=\begin{bmatrix}-A & \mathbb{0} & -\frac{1}{2}AD & -\frac{1}{2}A\begin{bmatrix}I_n & \mathbb{0}_{n\times 2n}\end{bmatrix}T^{-\frac{1}{2}}W_d & \mathbb{0} & \mathbb{0} & \mathbb{0}\\ * & -\frac{\kappa}{\mu}A^{-1} & -\frac{1}{2}D & -\frac{1}{2}\begin{bmatrix}I_n & \mathbb{0}_{n\times 2n}\end{bmatrix}T^{-\frac{1}{2}}W_d & \mathbb{0} & \mathbb{0} & \mathbb{0}\\ * & * & \frac{1}{2}E_{33} & \mathbb{0} & \mathbb{0} & \mathbb{0} & \mathbb{0}\\ * & * & * & \mathbb{0} & \mathbb{0} & \mathbb{0} & \mathbb{0}\\ * & * & \mathbb{0} & \mathbb{0} & \mathbb{0} & \mathbb{0} & \mathbb{0}\\ * & * & * & \mathbb{0} & \mathbb{0} & \mathbb{0} & \mathbb{0}\\ * & * & * & * & \mathbb{0} & \mathbb{0} & \mathbb{0}\\ * & * & * & * & * & \mathbb{0} & \mathbb{0}\\ * & * & * & * & * & * & \mathbb{0}\end{bmatrix},$$

where

$$E_{33}=AM\nabla^2U(\tilde{\theta}+\theta^s)+\nabla^2U(\tilde{\theta}+\theta^s)MA+M\mathbb{1}_n\mathbb{1}_n^\top A^{-1}+A^{-1}\mathbb{1}_n\mathbb{1}_n^\top M.$$

and $\mathcal{Q}$ is defined in (4.3.9).

Under the standing assumptions, $\mathcal{Q}<0$. Furthermore, the upper 2×2 block of Ξ_d is negative definite. Thus, by invoking [14, Lemma 11], it is concluded that the matrix sum in (4.3.15) is negative definite for some small

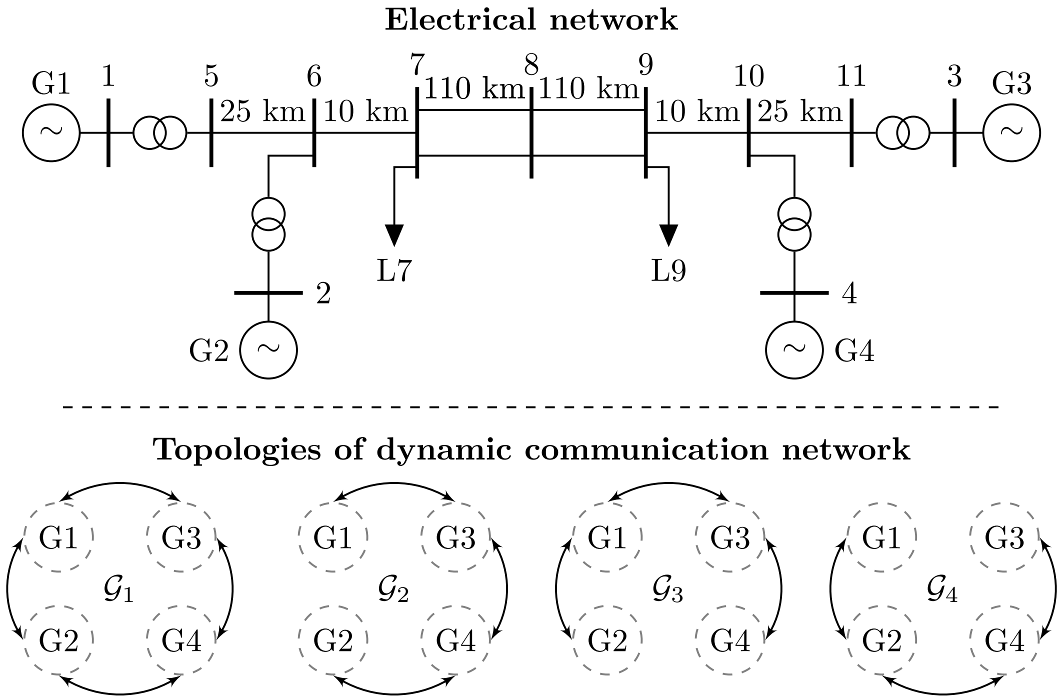

Figure 4.1: Kundur's two-area-four-machine test system taken from [1, Example 12.6] and the four employed topologies of the switched communication network.

$\epsilon > 0$. Consequently,

$$\dot{V} \leq -\nu \left(\|x\|_2^2\right)$$

for some (sufficiently small) $\epsilon \in \mathbb{R}_{>0}$ and $\nu \in \mathbb{R}_{>0}$. By invoking [26, Lemma 4.3], the origin of the system (4.3.6) is locally uniformly asymptotically stable.

□□□

Remark 4.3.4. *The proposed stability condition* (4.3.9)*,* (4.3.10) *is valid for any turbine-governor system that can be modeled as linear dynamics as long as Lemma 4.3.1 is satisfied.*

4.4 Numerical example

The efficacy of the stability condition in Proposition 4.3.3 is evaluated via a benchmark example based on Kundur's four-machine-two-area test system [1], see Fig. 4.1. This example has also been used in [14], where a related analysis is conducted for a power system model in which the generator dynamics are solely represented by the swing equation. The model used in [14] can be obtained from (4.2.6) by setting $T_m\dot{P}_m = T_s\dot{P}_s = \mathbb{0}_n$ for all $t \geq 0$, which yields

$$\begin{aligned} P_m &= -K^{-1}\omega + p, \\ T_p\dot{p} &= -I_n\omega_r - \sum_{m=1}^{2\bar{\mathcal{E}}} AL_{\ell,m}Ap(t-\tau_m), \end{aligned} \tag{4.4.1}$$

with angle and frequency dynamics as in (4.2.6).

The values of the main system parameters are given in [1] with $M = \mathrm{diag}(13.00, 13.00, 12.35, 12.35)$. The following modifications are made: damping coefficients $D_i = 2.3$ pu and droop gains $K_i = 0.05$ pu (with respect to the rated machine powers $S_{G,i} = [700, 700, 719, 700]$, $i = 1, \ldots, 4$). Also, the steam turbine is introduced as well as the governor time constants $T_m = \mathrm{diag}(0.125, 0.1, 0.125, 0.11)$ and $T_s = \mathrm{diag}(3.6, 1.8, 2.25, 4.5)$. Clearly, the assumption $\|T_s\|_p \ll \|M\|_p$ is not satisfied, see Remark 4.2.2. It is remarked that in the literature values for $T_{s,i}$ and $T_{m,i}$ up to $5-10$ s are reported [40, 50].

With regard to the communication uncertainties, four different communication topologies are considered, see Fig. 4.1. Furthermore, a fast-varying delay $\tau_m(t) = \tau(t)$ with $h_0 = 0.1\text{s} \leq \tau(t) \leq h_1 = 0.5$ s in (4.2.6) is considered. This delay is implemented as a piecewise continuous function with 2 ms sampling time.

The performance of the stability conditions given in Proposition 4.3.3 for the higher-order power system model (4.2.6) is compared with those derived in [14] for the reduced-order model (4.4.1) with $h_1 = 0$. To this end, as in [14], the controller time constants is set to $T_p = \frac{1}{0.05\kappa}A$, where $\kappa > 0$ is a free tuning parameter. For the given h_2, the maximum κ obtained via the stability conditions provided in [14] is $\bar{\kappa} = 16.0678$. Compared to this, the conditions of Proposition 4.3.3 are satisfied for $\hat{\kappa} = 0.902\bar{\kappa} = 14.4932$. This shows that the conditions of Proposition 4.3.3 do not introduce significant restrictions with regard to the admissible feedback gain, while they have the additional benefit of also guaranteeing stability in the presence of (non-passive) higher-order turbine-governor

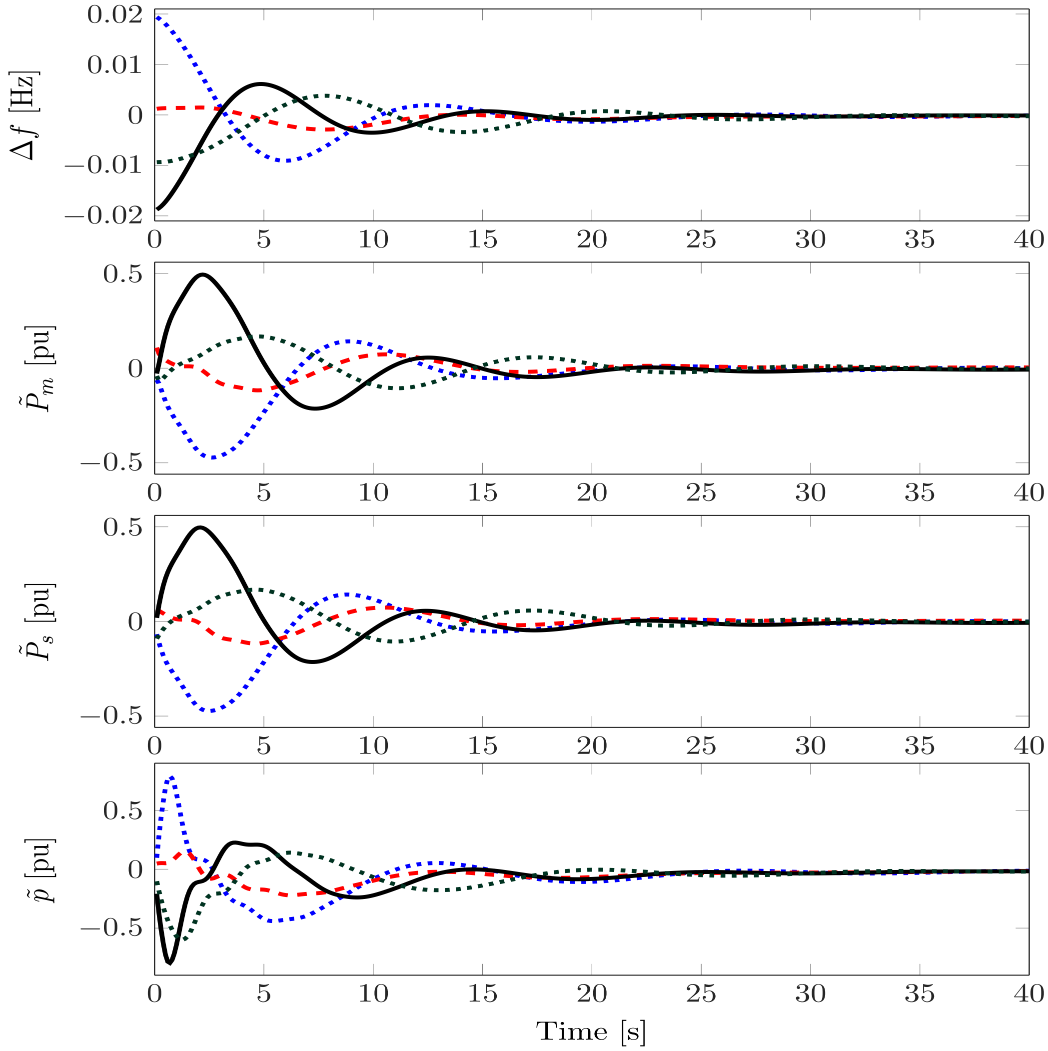

Figure 4.2: Simulation results with $\kappa = 17.4898$, $h_1 = 0.1s$, $h_2 = 0.5s$.

dynamics. Note that, even without delays or a switched communication network, disregarding these higher-order dynamics can lead to instability, see, e.g., the example in [24]. Furthermore, the proposed condition (4.3.9) with interval delays, is also compared with with [14]. By setting $h_0 = 0.1$s instead of $h_0 = 0$ and solving (4.3.9), the obtained result is $\hat{\kappa}_{inter} = 1.0843\bar{\kappa} = 17.4898$. This confirms that the proposed stability analysis with considering interval time-varying delays results in relatively improved stability conditions. The analysis is further confirmed in simulation. The results in Fig. 4.2 show that the system trajectories converge to an equilibrium point for $\kappa = 17.4898$ with $0.1\text{s} \leq \tau \leq 0.5$ s and the communication topologies are randomly switched every

5 s. Thus, despite the presence of communication uncertainties, the secondary frequency control objectives are achieved.

4.5 Summary

In this chapter, a robust stability analysis for a power system model with distributed consensus-based frequency control considering second-order turbine-governor dynamics, as well as heterogeneous fast-varying delays and time-varying communication topologies, has been performed. The analysis was conducted by introducing a novel coordinate transformation, which is instrumental to subsequently construct a strict LKF for the closed-loop power system dynamics. Moreover, both the LKF and the descriptor methods have been applied to develop robust stability conditions in the form of LMIs. The efficacy of the derived conditions has been illustrated via a numerical example. The example also shows that the proposed conditions, including the turbine-governor dynamics, do not result in more conservative result compare to the condition for the reduced-order model in [14].

Chapter 5

Delay-Robust Distributed Secondary Frequency Control: A Case Study

5.1 Introduction

The focus of the previous Chapter was on providing delay-robust stability conditions for consensus-based secondary frequency controllers. The standard practice in designing a secondary frequency controller and analysing the stability of the system is to use a reduced power system mode to provide a rigorous mathematical analysis [14, 23, 45, 65]. Furthermore, the numerical example provided in Chapter 4 was based on the reduced model, and it illustrated the effectiveness of the proposed robust stability conditions. However, when it comes to practical implementation, there is always the question of how the controller performs in the presence of unmodelled dynamics that have not been captured by the modelling assumptions used for the control design or stability analysis. Therefore, this chapter provides for the first time an extensive case study that evaluates the performance of a consensus-based secondary frequency control scheme on a realistic, full-detailed, medium-scale power system while explicitly considering communication delays

The employed model in this chapter consists of detailed models of SG with

Table 5.1: Comparison between the employed models in the control design and stability analysis and case study of this Chapter

Control design and stability analysis	**Case study**
Generator model (swing equation and turbine-governor dynamics)	Generator model (6^{th} order model with Exciter, AVR and PSS)
Kron-reduced model	Full network model
Lossless lines	Full π-model lines (lossy lines)
Decoupling between frequency and voltage dynamics (constant voltage)	Coupling between frequency and voltage dynamics (variable voltages)
–	Voltage sensitive loads

a full network model rather than the Kron-reduced model. Furthermore, the transmission lines are modeled as a π-model line with lossy lines. In addition, the voltage at all the buses is considered to be variable instead of constant, as considered for the case described in Chapter 4. Table 5.1 summarizes the differences between the employed model in the control design and stability analysis in Chapter 4 and the model described in this Chapter. Testing the delay-robust stability conditions in such a system is crucial in order to illustrate the efficacy of the conditions and the proposed assumptions.

Compared to related works [18, 28], the case study is not only limited to verify the steady-state frequency restoration with an economic dispatch but also explores the impact of communication delays as well as the interaction of the controller with unmodeled voltage phenomena.

5.2 Test system descriptions

In this Section, the well-known Nordic system is used [32], as sketched in Fig. 5.1. The system consists of three areas: North, Central, and South, with an equivalent external system connected to the North. It consists of 74 buses, 102 lines, and 42 transformers (20 of them equipped with On-Load Tap Changers). In addition, there are 20 generators throughout the system in which the North has hydro generation and the central/south has thermal generation, both of which are represented by dynamic synchronous machine models with relevant excitation, power system stabilisers and governors with

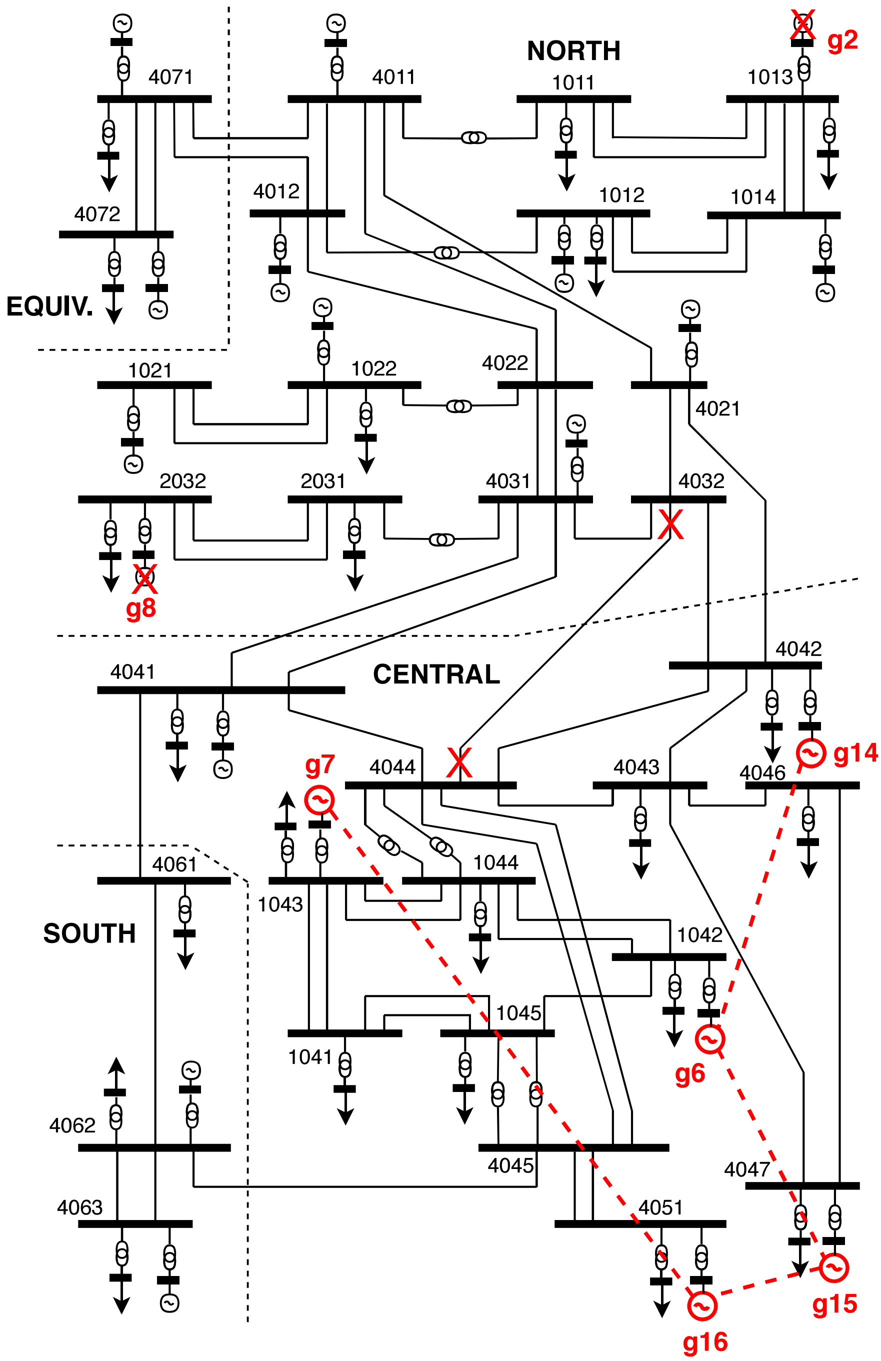

Figure 5.1: Schematic representation of the Nordic test system taken from [32]. The distributed control is implemented at five generators (g_6, g_7, g_{14}, g_{15}, and g_{16}). g_2 is used in case 1 and g_8 and branch 4032-4044 are used in cases 2 and 3, respectively.

varied parameters based on the generator type. Finally, the distribution loads are represented with voltage-sensitive, restorative models. All the dynamic models are detailed in [32]. An $N-1$ *insecure* operating point is used to analyze the controller performance. The primary frequency control is mainly carried out by the hydro generators in the North and Equiv areas (g_{20} is an equivalent generator and with a large participates the most in primary frequency control). Generator g_{13} is a synchronous condenser.

Two scenarios are considered in the case study presented in this Chapter:

- In the first scenario, consisting of Case 1, the effectiveness of the proposed delay-robust stability conditions in Chapter 4 (more specifically, Corollary 5.3.1) is tested. This is investigated by tripping a generator in the detailed dynamic system, leading to a frequency deviation, and checking the performance of the employed controller.

- The main purpose of the second scenario, consisting of Case 2 and Case 3, is to illustrate the interplay between the controller (4.2.1) and unmodelled voltage phenomena. This is implemented by tripping a large generator and losing a major corridor line.

5.3 Delay-robust stability condition

A constant uniform communication delay is considered with constant communication topology. Thus, by setting $\ell = 1$ in (4.3.8), the term in (4.3.8) can be rewritten as

$$\bar{\Psi} = W_d^\top T^{-\frac{1}{2}} \Psi T^{-\frac{1}{2}} W_d. \tag{5.3.1}$$

We then employ the following result for designing the gains of the controller in (4.2.6), the proof of which is given in Chapter 4.

Corollary 5.3.1. *Consider the system* (4.2.6)*. Fix* A*,* K*,* $\mathcal{L}$*,* T *and* D *as well as* $\tau \in \mathbb{R}_{>0}$*. Suppose that for all* $\bar{\Psi}$ *defined in* (5.3.1)*, there exist matrices* $R > 0 \in \mathbb{R}^{(3n-1)\times(3n-1)}$*,* $S > 0 \in \mathbb{R}^{(3n-1)\times(3n-1)}$*,* $P > 0 \in \mathbb{R}^{(3n-1)\times(3n-1)}$*,* $P_2 \in$

Table 5.2: The Participating generators

Generator No.	Location	Capacity (MW)
G_6	Central	468
G_7	Central	234
G_{14}	Central	819
G_{15}	Central	1404
G_{16}	Central	819

$\mathbb{R}^{(3n-1)\times(3n-1)}$, $P_3 > 0 \in \mathbb{R}^{(3n-1)\times(3n-1)}$ *satisfying*

$$\mathcal{Q}_d = \begin{bmatrix} -D & \mathcal{Q}_{d12} & \mathcal{Q}_{d13} & \mathbb{0}_{n\times(3n-1)} \\ * & \mathcal{Q}_{d22} & -\bar{\Phi}^\top P_3 + P - P_2^\top & R - P_2^\top \bar{\Psi} \\ * & * & -P_3 - P_3^\top + R & -P_3^\top \bar{\Psi} \\ * & * & * & -S - R \end{bmatrix} < 0, \tag{5.3.2}$$

where

$$\mathcal{Q}_{d12} = \frac{1}{2}\begin{bmatrix} I_n & \mathbb{0}_{n\times 2n} \end{bmatrix} T^{-\frac{1}{2}} W_d - \begin{bmatrix} \mathbb{0} & K^{-1} & I_n - K^{-1} \end{bmatrix} T^{-\frac{1}{2}} W_d P_2,$$
$$\mathcal{Q}_{d13} = -\begin{bmatrix} \mathbb{0} & K^{-1} & I_n - K^{-1} \end{bmatrix} T^{-\frac{1}{2}} W_d P_3, \qquad \mathcal{Q}_{d22} = -P_2^\top \bar{\Phi} - \bar{\Phi}^\top P_2 + S - R.$$

Then, the equilibrium point col$(\theta^s, \mathbb{0}_n, x^s) \in \mathbb{R}^{5n}$ *is locally uniformly asymptotically stable of the system* (4.3.6).

5.4 Implementation of secondary frequency controller

In this section, the gain of the distributed secondary frequency controller (4.2.1) for the described test system is chosen based on 5.3. The distributed control is implemented at five of the thermal generators in the Central area (g_6, g_7, g_{14}, g_{15}, and g_{16}) with the modified TGOV1 governor described by (2.2.6) and (4.2.1). Table 5.2 shows the information about the participating generators.

Moreover, for the communication network topology shown in Fig. 5.1 and a maximum communication delay of 200 ms, the controller parameters T_p

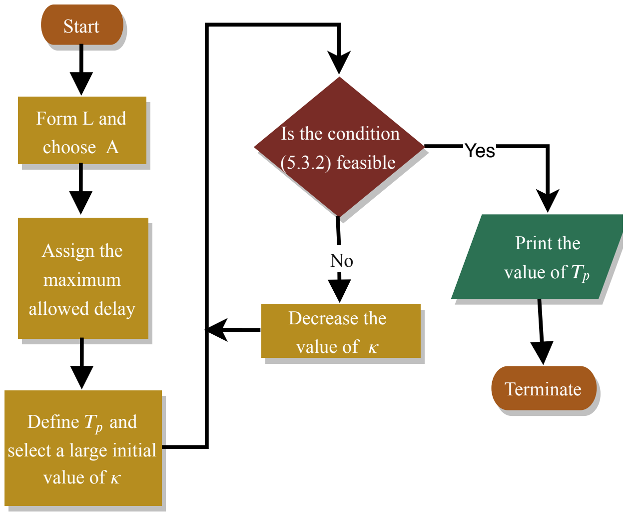

Figure 5.2: Flowchart of selection of the controller's parameters.

are selected as follows. First, the matrix $\mathcal{L}$ in (4.2.1) is formed based on the communication network topology and the matrix A in (4.2.1) is selected based on the generator marginal costs. Then, the controller time constants are defined as $T_p = \frac{1}{0.04\kappa}A$, where 0.04 is the droop gain for the primary control, $\kappa \in \mathbb{R}_{>0}$ is a tuning parameter and the communication delay is set to the maximum allowed $\tau = 200$ms. Then, we select a large initial value of κ (that is, a small T_p and fast-acting controller) and decrease its value until the the conditions (5.3.2) become feasible. This procedure gives us the fastest acting controller that satisfies the delay-robustness conditions. This process is summarised by the flowchart in Fig. 5.2. Moreover, this choice of T_P allows that generators with small cost coefficients (i.e., small A_{ii}) will react faster than the ones with large cost coefficients (i.e., large A_{ii}). Fig. 5.3 provides a feasibility map of the stability analysis conditions in (5.3.2) for the specific test system for different time delays and tuning parameter κ. The conditions are feasible in the shaded regions.

The feasibility of the analysis conditions (5.3.2) were implemented in MATLAB using Yalmip [107] and Mosek [110] while all the dynamic simulations below were carried out using the simulation software RAMSES [33].

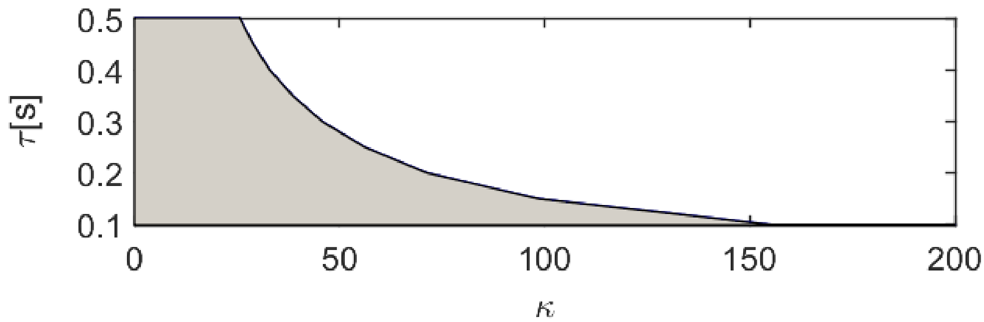

Figure 5.3: The feasibility map of condition (4.3.9) with different maximum communication delays.

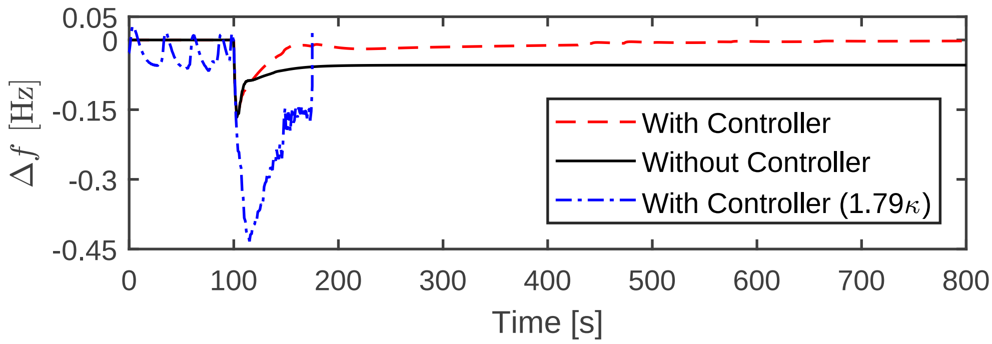

Figure 5.4: Case 1: Frequency deviation

5.4.1 Case 1: Tripping of 300MW generator g_2 in the North area

In this case, the 300MW thermal generator g_2 is tripped at $t = 100$s in the North area. This results in a load-generation unbalance hence leads to the frequency deviating from its nominal value ($\Delta\omega$). Consequently, the primary frequency response and the distributed secondary frequency controller from the participated generators are triggered. The frequency response is shown in Fig. 5.4, both with and without the proposed secondary frequency controller. It can be seen that in both variants the system is stable after the primary responses. The plot of the frequency without the controller (4.2.1) shows the frequency does not return to its nominal value. The proposed controller quickly restores the frequency to its nominal value, as desired.

Furthermore, to investigate the conservativeness of the proposed condition in Corollary 5.3.1, the value of κ, i.e. the response speed of the controller, is

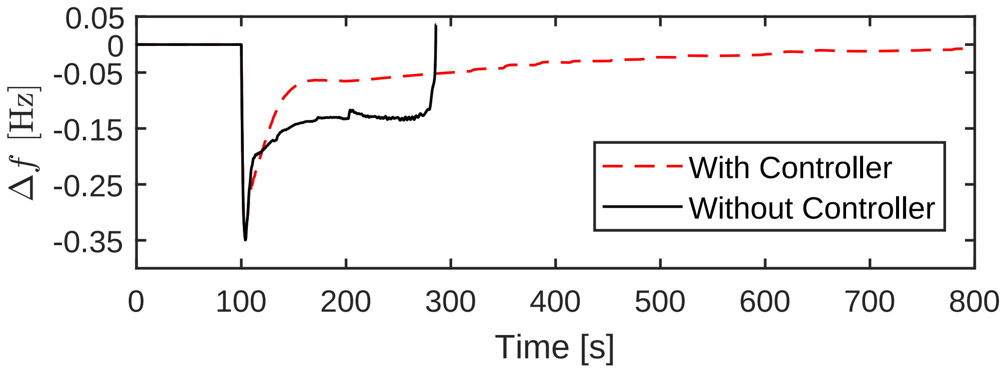

Figure 5.5: Case 2: Frequency deviation

increased, while the value of the communication delays $\tau = 200$ms is fixed. The performance of the system starts to significantly deteriorate from $\hat{\kappa} = 1.68\kappa$ until the system completely collapses at $\hat{\kappa} = 1.79\kappa$, as shown in Fig. 5.4. It is observed that the conditions in Proposition 5.3.1 are rather conservative for the considered scenario. Yet as discussed in [14], this may be explained by the fact that the conditions in Corollary 5.3.1 are equilibrium-independent and, hence, they are more conservative for equilibria with smaller phase angle differences (which is the case in the present scenario), but fairly accurate if the equilibrium phase angle differences are larger.

5.4.2 Case 2: Tripping of 750MW generator g_8 in the North area

Similar to the previous case, this case tests the controller when a larger thermal generator, g_8, with an active power production of 750MW, is tripped in the North area of the system at $t = 100$s. Due to the larger generator size, this will lead to a system collapse at $t \approx 240$s without additional control as shown in Fig. 5.5. The generation lost in the North causes depressed voltages in the Central area. As the voltages are restored (due to the combined effect of generator automatic voltage regulator (AVR) and on load tap changerss (OLTCs) actions), so is the load power consumption. The combined effect leads to a long-term voltage collapse [111], as shown in Fig. 5.6. Furthermore, Fig. 5.7 illustrates that there is an initial spike of increased power production during the primary reserves, followed by loss of power and a subsequent system

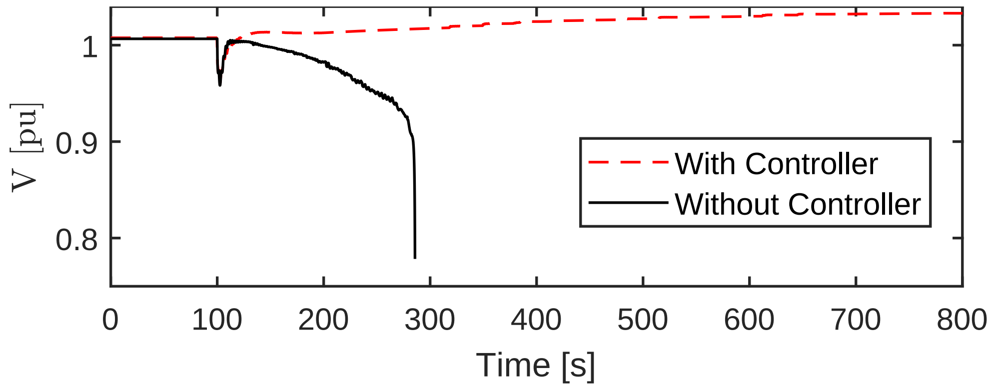

Figure 5.6: Case 2: Bus voltage deviation at bus 1044 in Central area

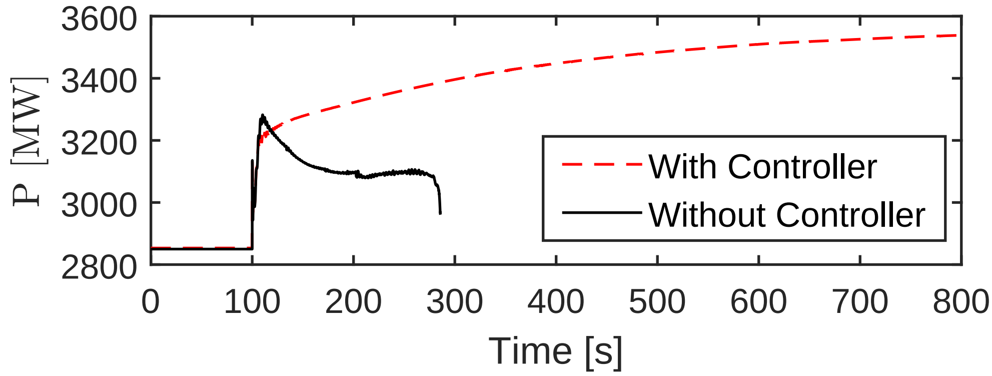

Figure 5.7: Case 2: Total active power output from the participating generators

collapse. The mechanism is detailed in [32].

When the secondary frequency controller is used, the active power injected in the Central area as a response to the under-frequency deviation, stabilises the system and restores the frequency to its nominal value, as shown in Fig. 5.5. This can also be seen in Fig. 5.7 wherein the total active power output of the generators participating in the secondary frequency control is shown.

As discussed in Chapter 4, the purpose of the controller (4.2.1) is to restore the frequency to its nominal value and ensure economic optimality. Fig. 5.8 shows the controller exchanged variables reaching consensus (identical marginal costs) in steady state after small deviations (see Fig. 5.8, zoom) immediately after the disturbance.

5.4.3 Case 3: Loss of major corridor line

In the considered test system, active power is transferred from the North area (where most of the generators are located) to the Central area (where most of

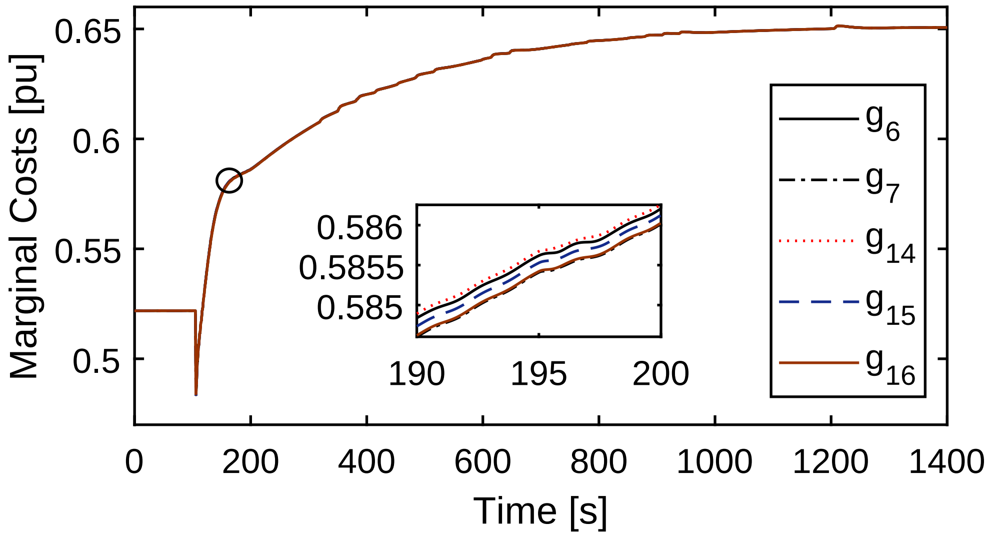

Figure 5.8: Case 2: Convergence of controller outputs

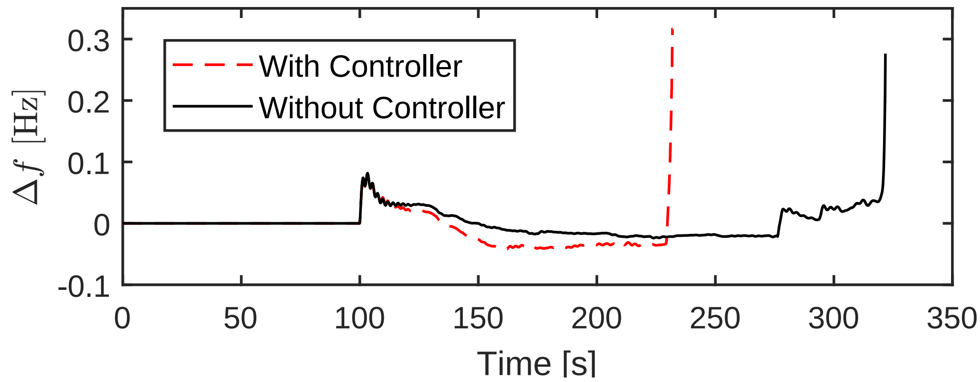

Figure 5.9: Case 3: Frequency deviation

the load is located). In this case, branch 4032-4044 located in the main corridor linking the Central and the North areas of the system is tripped. This event limits the ability of the transmission system to evacuate power to the Central area. This leads to a surplus of power in the North and a deficiency in the Central area resulting in an initial over-frequency (see Fig. 5.9) accompanied with depressed voltages in the Central area (see Fig. 5.10). Thereafter, the voltages in the Central area start being restored (along with the load power demand) and the frequency decreases below the nominal value.

Case 3 leads to a long-term voltage collapse, driven by the load restoration and the generator over-excitation limits. However, it can be seen from Figs. 5.9 and 5.10 that the proposed controller accelerates the system collapse.

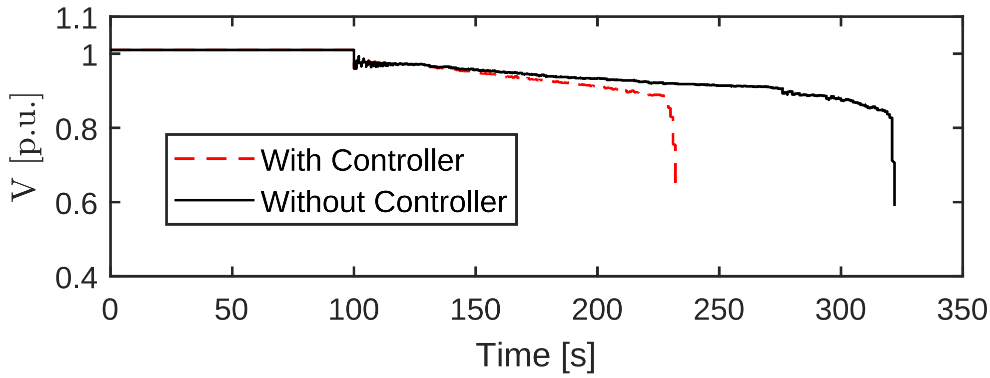

Figure 5.10: Case 3: Bus voltage of bus 1044 in Central area

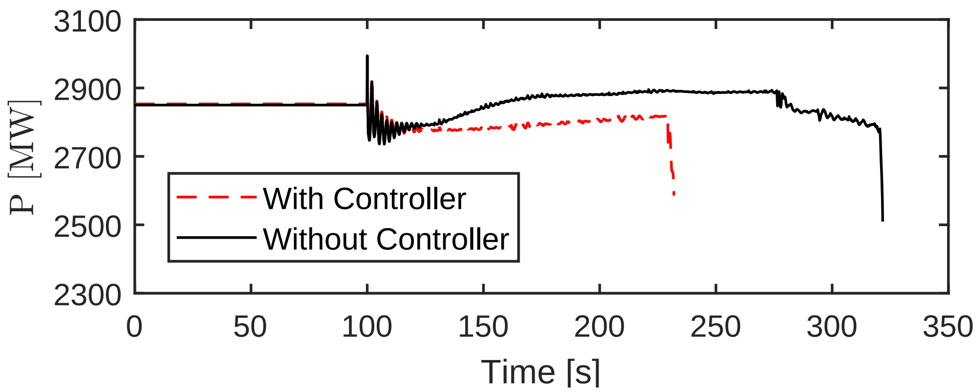

Figure 5.11: Case 3: Total active power output from the participating generators

The reason for the accelerated collapse is that the secondary controller reacts to the initial over-frequency by reducing the output power of the participating generators. Therefore, the power injected in the Central area is reduced, leading to a further reduction in bus voltages and thus accelerating the system collapse. Fig. 5.11 shows the total active power output of the generators participating in the secondary frequency control.

5.4.4 Discussion and summary

The three cases above show the performance of the proposed controller under different operating conditions. In Case 1, a frequency problem is initiated due to the tripping of a generator. In this case, the dynamics are dominated by the generator and governor frequency response (2.2.8) and the behaviour of the controller is exemplar. Furthermore the delay-robust stability conditions derived in Chapter 4 and employed in the present Chapter (see Corollary 5.3.1) have proven to be very effective in this scenario, despite the presence of unmodelled system dynamics.

In Cases 2 and 3, the frequency dynamics initiated by the disturbance strongly interact with the long-term voltage dynamics driven by the load restoration mechanisms and the generator limits, leading to a complex dynamical interplay. This voltage-driven behaviour is not modelled in the controller analysis and, as the case study reveals, results in unforeseen system behaviour. In Case 2, the long-term voltage dynamics coincide with an under-frequency excursion, thus the controller response supports the system restoration by injecting more active power in the Central area. On the contrary, the behaviour of the controller in Case 3 leads to an accelerated system collapse due to the over-frequency excursion right after the disturbance that reduces the power injected in the Central area, thus further depressing the voltages.

Overall the presented case study analysis demonstrates that the proposed consensus-based secondary frequency control law (4.2.1) provides a flexible alternative to the standard AGC with the advantages of a fully distributed implementation and of combining frequency restoration with economic dispatch in real-time. The latter property may, e.g., also be used to enable peer-to-peer electricity markets [112].

However, the present investigations show that the decoupling assumption between frequency and voltage dynamics can degrade the system's performance in pronounced voltage dynamics following a disturbance. This decoupling assumption, which is usually invoked when designing secondary frequency controllers [24, 28, 35, 42, 113] is made based on the physical weak coupling between the power and the voltage [1]. Nevertheless, in some systems, such as the given case study, this assumption can be violated. It is thus essential to be cautious when implementing the controller without considering such additional dynamics, in order to avoid deteriorating the overall system stability.

Chapter 6

General Conclusions

6.1 Summary of work and main contributions

Consensus algorithms are promising control schemes for secondary frequency control in next generation power systems. In this thesis, stability analysis and controller synthesis for delay-robust consensus-based secondary frequency controller were proposed and evaluated. The main contributions are summarized below:

- Chapter 3 jointly addressed the challenges of communication efforts, disturbance attenuation and robustness with respect to time delays. A design approach for a consensus-based secondary frequency controller in MGs was proposed that guarantees robustness with respect to uniform and heterogeneous fast-varying delays and simultaneously permits to trade off finite L_2-gain performance against the sparsity of the required communication network. More precisely, both the LKF and the descriptor methods were applied to develop a controller synthesis in the form of a constraint convex optimization problem. The proposed synthesis guarantees uniform local asymptotic stability for any operating point satisfying the usual safety requirement of the equilibrium phase angle differences being contained in an arc of length $\frac{\pi}{2}$. Furthermore, the relevance of the provided weighting parameters on the resulting closed-loop behaviour was illustrated via a two-step design case study based on the CIGRE benchmark MV distribution network. The numerical results show that the proposed approach can be used to identify minimal communication topologies, while at the same time guaranteeing desired delay robustness and disturbance attenuation properties. In addition, it was explained how the weighting factors have to be chosen to facilitate a trade-off between the L_2-performance and the required communication efforts.

- The work in Chapter 3 was directed toward the MG model wherein, the DGU dominates the generation units; in this case, a reduced-model limited to swing equation was employed. In Chapter 4, the delay robust stability conditions were proposed where second-order turbine-governor dynamics, heterogeneous fast-varying delays, and time-varying communication topologies were considered. This was addressed first by employing a novel coordinate transformation, which was instrumental in a subsequently construction of a strict LKF for the closed-loop power system dynamics. Then, similar to the description provided in the previous Chapter 3, both the LKF and descriptor methods were applied to develop robust stability conditions in the form of LMIs.

- Chapter 5 further investigated the performance of a consensus-based secondary frequency control via a case study on a detailed dynamic model of the Nordic test system. Two main aspects of interest were the robustness with respect to communication delays and unmodelled (voltage and higher-order generator) dynamics. Therefore, the controller was designed according to the delay-robust stability conditions derived in Chapter 4. It was found that in the event of generator outages, steady-state frequency restoration was achieved in an optimal manner also in the presence of communication delays and unmodelled dynamics. Thus, it was deduced that the conditions proposed in Chapter 4 were efficient. However, it was also shown that when complex voltage dynamics – not modelled in the control analysis phase – dominate the system behaviour, the controller might behave in an unexpected manner (stabilising or accelerating the system collapse).

6.2 Directions for future work

Possible extensions of the present PhD thesis are briefly described below:

- The proposed theoretical analysis in Chapters 3 and 4 is based on the standard assumptions in secondary frequency control. One of these assumptions is constant voltage at all the buses. However, the assumption of constant voltage could lead to deteriorate the overall performance as showed in Chapter 5. Thus, an extension of this study should investigate relaxing this assumption and considering the voltage dynamics in the controller design stage that might affect the controller and further complicate the controller developments. In addition to considering voltage dynamics, generator location and network topology also constitute important aspects to improve the system resilience and robustness against complex dynamic phenomena further.

- The reduced model in Chapter 3 is limited to a swing equation to incorporate both generation units: SG and converter-based unit. Thus, an interesting extension is to consider a high-order model consisting of the converter-based unit with all the controller dynamics, combined with SGs using the model employed in chapter 4. The latter also leads to complication of the stability condition and the controller synthesis.

- The work in this thesis is assuming the same communication delay affects both local and transmitted signals in the secondary frequency controller. Therefore, a possible extension of this work is to consider a more practical model to study the impact of the communication delays where these delays affect the transmitted signal through the communication network, with no impact of time delays on local information [114–116]. By using the definition of the Laplacian matrix in (2.3.24), the controller dynamics in (3.2.3) and (4.2.1) can be expressed as

$$\begin{aligned} \dot{p} &= K(\omega - \mathbb{1}_n\omega^d) - KQ\mathcal{D}Qp + KQ\mathcal{A}Qp(t-\tau(t)), \\ T_p\dot{p} &= -p + P_m - (1-K^{-1})\omega_r - Q\mathcal{D}Qp + Q\mathcal{A}Qp(t-\tau(t)). \end{aligned} \tag{6.2.1}$$

Then, the coordinate transformation and reductions in (3.3.1) and (4.3.2) are not usefull any more. This will lead to complicate the stability analysis and the controller synthesis. Investigating this new approach to tackle the problem and building up a new LKF jointly constitute a promising field of research.

- Another relevant direction for future research is the extension of the case study described in Chapter 5. This can be achieved by implementing a realistic communication layer with heterogeneous time-varying communication delays and investigating the performance of the controller under cyber-attacks. These aspects were not considered in the case study, and they critically rely on the existence of reliable data on the communication infrastructure. In addition, a comprehensive comparison between the performance of the distributed consensus based controller with the standard centralized AGC under communication delays is an interesting extension of the case study. This would require a similar approach of delay-robust stabiity conditions in Chapter 4 to be implemented in the case of AGC to achieve similar tuning criteria.

- The design procedure of the distributed secondary frequency controller in MG, in Chapter 3, was evaluated through simulation analysis. It is of interest to extend the results to validate the proposed design criterion experimentally.

- Another extension of the proposed work is to further investigate the applications of time-delay stability analysis and control design in MG and bulk power system. A well-known application is wide-area control in low-inertia power system. The effect of communication delays appears when the information flows from the i-th node to the WAMC center and vice versa. Therefore, the proposed approach explained in this work is considered a powerful tool to tackle this problem.

Bibliography

[1] P. Kundur, *Power system stability and control.* McGraw-Hill, 1994.

[2] M. A. El-Sharkawi, *Electric energy: an introduction.* CRC press, 2012.

[3] T. Garrity, "Getting smart," *IEEE Power and Energy Magazine*, vol. 6, pp. 38–45, March 2008.

[4] J. Machowski, J. Bialek, and J. Bumby, *Power system dynamics: stability and control.* J.Wiley & Sons, 2008.

[5] H. Farhangi, "The path of the smart grid," *IEEE Power and Energy Magazine*, vol. 8, pp. 18–28, January 2010.

[6] E. Santacana, G. Rackliffe, L. Tang, and X. Feng, "Getting smart," *IEEE Power and Energy Magazine*, vol. 8, pp. 41–48, March 2010.

[7] F. Milano, F. Dörfler, G. Hug, D. J. Hill, and G. Verbič, "Foundations and challenges of low-inertia systems (invited paper)," in *2018 Power Systems Computation Conference (PSCC)*, pp. 1–25, June 2018.

[8] U. Markovic, O. Stanojev, E. Vrettos, P. Aristidou, D. Callaway, and G. Hug, "Understanding Stability of Low-Inertia Systems," (in preparation).

[9] W. Winter, K. Elkington, G. Bareux, and J. Kostevc, "Pushing the limits: Europe's new grid: Innovative tools to combat transmission bottlenecks and reduced inertia," *IEEE Power and Energy Magazine*, vol. 13, pp. 60–74, Jan 2015.

[10] T. Green and M. Prodanovic, "Control of inverter-based micro-grids," *Electric Power Systems Research*, vol. Vol. 77, pp. 1204–1213, july 2007.

[11] J. D. Glover, M. S. Sarma, and T. J. Overbye, *Power system analysis and design*. Cengage Learning, 2011.

[12] J. Schiffer, D. Zonetti, R. Ortega, A. M. Stanković, T. Sezi, and J. Raisch, "A survey on modeling of microgridsâ€"from fundamental physics to phasors and voltage sources," *Automatica*, vol. 74, pp. 135–150, 2016.

[13] J. A. P. Lopes, A. G. Madureira, and C. C. L. M. Moreira, "A view of microgrids," *Wiley Interdisciplinary Reviews: Energy and Environment*, vol. 2, no. 1, pp. 86–103, 2013.

[14] J. Schiffer, F. Dörfler, and E. Fridman, "Robustness of distributed averaging control in power systems: Time delays & dynamic communication topology," *Automatica*, vol. 80, pp. 261–271, 2017.

[15] J. Guerrero, J. Vasquez, J. Matas, L. de Vicuna, and M. Castilla, "Hierarchical control of droop-controlled AC and DC microgrids; a general approach toward standardization," *IEEE Transactions on Industrial Electronics*, vol. 58, no. 1, pp. 158 –172, 2011.

[16] N. Grid, "System operability framework 2016," *National Grid*, 2016.

[17] F. Dörfler, S. Bolognani, J. W. Simpson-Porco, and S. Grammatico, "Distributed control and optimization for autonomous power grids," in *2019 18th European Control Conference (ECC)*, pp. 2436–2453, June 2019.

[18] C. Zhao, E. Mallada, S. H. Low, and J. Bialek, "Distributed plug-and-play optimal generator and load control for power system frequency regulation," *International Journal of Electrical Power & Energy Systems*, vol. 101, pp. 1 – 12, 2018.

[19] D. K. Molzahn, F. Dörfler, H. Sandberg, S. H. Low, S. Chakrabarti, R. Baldick, and J. Lavaei, "A survey of distributed optimization and control algorithms for electric power systems," *IEEE Transactions on Smart Grid*, vol. 8, no. 6, pp. 2941–2962, 2017.

[20] G. Strbac, N. Hatziargyriou, J. P. Lopes, C. Moreira, A. Dimeas, and D. Papadaskalopoulos, "Microgrids: Enhancing the resilience of the European megagrid," *IEEE Power and Energy Magazine*, vol. 13, no. 3, pp. 35–43, 2015.

[21] Q. Yang, J. A. Barria, and T. C. Green, "Communication infrastructures for distributed control of power distribution networks," *IEEE Transactions on Industrial Informatics*, vol. 7, no. 2, pp. 316–327, 2011.

[22] J. Schiffer, *Stability and power sharing in microgrids.* PhD thesis, Technische Universität Berlin, 2015.

[23] A. Kasis, N. Monshizadeh, and I. Lestas, "Secondary frequency control with on-off load side participation in power networks," *IEEE Transactions on Control of Network Systems*, pp. 1–1, 2019.

[24] S. Trip and C. De Persis, "Distributed optimal load frequency control with non-passive dynamics," *IEEE Transactions on Control of Network Systems*, vol. 5, no. 3, pp. 1232–1244, 2018.

[25] E. Fridman, "Tutorial on Lyapunov-based methods for time-delay systems," *Europ. Journal of Control*, vol. 20, no. 6, pp. 271–283, 2014.

[26] E. Fridman, *Introduction to time-delay systems: analysis and control.* Birkhäuser, 2014.

[27] S. Boyd, L. El Ghaoui, E. Feron, and V. Balakrishnan, *Linear matrix inequalities in system and control theory*, vol. 15. Siam, 1994.

[28] A. Kasis, N. Monshizadeh, and I. Lestas, "A novel distributed secondary frequency control scheme for power networks with high order turbine

governor dynamics," in *European Control Conference (ECC)*, pp. 2569–2574, 2018.

[29] R. Olfati-Saber and R. M. Murray, "Consensus problems in networks of agents with switching topology and time-delays," *IEEE Transactions on Automatic Control*, vol. 49, no. 9, pp. 1520–1533, 2004.

[30] J. Hespanha, P. Naghshtabrizi, and Y. Xu, "A survey of recent results in networked control systems," *Proceedings of the IEEE*, vol. 95, no. 1, pp. 138–162, 2007.

[31] R. Olfati-Saber, J. A. Fax, and R. M. Murray, "Consensus and cooperation in networked multi-agent systems," *Proceedings of the IEEE*, vol. 95, no. 1, pp. 215–233, 2007.

[32] T. Van Cutsem, M. Glavic, W. Rosehart, J. Andrade dos Santos, C. Cañizares, M. Kanatas, L. Lima, F. Milano, L. Papangelis, R. Andrade Ramos, *et al.*, "Test systems for voltage stability analysis and security assessment," tech. rep., IEEE, 2015.

[33] P. Aristidou, D. Fabozzi, and T. Van Cutsem, "Dynamic simulation of large-scale power systems using a parallel schur-complement-based decomposition method," *IEEE Transactions on Parallel and Distributed Systems*, vol. 25, no. 10, pp. 2561–2570, 2014.

[34] Q. Zhu, W. Yao, L. Jiang, C. Luo, and Q. H. Wu, "Load frequency control with dynamic demand control for deregulated power system," in *2014 IEEE PES General Meeting — Conference Exposition*, pp. 1–5, July 2014.

[35] L. Jiang, W. Yao, Q. Wu, J. Wen, S. Cheng, *et al.*, "Delay-dependent stability for load frequency control with constant and time-varying delays," *IEEE Transactions on Power Systems*, vol. 27, no. 2, p. 932, 2012.

[36] H. Bevrani and T. Hiyama, “A control strategy for LFC design with communication delays,” in *2005 International Power Engineering Conference*, pp. 1087–1092 Vol. 2, Nov 2005.

[37] X. Li, R. Wang, and L. Jiang, “Stability analysis of load frequency control for power systems with large delay periods based on switching technique,” in *2015 American Control Conference (ACC)*, pp. 1101–1106, July 2015.

[38] L. Jin, C. Zhang, Y. He, L. Jiang, and M. Wu, “Delay-dependent stability analysis of multi-area load frequency control with enhanced accuracy and computation efficiency,” *IEEE Transactions on Power Systems*, vol. 34, pp. 3687–3696, Sep. 2019.

[39] C. Duan, C. Zhang, L. Jiang, W. Fang, and W. Yao, “Structure-exploiting delay-dependent stability analysis applied to power system load frequency control,” *IEEE Transactions on Power Systems*, vol. 32, pp. 4528–4540, Nov 2017.

[40] C. K. Zhang, L. Jiang, Q. H. Wu, Y. He, and M. Wu, “Delay-dependent robust load frequency control for time delay power systems,” *IEEE Transactions on Power Systems*, vol. 28, pp. 2192–2201, Aug 2013.

[41] N. Vafamand, M. H. Khooban, T. Dragičević, J. Boudjadar, and M. H. Asemani, “Time-delayed stabilizing secondary load frequency control of shipboard microgrids,” *IEEE Systems Journal*, vol. 13, pp. 3233–3241, Sep. 2019.

[42] T. Stegink, C. De Persis, and A. van der Schaft, “A unifying energy-based approach to stability of power grids with market dynamics,” *IEEE Transactions on Automatic Control*, vol. 62, no. 6, pp. 2612–2622, 2017.

[43] N. Li, C. Zhao, and L. Chen, “Connecting automatic generation control and economic dispatch from an optimization view,” *IEEE Transactions on Control of Network Systems*, vol. 3, no. 3, pp. 254–264, 2016.

[44] L. Chen and S. You, "Reverse and forward engineering of frequency control in power networks," *IEEE Transactions on Automatic Control*, vol. 62, no. 9, pp. 4631–4638, 2017.

[45] S. Trip, M. Bürger, and C. D. Persis, "An internal model approach to (optimal) frequency regulation in power grids with time-varying voltages," *Automatica*, vol. 64, pp. 240 – 253, 2016.

[46] F. Dörfler, J. W. Simpson-Porco, and F. Bullo, "Breaking the hierarchy: Distributed control and economic optimality in microgrids," *IEEE Transactions on Control of Network Systems*, vol. 3, no. 3, pp. 241–253, 2016.

[47] J. Schiffer and F. Dörfler, "On stability of a distributed averaging PI frequency and active power controlled differential-algebraic power system model," in *European Control Conference (ECC)*, pp. 1487–1492, 2016.

[48] N. Chuang, "Robust H^∞ load-frequency control in interconnected power systems," *IET Control Theory Applications*, vol. 10, no. 1, pp. 67–75, 2016.

[49] W. Tan and Z. Xu, "Robust analysis and design of load frequency controller for power systems," *Electric Power Systems Research*, vol. 79, no. 5, pp. 846 – 853, 2009.

[50] A. N. Venkat, I. A. Hiskens, J. B. Rawlings, and S. J. Wright, "Distributed MPC strategies with application to power system automatic generation control," *IEEE Transactions on Control Systems Technology*, vol. 16, pp. 1192–1206, Nov 2008.

[51] H. Bevrani and T. Hiyama, "On load-frequency regulation with time delays: Design and real-time implementation," *IEEE Transactions on Energy Conversion*, vol. 24, pp. 292–300, March 2009.

[52] J. W. Simpson-Porco, F. Dörfler, and F. Bullo, "Synchronization and power sharing for droop-controlled inverters in islanded microgrids," *Automatica*, vol. 49, no. 9, pp. 2603 – 2611, 2013.

[53] A. Bidram, F. Lewis, and A. Davoudi, "Distributed control systems for small-scale power networks: Using multiagent cooperative control theory," *IEEE Control Systems*, vol. 34, no. 6, pp. 56–77, 2014.

[54] C. De Persis and N. Monshizadeh, "Bregman storage functions for microgrid control," *IEEE Transactions on Automatic Control*, 2017.

[55] X. Wu, F. Dörfler, and M. Jovanović, "Topology identification and design of distributed integral action in power networks," in *American Control Conference (ACC)*, pp. 5921–5926, 2016.

[56] E. Tegling, M. Andreasson, J. W. Simpson-Porco, and H. Sandberg, "Improving performance of droop-controlled microgrids through distributed PI-control," in *American Control Conference (ACC)*, pp. 2321–2327, 2016.

[57] A. Krishna, C. A. Hans, J. Schiffer, J. Raisch, and T. Kral, "Steady state evaluation of distributed secondary frequency control strategies for microgrids in the presence of clock drifts," in *2017 25th Mediterranean Conference on Control and Automation (MED)*, pp. 508–515, July 2017.

[58] S. Lee, C. Lee, M. Park, and O. Kwon, "Delay effects on secondary frequency control of micro-grids based on networked multi-agent," in *16th International Conference on Control, Automation and Systems (ICCAS)*, pp. 655–659, 2016.

[59] J. Lai, H. Zhou, X. Lu, X. Yu, and W. Hu, "Droop-based distributed cooperative control for microgrids with time-varying delays," *IEEE Transactions on Smart Grid*, vol. 7, no. 4, pp. 1775–1789, 2016.

[60] E. A. A. Coelho, D. Wu, J. M. Guerrero, J. C. Vasquez, T. Dragičević, Č. Stefanović, and P. Popovski, "Small-signal analysis of the microgrid secondary control considering a communication time delay," *IEEE Transactions on Industrial Electronics*, vol. 63, no. 10, pp. 6257–6269, 2016.

[61] S. Liu, X. Wang, and P. X. Liu, "Impact of communication delays on secondary frequency control in an islanded microgrid," *IEEE Transactions on Industrial Electronics*, vol. 62, pp. 2021–2031, April 2015.

[62] C. Ahumada, R. Cárdenas, D. Sáez, and J. M. Guerrero, "Secondary control strategies for frequency restoration in islanded microgrids with consideration of communication delays," *IEEE Transactions on Smart Grid*, vol. 7, pp. 1430–1441, May 2016.

[63] C. Kammer and A. Karimi, "Robust distributed averaging frequency control of inverter-based microgrids," in *IEEE 55th Conference on Decision and Control (CDC)*, pp. 4973–4978, 2016.

[64] H. Bevrani, M. R. Feizi, and S. Ataee, "Robust frequency control in an islanded microgrid: H_∞ and μ -synthesis approaches," *IEEE Transactions on Smart Grid*, vol. 7, pp. 706–717, March 2016.

[65] L. Guo, C. Zhao, and S. Low, "Cyber network design for secondary frequency regulation: A spectral approach," *Power Systems Computation Conference (PSCC)*, 2018.

[66] X. Zhang and A. Papachristodoulou, "Redesigning generation control in power systems: Methodology, stability and delay robustness," in *53rd IEEE Conference on Decision and Control*, pp. 953–958, Dec 2014.

[67] J. D. Glover, *Power system analysis and design*. Boston, Mass: Cengage Learning, sixth ed., 2017.

[68] A. R. Bergen, *Power systems analysis*. Pearson Education India, 2009.

[69] G. Andersson, “Modelling and analysis of electric power systems,” *ETH Zurich*, pp. 5–6, 2008.

[70] S. Caliskan and P. Tabuada, “Compositional transient stability analysis of multimachine power networks,” *IEEE Transactions on Control of Network Systems*, vol. 1, pp. 4–14, March 2014.

[71] P. Pourbeik *et al.*, “Dynamic models for turbine-governors in power system studies,” *IEEE Task Force on Turbine-Governor Modeling*, 2013.

[72] P. M. Anderson and A. A. Fouad, *Power system control and stability*. John Wiley & Sons, 2008.

[73] M. I. Alomoush, “Load frequency control and automatic generation control using fractional-order controllers,” *Electrical Engineering*, vol. 91, no. 7, pp. 357–368, 2010.

[74] P. Sauer and M. Pai, *Power system dynamics and stability.* Prentice Hall, 1998.

[75] U. Markovic *et al.*, “Understanding Stability of Low-Inertia Systems,” *IEEE Trans. Power Syst.*, 2019 (under review).

[76] J. Guerrero, P. Loh, M. Chandorkar, and T. Lee, “Advanced control architectures for intelligent microgrids – part I: Decentralized and hierarchical control,” *IEEE Trans. Ind. Electron.*, vol. 60, no. 4, pp. 1254–1262, 2013.

[77] J. Schiffer, D. Goldin, J. Raisch, and T. Sezi, “Synchronization of droop-controlled microgrids with distributed rotational and electronic generation,” in *52nd IEEE Conference on Decision and Control (CDC)*, (Florence, Italy), pp. 2334–2339, 2013.

[78] Q. Zhong and G. Weiss, “Synchronverters: Inverters that mimic synchronous generators,” *IEEE Transactions on Industrial Electronics*, vol. 58, no. 4, pp. 1259–1267, 2011.

[79] H. Tu, Y. Du, H. Yu, S. Lukic, M. Metelko, P. Volgyesi, A. Dubey, and G. Karsai, “A hardware-in-the-loop real-time testbed for microgrid hierarchical control,” in *2018 IEEE Energy Conversion Congress and Exposition (ECCE)*, pp. 2053–2059, 2018.

[80] J. Schiffer, R. Ortega, A. Astolfi, J. Raisch, and T. Sezi, “Conditions for stability of droop-controlled inverter-based microgrids,” *Automatica*, vol. 50, no. 10, pp. 2457–2469, 2014.

[81] V. Venkatasubramanian, H. Schattler, and J. Zaborszky, “Fast time-varying phasor analysis in the balanced three-phase large electric power system,” *IEEE Transactions on Automatic Control*, vol. 40, no. 11, pp. 1975–1982, 1995.

[82] Y. Wang, P. Yemula, and A. Bose, “Decentralized communication and control systems for power system operation,” *IEEE Trans. Smart Grid*, vol. 6, no. 2, pp. 885–893, 2015.

[83] P. Kansal and A. Bose, “Smart grid communication requirements for the high voltage power system,” in *IEEE PES General Meeting*, 2011.

[84] Y. Ghaedsharaf, C. Somarakis, F. Dörfler, and N. Motee, “Wide-area control of power networks with time-delay,” *IFAC*, vol. 51, no. 23, pp. 277 – 282, 2018.

[85] G. Tzounas, M. Liu, M. A. A. Murad, and F. Milano, “Stability analysis of wide area damping controllers with multiple time delays,” *IFAC-PapersOnLine*, vol. 51, no. 28, pp. 504 – 509, 2018.

[86] H. K. Khalil, *Nonlinear systems*, vol. 3. Prentice Hall, 2002.

[87] P. Park, “A delay-dependent stability criterion for systems with uncertain time-invariant delays,” *IEEE Transactions on Automatic control*, vol. 44, no. 4, pp. 876–877, 1999.

[88] E. Fridman, "New Lyapunov-Krasovskii functionals for stability of linear retarded and neutral type systems," *Systems & Control Letters*, vol. 43, no. 4, pp. 309–319, 2001.

[89] E. Fridman and U. Shaked, "A descriptor system approach to H_∞control of linear time-delay systems," *IEEE Transactions on Automatic Control*, vol. 47, no. 2, pp. 253–270, 2002.

[90] J. Sun and J. Chen, "A survey on Lyapunov-based methods for stability of linear time-delay systems," *Frontiers of Computer Science*, pp. 1–13, 2016.

[91] M. Wu, Y. He, and J.-H. She, *Stability analysis and robust control of time-delay systems*. Springer, 2010.

[92] K. Ramakrishnan and G. Ray, "Delay-dependent stability criteria for linear systems with multiple time-varying delays," in *TENCON 2009 - 2009 IEEE Region 10 Conference*, pp. 1–6, Jan 2009.

[93] J. Li, Z. Chen, D. Cai, W. Zhen, and Q. Huang, "Delay-Dependent Stability Control for Power System With Multiple Time-Delays," *IEEE Transactions on Power Systems*, vol. 31, no. 3, pp. 2316–2326, 2016.

[94] T. Li, M. Wu, Y. He, and W. Cao, "New delay-dependent steady state stability analysis for WAMS assisted power system," in *Control Conference (CCC), 2010 29th Chinese*, pp. 5734–5739, IEEE, 2010.

[95] R. Diestel, *Graduate texts in mathematics: Graph theory*. Springer, 2000.

[96] C. Godsil and G. Royle, *Algebraic Graph Theory*. Springer, 2001.

[97] P. Lin and Y. Jia, "Average consensus in networks of multi-agents with both switching topology and coupling time-delay," *Physica A: Statistical Mechanics and its Applications*, vol. 387, no. 1, pp. 303–313, 2008.

[98] A. van der Schaft, *L2-gain and passivity techniques in nonlinear control*. Springer, 2000.

[99] S. Trip, M. Bürger, and C. De Persis, "An internal model approach to (optimal) frequency regulation in power grids with time-varying voltages," *Automatica*, vol. 64, pp. 240–253, 2016.

[100] C. Bovy, H. Mertodimedjo, G. Hooghiemstra, H. Uijterwaal, and P. Van Mieghem, "Analysis of end-to-end delay measurements in internet," in *Proceedings of Passive and Active Measurement (PAM)*, pp. 26–33, 2002.

[101] S. Schuler, D. Zelazo, and F. Allgöwer, "Robust design of sparse relative sensing networks," in *2013 European Control Conference (ECC)*, pp. 1860–1865, July 2013.

[102] X. Wu, F. Dörfler, and M. R. Jovanović, "Input-output analysis and decentralized optimal control of inter-area oscillations in power systems," *IEEE Trans. Power Syst.*, vol. 31, no. 3, pp. 2434–2444, 2016.

[103] S. Schuler, U. Münz, and F. Allgöwer, "Decentralized state feedback control for interconnected systems with application to power systems," *Journal of Process Control*, vol. 24, no. 2, pp. 379–388, 2014.

[104] E. Candes, M. Wakin, and S. Boyd, "Enhancing sparsity by reweighted ℓ_1 minimization," *Journal of Fourier Analysis and Applications*, vol. 14, no. 5, pp. 877–905, 2008.

[105] P. Park, J. Ko, and C. Jeong, "Reciprocally convex approach to stability of systems with time-varying delays," *Automatica*, vol. 47, no. 1, pp. 235–238, 2011.

[106] S. Boyd and L. Vandenberghe, *Convex optimization*. Cambridge University Press, 2004.

[107] J. Löfberg, "YALMIP : a toolbox for modeling and optimization in MATLAB," in *IEEE Int. Symposium on Computer Aided Control Systems Design*, pp. 284 –289, Sept. 2004.

[108] Z. Styczynski, A. Orths, K. Rudion, A. Lebioda, and O. Ruhle, "Benchmark for an electric distribution system with dispersed energy resources," in *IEEE PES Transmission and Distribution Conference and Exhibition*, pp. 314–320, May 2006.

[109] K. Rudion, A. Orths, Z. Styczynski, and K. Strunz, "Design of benchmark of medium voltage distribution network for investigation of DG integration," in *IEEE Power Engineering Society General Meeting*, 2006.

[110] M. ApS, *The MOSEK optimization toolbox for MATLAB manual. Version 8.0.0.64*, 2017.

[111] T. Van Cutsem and C. Vournas, *Voltage Stability of Electric Power Systems.* Springer US, 1998.

[112] E. Sorin, L. Bobo, and P. Pinson, "Consensus-based approach to peer-to-peer electricity markets with product differentiation," *IEEE Transactions on Power Systems*, vol. 34, pp. 994–1004, March 2019.

[113] C. Zhao, E. Mallada, S. H. Low, and J. Bialek, "Distributed plug-and-play optimal generator and load control for power system frequency regulation," *Int. J. Electr. Power Energy Syst.*, 2018.

[114] A. Seuret, D. V. Dimarogonas, and K. H. Johansson, "Consensus under communication delays," in *2008 47th IEEE Conference on Decision and Control*, pp. 4922–4927, 2008.

[115] L. Moreau, "Stability of continuous-time distributed consensus algorithms," in *43rd Conference on Decision and Control*, vol. 4, pp. 3998–4003, IEEE, 2004.

[116] T. Zhang and H. Yu, "Average consensus in networks of multi-agent with multiple time-varying delays.," *IJCNS*, vol. 3, no. 2, pp. 196–203, 2010.